TEES AERO 91-1

CONTROL ALGORITHMS FOR AEROBRAKING IN THE MARTIAN ATMOSPHERE

Final Report

Submitted by the

TEXAS ENGINEERING EXPERIMENT STATION

to the

NASA LYNDON B. JOHNSON SPACE CENTER
Houston, Texas

Prepared by
Dr. Donald T. Ward. and Dr. Buford W. Shipley, Jr

Aerospace Engineering Division
Texes Engineering Experiment Station
College Station, Texas 77843-3141

September 1991

TEES AERO 91-1

CONTROL ALGORITHMS FOR AEROBRAKING IN THE MARTIAN ATMOSPHERE

Final Report

Submitted by the

TEXAS ENGINEERING EXPERIMENT STATION

to the

NASA LYNDON B. JOHNSON SPACE CENTER
Houston, Texas

Prepared by
Dr. Donald T. Ward. and Dr. Buford W. Shipley, Jr

Aerospace Engineering Division
Texes Engineering Experiment Station
College Station, Texas 77843-3141
September 1991

ABSTRACT

The Analytic Predictor Corrector (APC) and Energy Controller (EC) atmospheric guidance concepts have been adapted to control an interplanetary vehicle aerobraking in the Martian atmosphere. Modifications are made to the APC to improve its robustness to density variations. These modifications include adaptation of a new exit phase algorithm, an adaptive transition velocity to initiate the exit phase, refinement of the reference dynamic pressure calculation and two improved density estimation techniques. The modified controller with the hybrid density estimation technique is called the Mars Hybrid Predictor Corrector (MHPC), while the modified controller with a polynomial density estimator is called the Mars Predictor Corrector (MPC).

A Lyapunov Steepest Descent Controller (LSDC) is adapted to control the vehicle. The LSDC lacked robustness, so a Lyapunov tracking exit phase algorithm is developed to guide the vehicle along a reference trajectory. The equilibrium glide entry phase is employed for the first part of the trajectory. This algorithm, when using the hybrid density estimation technique to define the reference path, is called the Lyapunov Hybrid Tracking Controller (LHTC). With the polynomial density estimator used to define the reference trajectory, the algorithm is called the Lyapunov Tracking Controller (LTC).

These four new controllers are tested using a six degree of freedom computer simulation to evaluate their robustness. MARS-GRAM is used to develop realistic atmospheres for the study. The atmospheres are then perturbed using square wave density pulses. The MHPC, MPC, LHTC and LTC show dramatic improvements in robustness over the APC and EC. The MHPC, MPC, LHTC and LTC all complete the initial phase of testing (using square wave density pulses) with no failures. The second phase tests the MHPC, MPC, LHTC and LTC against atmospheres where the inbound and outbound density functions are different. Square wave density pulses are again used, but only for the outbound leg of the trajectory. Additionally, sine waves, in both altitude and range, are used to perturb the density function. All four new controllers are able to compensate for the outbound leg density pulses with no hard failures, but the algorithms are sensitive to large amplitude density pulses. Additionally, these control algorithms are sensitive to large amplitude sine waves, particularly sine waves in range. The hybrid density estimator responds poorly to sine waves in range with wavelength between twenty and two hundred nautical miles. The polynomial density estimator is sensitive to wavelengths between five hundred and two thousand nautical miles. Overall, the polynomial density estimator performs better than the hybrid density estimator. The Lyapunov tracking phase performs better than the predictor correctors and the LTC is the most robust control algorithm examined.

ACKNOWLEDGEMENTS

Many individuals deserve special thanks for their contributions to this research effort. First and foremost, Mr. Bob Ess and Mr. Steve Fitzgerald of NASA's Lyndon B. Johnson Space Center provided unswerving support under NASA P.O. T-1238R. They were always there to help with either technical or administrative problems. Dr. John Junkins and Dr. S.R. Vadali deserve special credit for their helpful suggestions and expert advice. Mr. Clifford DePrang spent many hours on this project and his contributions are sincerely appreciated. Mr. Mike Niestroy gave freely of his time in helping bring up the simulations on the Silicon Graphics workstation, even when he was busiest on his own research project. Similarly, Larry Kealey deserves special thanks for all of his help in preparing the documentation of the research on the NeXT computer. Additional thanks go to Dr. Thomas Linehan and Architecture Visualization Laboratory for allowing me to use their computer resources. Without their support this research could not have been completed on time. The Air Force Institute of Technology, especially Captain Shipley's program manager Captain Steve Payne, were steadfastly supportive.

TABLE OF CONTENTS

TABLE OF CONTENTS (CONT)

TABLE OF CONTENTS (CONT)

LIST OF TABLES

LIST OF FIGURES

LIST OF FIGURES (CONT)

LIST OF FIGURES (CONT)

LIST OF FIGURES (CONT)

LIST OF FIGURES (CONT)

NOMENCLATURE

A	Plant Matrix for Density Estimator
a	Orbit Semi-Major Axis
$\hat{C}$	Estimate of Coefficients c_1 - c_7
c_1 - c_7	Coefficients of Polynomial Used in Density Estimator
C_D	Aerodynamic Drag Coefficient
C_L	Aerodynamic Lift Coefficient
D	Drag Force
e	Orbit Eccentricity
E	Keplerian Energy to Mass Ratio
$\tilde{E}$	Residual Error Matrix
g	Local Gravitational Acceleration
$G_{\dot{h}}$	Gain On Altitude Rate Error
$G_{\bar{q}}$	Gain On Dynamic Pressure Error
H	Cosine of Angle Between the Gradient of the Descent Function and the State Space Velocity Vector
h	Altitude
h_1	Reference Altitude (250,000 ft)
hS	Density Scale Height
J	Cost Function
K	Gain Term
$K_{\bar{q}}$	Multiplier Used to Calculate Reference Dynamic Pressure
K_ρ	Density Multiplier
L	Lift Force
M_D	Vehicle Ballistic Coefficient
m	Vehicle Mass
P	Covariance Matrix
$\bar{q}$	Dynamic Pressure
R or r	Orbital Radius

R_a	Apocenter Radius
R_p	Pericenter Radius
S	Aerodynamic Reference Area
t	Time from Atmospheric Entry
u	Control Variable = cos (Φ)
V	Inertial Velocity
$\hat{V}$	Target Velocity
V_r	Atmospheric Relative Velocity
V_{trig}	Transition Velocity for Switch From Equilibrium Glide phase to Exit Phase
W	Lyapunov Descent Function
$\overline{W}$	Matrix of Weight Functions
w	Vehicle Weight
x_1	State Variable - Normalized Altitude
x_2	State Variable - Normalized Velocity
x_3	State Variable - Flight Path Angle
$\hat{x}$	Target States for Lyapunov Controllers
$\tilde{Y}$	Matrix of Normalized Density Measurements
β	Angle Between the Gradient of the Descent Function and the State Space Velocity Vector
γ	Inertial Flight-path-Angle
μ	Martian Gravitational Constant
λ	Lagrange Multipliers
ρ	Density
$\hat{\rho}$	Density Used to Normalize Density Measurements
τ	Normalized Time
σ	Normalized Density
ϕ	Rotation Angle for Ellipse Used in Lyapunov Descent Function
φ	Weighted Quadratic Function of Residual Errors
Φ	Bank Angle
ψ	Terminal Constraints

Superscripts

$\dot{()}$	Overdot - Derivative With Respect to Time
T	Transpose

Subscripts

0	Reference
a	At Apocenter
c	Commanded
d	Derived
e	Entry
f	Final
g	Gain
I	Inertial
p	At Pericenter
r	Relative
x	Exit

Acronyms

AFE	Aeroassisted Flight Experiment
APC	Analytic Predictor Corrector
EC	Energy Controller
GEO	Geosynchronous Earth Orbit
LEO	Low Earth Orbit
LHTC	Lyapunov Hybrid Tracking Controller
LSDC	Lyapunov Steepest Descent Controller
LTA	Lyapunov Tracking Algorithm
LTC	Lyapunov Tracking Controller
MARS-GRAM	Mars Global Reference Atmosphere Model
MHPC	Mars Hybrid Predictor Corrector
MPC	Mars Predictor Corrector
MRSR	Mars Rover/Sample Return
NASA	National Aeronautics and Space Administration
STS	Space Transportation System

CHAPTER I

INTRODUCTION

When orbital transfer is required near a celestial body with an atmosphere of sufficient altitude and density, it is often advantageous to utilize aerodynamic forces to aid in the transfer[1-11]. Aerodynamic drag forces are used to reduce the kinetic energy, while aerodynamic lift forces are used to control the trajectory during the maneuver. The result is a vehicle weight savings equivalent to the propellant necessary to perform the maneuver. The critical factor for success in the aerobraking maneuver is the performance of the guidance control system. The National Aeronautics and Space Administration plans a 1992 launch of the Aeroassisted Flight Experiment (AFE) to serve as a proof-of-concept and test vehicle for aerobraking orbital maneuvers[12]. Meanwhile, an aeroassisted orbital transfer maneuver is planned for the Mars Rover/Sample Return (MRSR) Mission to reduce the orbit energy from the hyperbolic Martian approach orbit to capture into a low Mars orbit with a commensurate ΔV savings of over 8000 ft/s when compared with an all propulsive mission[13].

Fig. 1 shows the proposed interplanetary mission concept. The vehicle will be launched from Earth into an elliptical heliocentric orbit. The vehicle will travel almost eight months in this interplanetary orbit making mid-course corrections as necessary to intercept Mars. When the vehicle reaches Mars there will be 6 km/sec difference between the velocity of the vehicle and Mars orbital velocity. Without some method of changing the vehicle's velocity it would swing by Mars without capturing into a Martian orbit. The proposed method for imparting this velocity change is to use the aerodynamic forces imparted by the Martian atmosphere. The final mid-course correction to the interplanetary orbit will allow the vehicle to enter the Martian atmosphere as shown in Fig. 2. The typi-

Journal model is *AIAA Journal of Aircraft.*

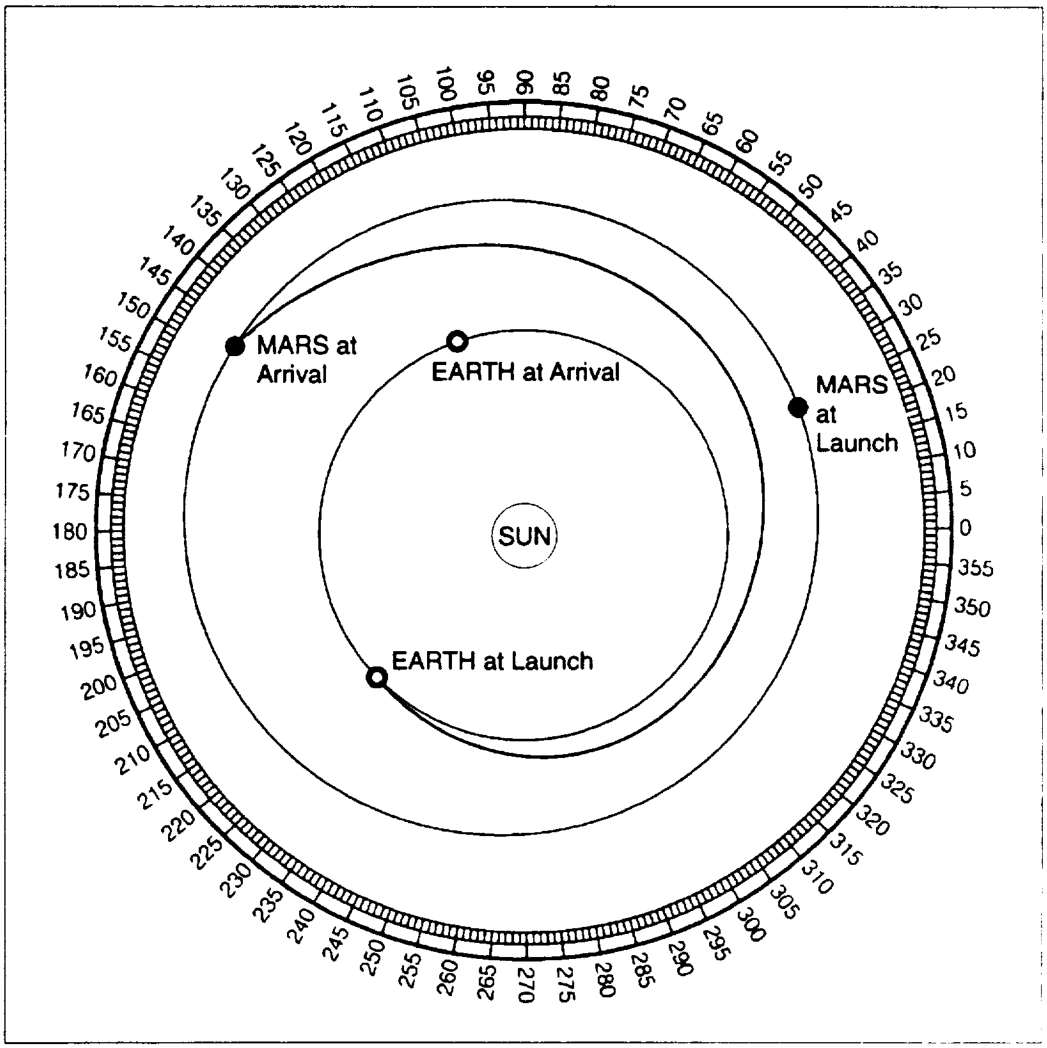

Fig. 1 Proposed Interplanetary Mission Concept (Adapted from Reference 14)

cal sequence of events for an aerobraking maneuver call for the vehicle to plunge into the atmosphere and fly deep in the atmosphere until the velocity is appropriately reduced. The vehicle then executes a pullout maneuver exiting the atmosphere in a low Mars orbit. Finally, a series of propulsive maneuvers are performed to transition the vehicle into the desired final orbit.

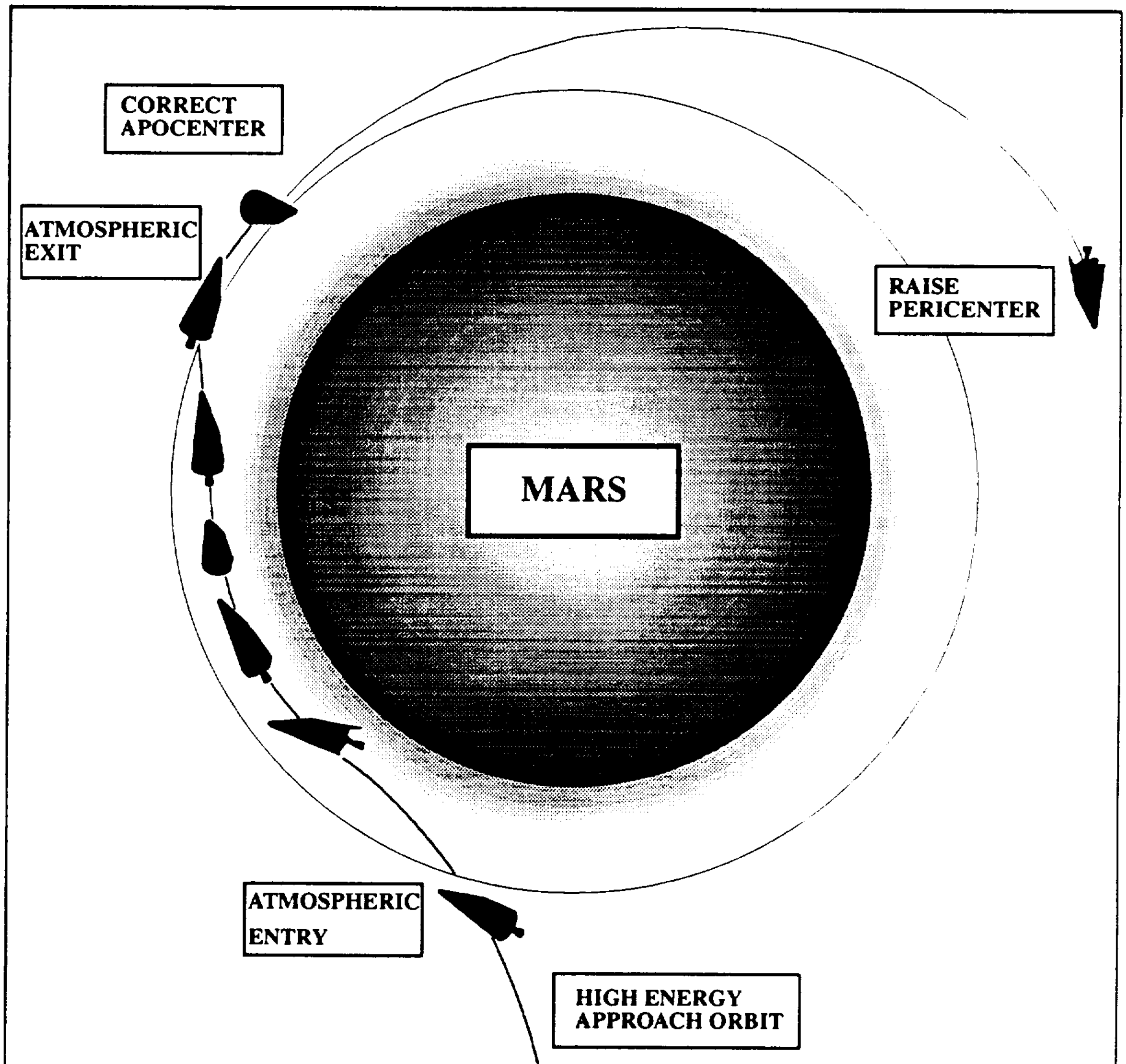

Fig. 2 Aerobraking Maneuver Sequence of Events
(Adapted from Reference 14)

In the past, for space missions reentering the Earth's atmosphere, only the destination coordinates have been specified. In targeting to the correct orbit following the aerobraking maneuver the guidance system must accurately control the final position of the vehicle as well as the final velocity vector. The atmospheric lift and drag forces affecting the vehicle are proportional to the atmospheric density, but atmospheric density is highly variable[15-22]. The guidance algorithm must be robust enough to control to the final state even with these uncertainties. The focus of this report is to study the relative merits of several existing and novel guidance algorithms, with particular emphasis upon the extent to which the algorithms tolerate our ignorance of the Martian atmosphere.

Although robustness with respect to density variations was a prime factor in developing and choosing the guidance scheme for the AFE[3,10-11,23-25]it becomes even more critical for the Mars mission. Scientists have worked for many years to characterize the Earth's atmosphere. Accelerometer data gathered during space shuttle returns have allowed us to characterize not only the average density values but also the expected magnitude and frequency of the random density variations[15-17]. In designing the AFE guidance system the Earth's upper atmosphere in the region 250000-400000 feet, was assumed to have density variations of ±25% from standard values over small altitude intervals[15]. The Martian atmosphere goes through global atmospheric expansions and contractions equivalent to an atmospheric shift of 10 km[22]. Additionally, data gathered from the Viking I and Viking II landers show density variations of 20 to 30% over small altitude intervals in the aerobraking region[18-19]. Since we have only two sets of density measurements from the Martian aerobraking region, we must expect even larger density variations to occur. It is conjectured that density shears of 60% or greater may be encountered. Development of a robust controller capable of acceptable performance given the large, unpredictable density variations in the Martian atmosphere is, therefore, vital to the success of the MRSR mission.

Background

The basic technology required to perform hypersonic flight in an atmosphere was developed in the 1950s to support the development of intercontinental ballistic missiles[26]. Technology was extended to allow the Mercury and Gemini projects to dissipate kinetic energy by entering the atmosphere with low ballistic coefficient vehicles. Major advances in entry technology were made during the Apollo program, especially in the areas of navigation, guidance and control during atmospheric maneuvering. With the Space Transportation System (STS) came a reusable capability to deploy and retrieve satellites from Low Earth Orbit (LEO). Deployment of the Space Station will provide a permanent base in LEO capable of performing maintenance and repair of satellites. However, with a large percentage of satellites in Geosynchronous Earth Orbit (GEO)an economical system of deploying satellites to GEO and then returning them to LEO is required. The National Aeronautics and Space Administration (NASA) has developed an aerobraking vehicle, the AFE, to meet the return requirement[12]. In designing the Mars Rover/Sample Return mission an aerobraking phase similar to that of the AFE is envisioned to dissipate kinetic energy from the hyperbolic Martian approach orbit leaving the satellite in a Low Mars Orbit[13].

The AFE, scheduled for launch in 1992 will serve as a proof of concept and test vehicle for aerobraking. AFE will enter the atmosphere with the same velocity as a vehicle returning from GEO. The vehicle will fly trimmed at a constant angle of attack, and therefore, at near a constant lift to drag (L/D) ratio. AFE will roll about the velocity vector to modulate the in plane portion of the lift to control the trajectory while drag dissipates kinetic energy. The vehicle will exit the atmosphere, after an appropriate energy reduction, with exit velocity and flight path angle such that the final orbit will rendezvous, at apogee, with the desired LEO. The mission concept for the Mars aerobrake is expected to be quite similar, but of course, for the MRSR objectives.

The complexity of the competing inequality and equality constraints placed on an aerobraking maneuver make definition of an optimal, robust control algorithm extremely difficult. The simplest controllers are open loop controllers designed to optimize the trajectory for a specific atmosphere, entry conditions and vehicle design. Talay, et al,[3] optimized a bank angle history for a nominal 1962 atmosphere using a trajectory optimization code. When this bank angle history was used in trajectory simulations with off-nominal atmospheres in several cases the vehicle either exited the atmosphere early or failed to exit at all. Vinh[4] first formulated an *optimal*, minimum fuel, control problem using a combined propulsive and aerodynamic transfer. He shows that an *optimal* combined propulsive/aerodynamic orbit transfer will require only 32% of the total ΔV required for an all propulsive maneuver for an orbit transfer from GEO to LEO. Then Vinh, et al,[27] produce an explicit guidance scheme for the aerobraking phase of a drag modulated aeroassisted transfer between elliptical orbits. They find the optimal strategy consists of bang-bang control but then point out that the strategy is difficult to realize because the switching time must be very accurate, "within a fraction of a second to avoid crashing." They propose an alternative strategy whereby the drag is controlled between minimum and maximum values as a function of the current state. Kechichian, et al,[28] also acknowledge that for a drag modulated vehicle bang-bang control is optimum for minimizing the total ΔV required to achieve the desired orbit, but in an effort to reduce the sensitivity to switch point timing a new C_{Dmax}-C_{Dmin}-C_{Dmax} controller is developed to add an additional degree of control. Sensitivity analysis shows that this control scheme has essentially zero sensitivity to an atmospheric density profile of $\pm 15\%$ of nominal but an entry corridor width of $\pm 0.1°$ should be maintained to avoid excessive ΔV requirements.

Much work has been performed in the area of optimal aeroassisted plane changes. Hull, et al,[29] derives an optimal guidance scheme for performing an aeroassisted plane change between circular orbits. They assume a parabolic drag polar for the vehicle and use Loh's constant[30] to include gravitational terms and apparent lift terms in the analysis. They find bank angle and angle of attack time histories which minimize the total ΔV required to perform the maneuver by maximizing the exit velocity following the aero phase. Plane changes of 10 to 40 degrees are demonstrated. Later the problem is reformulated[31] using heading as the independent variable and assuming that Loh's term may be either positive or negative. They show that only one solution exists and that it may be found by solving a fourth order polynomial. Hull, McClendon, and Speyer[32] then reform the problem assuming an elliptic drag polar and obtain similar results. They show that near the end of the atmospheric turn Loh's term is not constant which may cause extremely high angles of attack. Finally, Hull and co-workers[33] assume Loh's term is piecewise constant during the turn and reformulate the problem. Using the method of successive approximations they construct a control law which results in a final velocity within 1% of the *true* optimal final velocity for a 40° plane change and results in a very reasonable maximum angle of attack of 30°. Johannesen, et al,[5] formulate an approximate control law for lift and bank angle to maximize orbit plane change using an aeroassist maneuver. The control law is tested for a wide range of speed ratios V_e/V_f. They observe that the maximum turn angle for any speed ratio is proportional to the maximum lift-to-drag ratio.

Two unique methods of determining atmospheric guidance control laws have been developed. Mease and McCreary[6] propose using an approximate closed form solution of the equations of motion. Their solution divides the trajectory into three regions. During the beginning and end of the trajectory the gravitational terms are assumed to dominate, while in the mid-portion of the trajectory aerodynamic terms are assumed to dominate. The solutions for each of these regions is combined using the method of matched asymptotic expansion. Final apocenter values within 9% of the targeted values are demonstrated for a wide range of entry flight path angles for a simulated Mars aerocapture mission. The other unique method developed by Lee and Grantham[7] uses Lyapunov optimal feedback control to minimize the ΔV required to raise perigee following an aerobraking maneuver. This method calculates a descent function and then seeks to move the system in a preferred direction, opposite the gradient of the descent function. The Lyapunov feedback controller is compared with an optimal open loop controller derived using calculus of variations for the nominal 1962 standard atmosphere. Superior, robust performance for the Lyapunov controller is demonstrated for both the standard atmosphere and a shuttle-derived atmosphere.

Control laws developed using optimal control theory offer excellent performance in numerical simulations, but those methods which require extensive computation for each control update have been at a distinct disadvantage due to limitations of onboard computing capability. For this reason several simplified guidance schemes have been developed. Letts and Pelekanos[8] developed a control law using bank-angle modulation of the lift vector to establish a constant axial deceleration level until the required exit velocity is reached, when full lift up is commanded. They show that ΔV required to circularize following the aerobrake maneuver increases approximately 35 m/s for each percent change from the nominal value for an atmosphere that is multiplied by a constant density bias. Gamble, et al,[23] develop a control scheme similar to that of Letts and Pelakanos except Gamble's method commands to an equilibrium glide rather than a constant axial deceleration until the desired velocity is achieved. After the desired velocity is achieved, full lift up is again commanded for atmospheric exit. Gamble finds that a 50% increase in density has little effect on the total ΔV required but a 50% decrease in density increased ΔV required by about 35% due to problems in establishing the equilibrium glide. Cerimele, et al,[24] use Gamble's equilibrium glide phase during the entry portion of the trajectory, but then switch to a reference drag profile like Letts and Pelekanos for the exit portion of the trajectory. Density shears in the atmosphere are simulated and the ΔV required following the aerobraking maneuver is found to be very sensitive to density ratios exceeding ±30% occurring over altitude ranges of 1,000 to 10,000 ft. Cerimele and Gamble[9] produce an analytic predictor corrector guidance algorithm, again using the equilibrium glide entry phase but with a predictor corrector exit phase designed to target apogee more accurately. The predictor corrector algorithm assumes a constant altitude rate and an exponential atmosphere to predict apogee. The predictor algorithm iterates altitude rate until a value is found which produces the desired apogee. The vehicle is then commanded to this altitude rate. An interesting feature added to this algorithm is a low pass density filter. Density is computed on-board based on accelerometer data. Calculated density is then compared against predicted density values and future predicted values are adjusted accordingly. This guidance algorithm was tested numerically using combined dispersions of ±0.2° in entry flight path angle, ±20% density variations and ±33% L/D. The final apogee value was within 2 nm of the target value in all cases. Gamble, et al,[34] present three atmospheric guidance concepts for aeroassist orbit transfer vehicles. The first method presented is the Analytic Predictor Corrector, already discussed. The second is a Numerical Predictor Corrector algorithm which numerically integrates a trajectory assuming constant bank angle magnitude and an assumed density profile. The bank angle is iterated until the desired apogee is computed and the vehicle is commanded to this bank angle. The final control algorithm presented is the Energy Controller which guides the vehicle to a desired energy state at atmospheric exit. The energy gain, defined as the ratio of energy rate to energy error, is controlled so that energy error exponentially goes to zero at atmospheric exit. The energy gain command is converted to an altitude rate command which in turn is converted to a bank angle command. Their results show that all three algorithms are capable of maintaining the final apogee within 10 nm and ΔV within 50 ft/sec of the nominal values for test cases with dispersions of ±4 nm in perigee, ±50% in density, ±50% in W/C_DA and +50% in L/D. The analytic predictor corrector and Energy Controller show slightly worse results for the -50% L/D case.

Fitzgerald and Ward[10-11] investigate the sensitivity to density shears of the Analytic Predictor Corrector and Energy Controller algorithms while guiding the AFE vehicle. They consider spike and step shaped density dispersions of ±10 and ±20% magnitude with durations of 5,000 and 10,000 feet, starting at altitudes between 260K and 295K ft. ΔV increases up to 60% for the Energy Controller and 41% for the APC are demonstrated. Fitzgerald[11] then formulates a Hybrid Predictor Corrector algorithm which uses the atmospheric density profile determined during the entry phase in the predictor corrector of the exit phase. This significantly reduces the sensitivity to density shears for atmospheres where the exit atmosphere matches the entry profile.

Meyerson and Cerimele[13] review the aeroassist vehicle requirements for the Mars Rover/Sample Return Mission. They use a modified analytic predictor corrector algorithm referred to as HYPAS as the controller for vehicles with L/D ranging from 0.3 to 1.5. Additionally, entry velocities from 5.79 to 9.20 km/sec were investigated. A recommendation of this study is, "to refine the HYPAS guidance algorithm to control the trajectory more accurately in the exit phase." They recommend using two exponential atmosphere models in the guidance predictor.

"The Mars atmosphere is highly variable on a daily, seasonal and annual basis[18]." The thin atmosphere and solar heating produce a large daily temperature range which translates to a large daily density fluctuation[18-21]. Fig. 3 shows that at the surface the Martian atmospheric density is approximately two orders of magnitude less than that of the Earth's atmosphere and at aerobraking altitudes there is still more than an order of magnitude difference between the density of Earth and that of Mars. "On an annual basis,

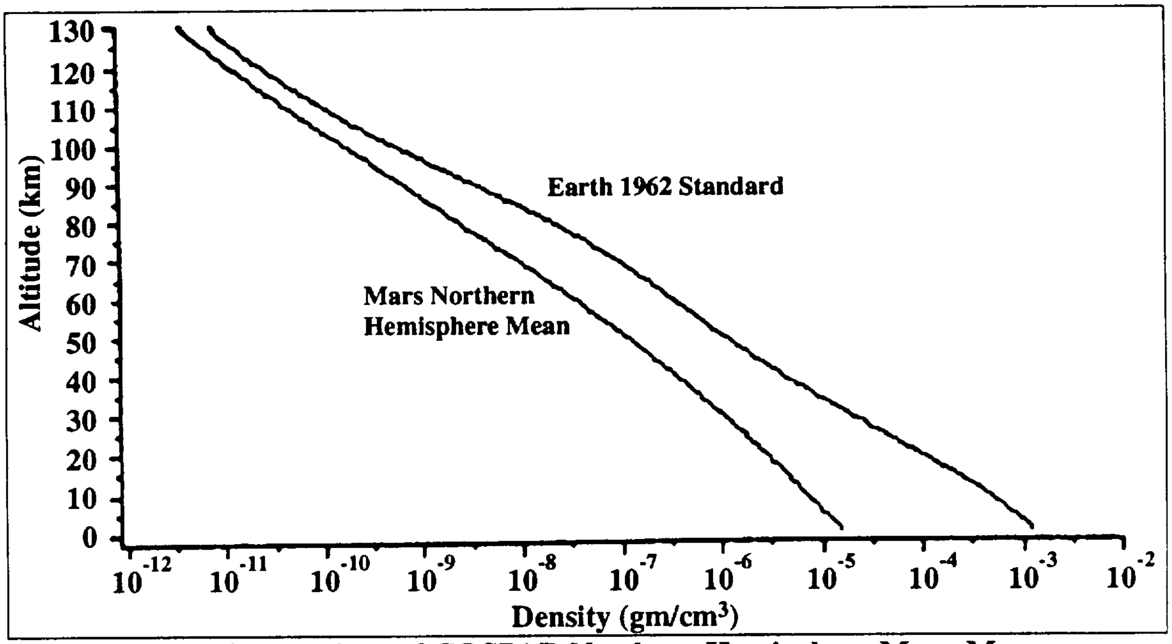

Fig. 3 Comparison of COSPAR Northern Hemisphere Mean Mars Density Model and 1962 U.S. Standard Earth Atmosphere (Adapted from Reference 19)

the atmospheric pressure at the surface changes by ±15% due to condensation and sublimation of the CO_2[17]," which produces a global expansion and contraction of the atmosphere of roughly 10km. Fig. 4 presents the density deviations of the COSPAR high density model and the COSPAR low density model relative to the COSPAR Northern Hemisphere Mean Model. Global dust storms absorb radiation high in the atmosphere, thereby increasing the upper atmosphere temperature and causing a large scale expansion of the atmosphere. The density is then substantially increased at orbital and entry altitudes. Additionally, density of the Martian atmosphere varies widely on a daily basis. Fig. 5 shows the expected morning and afternoon density profiles calculated for summer at the Viking 1 lander location while Fig. 6 shows the calculated density profiles for winter at the Viking 1 lander location. These figures show that at aerobraking altitudes the density may vary by as much as 100 to 150% on a daily basis. The Viking 1 and 2 landers measured atmospheric properties during their descent and recorded peak to peak density varia-

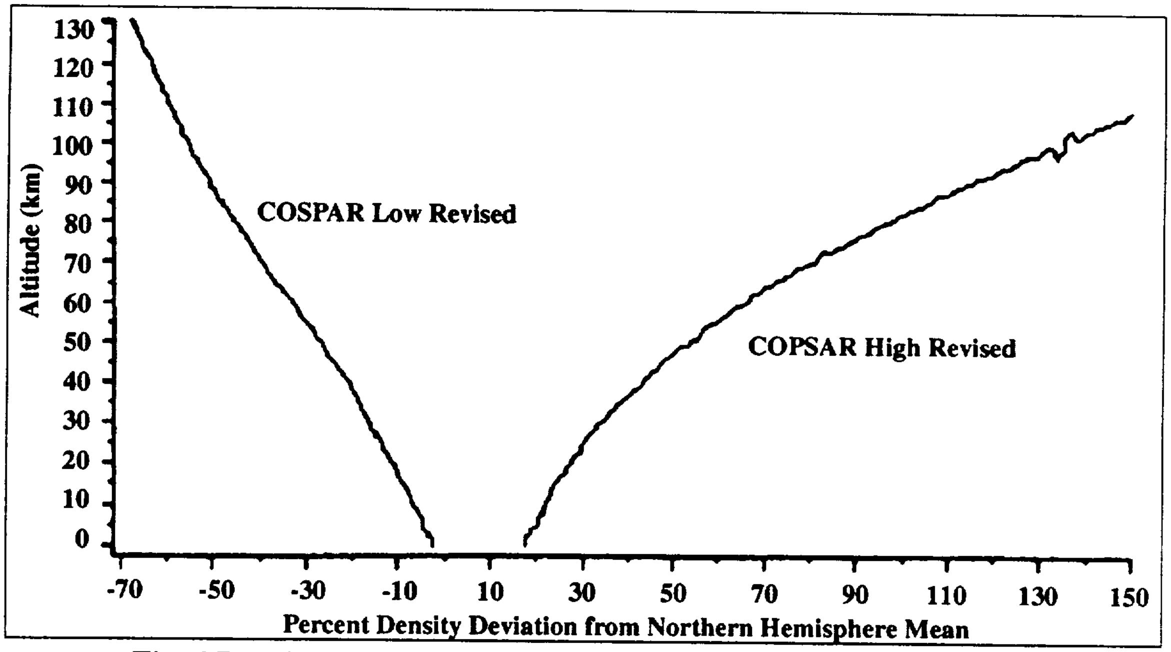

Fig. 4 Density Deviations of the COSPAR Low-Cool and COSPAR High-Warm Density Models as Compared to the COSPAR Northern Hemisphere Mean Model (Adapted from Reference 19)

tions in the aerobraking region of 30% over a 15 km altitude band and 20% over a 10 km region[18-21]. Fig. 7 and Fig. 8 present the density variations measured by Viking 1 and Viking 2 respectively during their descent to Mars. The Mars Global Reference Atmosphere Model (MARS-GRAM)[35] characterizes Mars atmospheric properties, density, temperature, pressure and wind speed and direction, as functions of date, time, latitude, longitude, altitude, solar activity and dust storm activity.

This report will characterize the sensitivity of selected aerobraking guidance algorithms with respect to density variations of the type and magnitude expected in the Martian atmosphere to determine their suitability to perform the MRSR Mission. A guidance algorithm capable of acceptable performance in spite of the uncertainty in Martian atmospheric density or methods of reducing the uncertainty will be developed. To attain this goal the following research objectives are proposed.

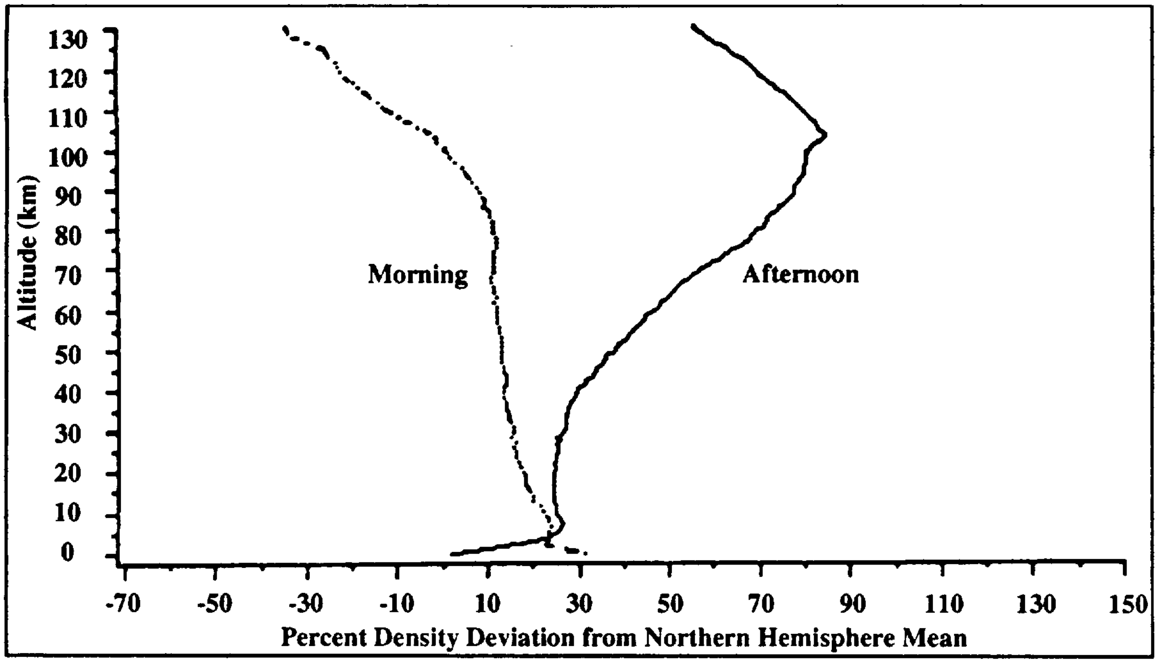

Fig. 5 Morning and Afternoon Density Profiles Calculated for the Viking 1 Lander Location During the Summer (Adapted from Reference 19)

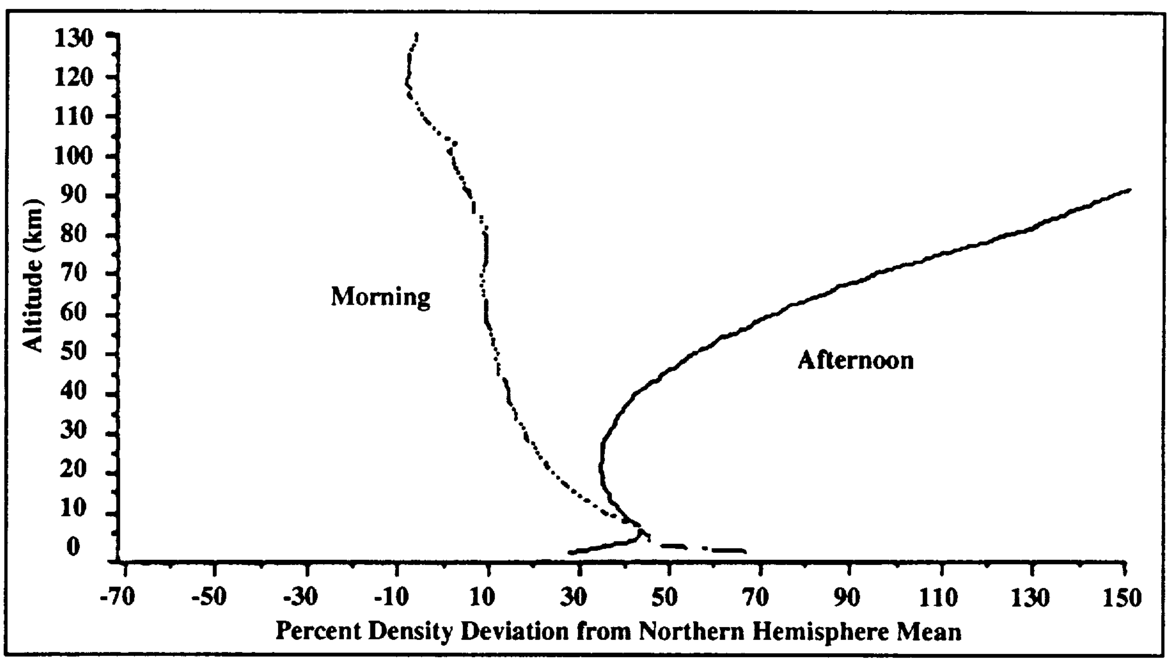

Fig. 6 Morning and Afternoon Density Profiles Calculated for the Viking 1 Lander Location During the Winter (Adapted from Reference 19)

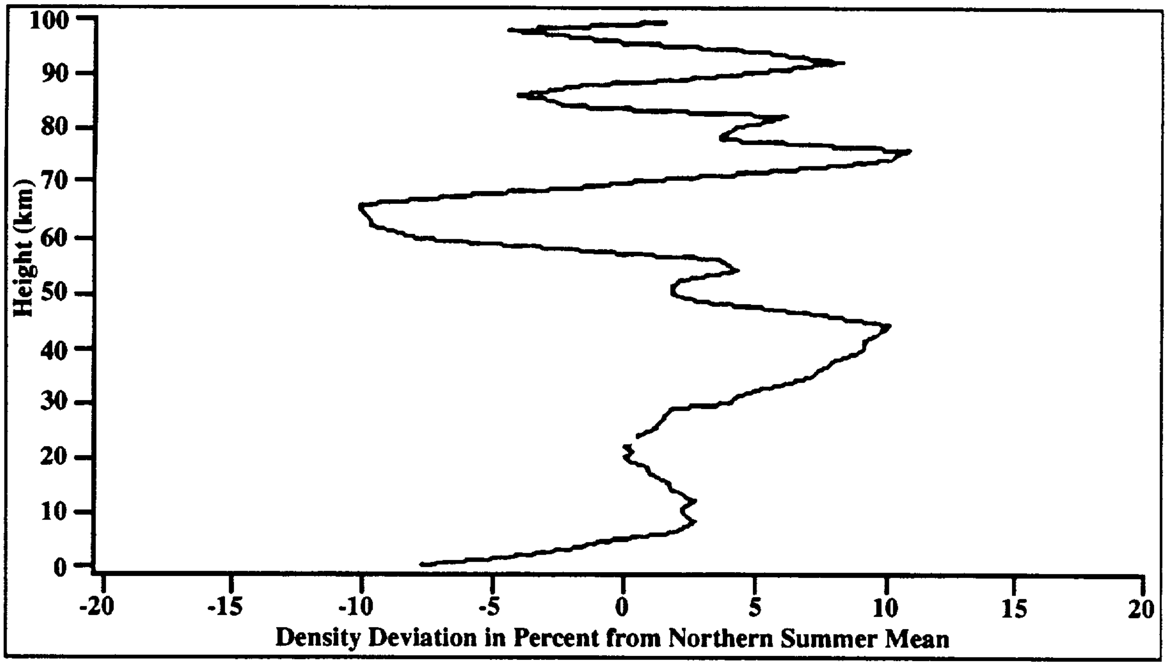

Fig. 7 Viking 1 Measured Density Profile
(Adapted from Reference 19)

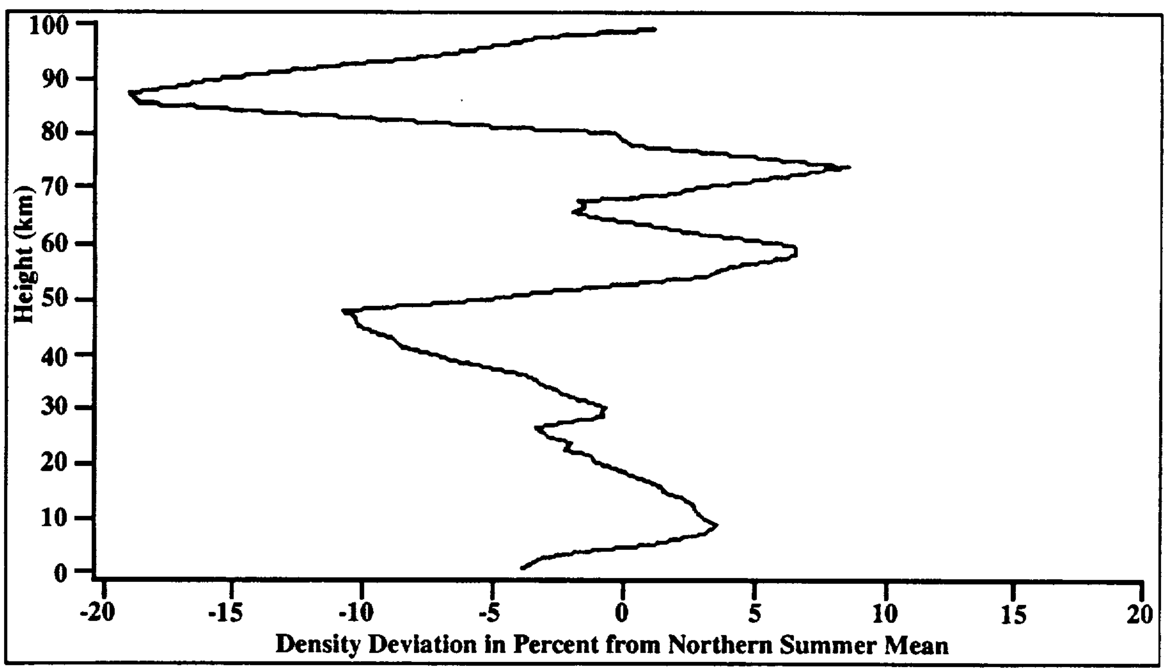

Fig. 8 Viking 2 Measured Density Profile
(Adapted from Reference 19)

Research Objectives

When designing a control law for an aeroassist maneuver, an exponential variation of atmosphere density with altitude is an extremely attractive computational simplification. However, given the large density biases and density shears of the Martian atmosphere[18-21], a guidance algorithm optimized for the MRSR vehicle aerobraking in the assumed exponential atmosphere may demonstrate poor performance and potentially catastrophic failures if realistically off-nominal conditions are encountered[13]. Especially when errors in navigation accuracy and/or vehicle L/D are also considered, the results of using any fixed density model may be catastrophic, with the vehicle either not being captured into a Martian orbit or failing to exit the Martian atmosphere. As a result, the sensitivity of MRSR atmospheric guidance to perturbations in density as well as to navigation errors and L/D errors is critical to the success of the mission.

A systematic method of evaluating the effects of density biases and density shears in combination with navigation errors and L/D errors on an MRSR atmospheric guidance algorithm is sought. The methods established will be used to evaluate candidate guidance algorithms, including algorithms developed in this report. Toward these objectives, the first task is to determine the expected extremes in Martian density. MARS-GRAM[35] will be utilized for this task. The highest and lowest density atmospheres expected are determined as a function of season, time of day, solar activity and dust storm activity. Since there have only been two space probes which have measured density through the Martian aerobraking region, the nature and magnitude of expected worst case density shears is not known precisely and must be estimated. These atmosphere extremes are checked against the Mars standard atmospheres[18] and the Viking data[18-19]. There is a proposal for the Mars Aeronomy Observer (MAO)[20-21] to send additional probes to the Martian surface to gather more data quantifying these shears; but, this mission is still years away. The expected navigational accuracy and probable L/D errors are also be determined.

Secondly, the Analytic Predictor Corrector algorithm,[9] the algorithm chosen for the AFE mission, and the Energy Controller[34] are fine tuned for the MRSR mission. Then the sensitivity of these algorithms when faced with these density biases, density shears, navigation and L/D errors are determined. The six degree-of-freedom Program to Optimize Simulated Trajectories (POST)[36] is used in this analysis. The sensitivity of these algorithms is visually presented by plotting three dimensional sensitivity surfaces with the qualitative objective of finding the worst combinations of dispersions and defining the performance bounds of these two controllers. Methods of improving the performance of these algorithms, especially methods of using information derived early in the trajectory, to improve the performance in the latter portions of the trajectory (similar to the methods proposed by Fitzgerald in his Hybrid Predictor Corrector algorithm) are evaluated. Two new algorithms called the Mars Hybrid Predictor Corrector (MHPC) and the Mars Predictor Corrector (MPC) are developed. These two algorithms differ only in their density estimation techniques. This task, along with developing the new algorithm proposed below, are crucial to the research and secondary only to the task of defining absolute robustness limits.

The third order of business is to explore more elegant ways to optimize the controller, especially ways of improving the robustness. A potential candidate Lyapunov Steepest Descent Controller[7] (LSDC) similar to the one suggested by Lee and Grantham is coded and its performance tested against the same perturbations as the others. Two new algorithms are developed, again differing only in their density estimation techniques. They are called the Lyapunov Tracking Controller (LTC) and the Lyapunov Hybrid Tracking Controller (LHTC).

Finally, and most important of all, the robustness limits of the improved MPC, MHPC, LTC and LHTC controllers are characterized. The guidance performance is thoroughly tested to find the tolerable limits on density bias and density shear given the probable errors in navigation and L/D. POST is used to test the guidance algorithms, using the Viking atmosphere profiles[18-19]. The limits on atmosphere dispersions, considering the inherent navigation and probable L/D errors, under which acceptable controller performance will occur is clearly defined from the results of these simulations.

These limits are checked against the worst case perturbations expected for the mission[18-19,35]. Conclusions are drawn regarding the performance of these algorithms when faced with the expected density variations, as well as possible variations in vehicle lift to drag ratio and entry flight path angle. Recommendations for future study are then presented.

Organization of the Report

Improvements made to the Analytic Predictor Corrector and Hybrid Predictor Corrector control algorithms are presented in Chapter II. Derivation of the LSDC and a LTA are presented in Chapter III. Chapter IV details the model used for the trajectory simulations and the atmospheric models. Vehicle mass and aerodynamic data are presented along with atmospheric entry conditions. The controller test program is outlined and the perturbations in atmospheric density, vehicle lift and drag, and entry conditions which were used in the test program are presented. Finally the performance of the various controllers is presented. In Chapter V the four best performing controllers, the MPC, MHPC, LTA and the LHTA algorithms, are tested against each other in a head to head fashion. The perturbation limits which define the edge of the envelope where acceptable performance is attainable are determined. Conclusions and recommendations are presented in Chapter VI.

CHAPTER II

IMPROVEMENTS TO THE PREDICTOR CORRECTOR ALGORITHM

The Analytic Predictor Corrector controller, discussed by Cerimele and Gamble[9], is the control algorithm selected for the AFE[12]. This controller was adapted to the MRSR problem and tested against expected perturbations in the Martian atmosphere as well as perturbations in entry conditions and vehicle lift and drag characteristics. While testing the Analytic Predictor Corrector controller, several areas were found where improvements could be made. The constant multiplier used to determine the reference dynamic pressure was changed in an effort to gain robustness and prevent premature exit from the atmosphere. Borrowing a technique first employed by Fitzgerald[11], an improved atmospheric model used by the predictor step to determine velocity loss during the exit phase was also incorporated. Then a new method of estimating density incorporating a polynomial to fit the normalized density function was developed[42]. A modified exit phase, first developed at the Charles Stark Draper Laboratory[43,44], was incorporated and tested, first without and then with the improved atmospheric models. The new exit phase also assumes a constant altitude rate to compute the velocity loss due to aerodynamic drag. However, instead of predicting the exit state and iterating altitude rate to target the desired apocenter, the velocity required to attain the desired apocenter altitude is computed based on the current state and an estimate of the remaining velocity loss due to aerodynamic drag. The iteration is simplified to a single step altitude rate correction. With the large density shifts present in the Martian atmosphere and the uncertainties in vehicle and entry conditions the velocity at which the controller transitions from the equilibrium glide phase to the exit phase (incorporated as a controller constant for the APC controller operating in the Earth atmosphere) was changed to an adaptive parameter.

The predictor corrector algorithm developed here which uses a variation of Fitzgerald's density estimation scheme is referred to as the Mars Hybrid Predictor Corrector (MHPC). The algorithm which incorporates the polynomial density estimator is called simply the Mars Predictor Corrector (MPC) algorithm. The modifications presented here convert the predictor corrector algorithm from a good controller for guiding the aerobraking phase of a space vehicle returning from Geosynchronous Earth Orbit (GEO) into a robust control algorithm capable of accurately guiding an interplanetary probe through an aerobraking maneuver in the Martian atmosphere.

Reference Dynamic Pressure Calculation

The equilibrium glide phase of the APC controller seeks an equilibrium condition with the vehicle following a reference dynamic pressure path. The reference dynamic pressure is calculated as a multiple, $K_{\bar{q}}$, of the dynamic pressure required to maintain equilibrium with the lift vector oriented down. Gamble, et al[34], recommend that this multiplier be 1.33 for the AFE which aerobrakes in the Earth's atmosphere.

$$\bar{q}_{ref} = \left[-\frac{K_{\bar{q}}w}{C_L S}\right]\left[1 - \frac{V^2}{gR}\right] \tag{1}$$

Ideally, to have the minimum ΔV required after the aerobraking maneuver the velocity of the vehicle should be decreased as high in the atmosphere as possible. Some studies have considered, as a minimum ΔV aeromaneuver, the case of a vehicle with infinite lift skimming the edge of the atmosphere until the velocity has decreased by the appropriate amount so the vehicle can be released into a Hohman Transfer orbit from the circular orbit at the edge of the atmosphere to the desired orbit[7]. However, decreasing the velocity high in the atmosphere means flying in a region of lower density and consequently lower dynamic pressure. Flying higher requires the in-plane component of the lift vector to be oriented more downward to maintain equilibrium. This idealization is satisfactory only with a smooth exponential density profile; density shears are not allowed. If the vehicle is flying in equilibrium using 50% of the lift down capability ($\Phi = \pm 120°$) and a density shear is encountered which decreases the density by 50% suddenly, full lift down will be required to maintain equilibrium. In actuality, because of time lags between the encounter of a density shear and the vehicle's response, coupled with the potential necessity of reducing a positive altitude rate, the minimum acceptable reference dynamic pressure to maintain control, if the density suddenly decreases by 50%, is considerably more than twice that required to maintain equilibrium in a full lift down configuration.

One potential drawback to increasing $K_{\bar{q}}$ is that the trajectory loads are increased over a portion of the flight. Heat rates and vehicle acceleration loads are increased for the portion of the portion of the trajectory after the minimum altitude point until the transition to the exit phase, however, for the range of $K_{\bar{q}}$ between 1.33 and 4.5 the maximum heat rates, g loading, the minimum altitude, and even the maximum dynamic pressure do not change. 4.5 was the largest value which would not adversely affect the peak trajectory loads. Furthermore, it has been found that the total heat integrated heat load calculated is lower for a higher value of $K_{\bar{q}}$ because the vehicle's deceleration is greater and less time is required to reduce the vehicle's velocity.

Fig. 9 presents the altitude time histories and Fig. 10 presents the velocity time histories for trajectories flown through a nominal Martian atmosphere perturbed with a square wave pulse of 20,000ft duration located between 140,000ft and 160,000ft altitude. This pulse multiplies the nominal density function by 0.5 in this altitude region. The three curves presented in each figure represent $K_{\bar{q}}$ values of 1.33, 2.2 and 4.5. Notice that the trajectories where $K_{\bar{q}}$ equals 1.33 and 4.5 perform well. The final apocenter is within three nautical miles of the targeted 270 nm for both cases. However, the trajectory flown

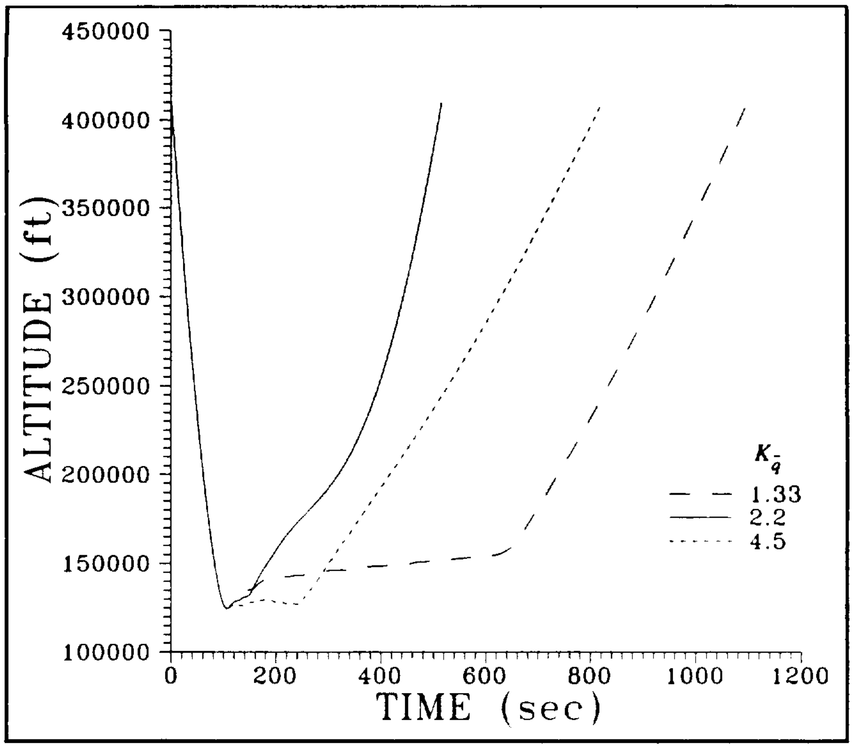

Fig. 9 Altitude Time Histories Varied $K_{\bar{q}}$ Values

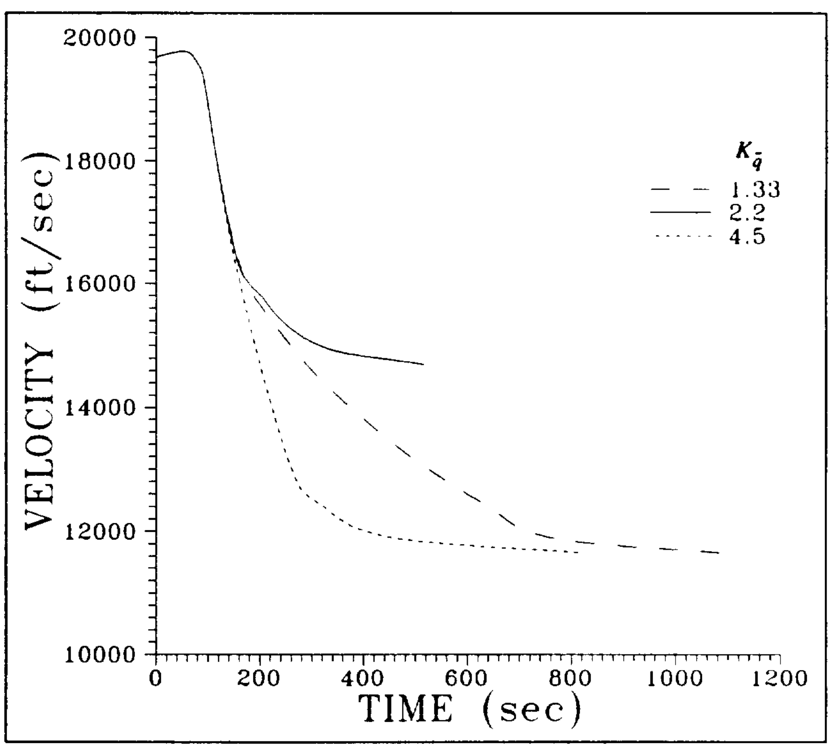

Fig. 10 Velocity Time Histories Varied $K_{\bar{q}}$ Values

with $K_{\bar{q}}$ equal to 2.2 skips out, or exits the atmosphere early while the velocity is still too high. Skip outs are difficult to predict because they are caused by a sudden negative density shear which reduces the vehicle's available lift and drag force. If this negative density shear occurs when the vehicle is in a relatively safe regime where the sudden decrease in density will not place the vehicle in a critical situation, a skip out may not occur. If the vehicle has a positive altitude rate while reversing the bank with the lift vector oriented up, or if the control scheme allows the vehicle to overshoot the reference dynamic pressure trajectory, thus temporarily flying at a dynamic pressure lower than the reference value, a skip out is quite likely. Combinations of these factors are an even greater challenge for the controller when a sudden negative density shear is encountered. Increasing $K_{\bar{q}}$ will not always prevent a skip out, but increasing $K_{\bar{q}}$ does tend to reduce the probability of a skip out. Indeed, with $K_{\bar{q}}$ set to 4.5 (the largest value possible without adversely affecting peak trajectory loads) no skip outs were encountered during the validing simulations.

With the uncertainties in the Martian atmosphere the slight penalty in ΔV required to increase this multiplier to 4.5 (less than 10 ft/sec), when compared to the 1.33 value recommended for the Earth atmosphere, seems to be a small penalty to gain additional robustness and limit the possibility of a premature skip out. $\bar{q}_{\text{ref}}$ is therefore calculated

$$\bar{q}_{\text{ref}} = \left[-\frac{4.5w}{C_L S}\right]\left[1 - \frac{V^2}{gR}\right]. \tag{2}$$

Improved Exit Phase Density Models

The second area of improvement is the density estimation technique. Good density estimation is critical for the success of any Martian aerobraking. With the wide density variations possible in the Martian atmosphere, the correct path, given an estimate of future density, may prove disastrous if that estimate is wrong. Given that the MRSR vehicle will traverse over 1000 nautical miles during the aerobraking maneuver it is entirely conceivable that the density function encountered may vary as much as the 100 to 150% variation in density between morning and afternoon presented in Fig. 5 and Fig. 6. The density estimation technique must not only develop a profile of density versus altitude, but must continue to update this estimate throughout the trajectory based on the latest accelerometer-based density measurement. Two methods for performing this task are suggested here.

Hybrid Density Estimator

One possible approach is to model the atmosphere like Fitzgerald did[11]. During the entry phase accelerometer-derived density is recorded near each 1000 ft altitude interval along with the altitude for each density measurement. Then, during the exit phase, the predictor step uses these measurements to predict the velocity loss due to atmospheric drag. One difference between our approach and that of Fitzgerald is the inclusion of a density multiplier derived from accelerometer-generated density measurements which continue to update the density estimated throughout the trajectory.

The accelerometer-generated density measurements taken during the entry phase of the aerobraking maneuver are, quite likely, the best estimate of the atmospheric density function available for the exit phase of the trajectory. These measurements will be close, in both space and time, to the density for the remainder of the flight. They will indicate the general state of the atmosphere, that is whether the CO_2 is in a condensed or sublimated state, and they will provide an indication of the vertical wave structure of the atmosphere. They will not provide any information on horizontal waves which may affect density on the outbound leg. To compensate for this latter shortcoming, a density multiplier and a low pass filter like the one presented for the APC[9, 34] were used. However, instead of dividing derived density by the density predicted by an exponential function, the divisor is the density predicted from the measurements taken during the entry phase.

$$\rho_{\text{model}} = \rho_1 e^{-(h-h_1)/\text{hS}} \tag{3}$$

where ρ_1 is the density which was measured at the lower edge of the current altitude band, h_1 is the altitude at which this measurement was taken, and hS is the scale height for the atmosphere computed between this density measurement and the next measurement approximately 1000 ft higher.

$$\text{hS} = \left[\frac{\log(\rho_2/\rho_1)}{h_1 - h_2}\right]^{-1} \tag{4}$$

The density multiplier is then computed by dividing the accelerometer derived density by the density predicted for the current altitude, using the density model derived during entry. The result is filtered using a low pass filter to remove high frequency density deviations which would have minimal effect on the post-aerobraking apocenter.

$$K_\rho = (1-K)K_\rho + K(\rho_d/\rho_{\text{model}}) \tag{5}$$

To use this modified atmosphere in the predictor step, rewrite the expression relating rate of change of velocity and rate of change of altitude[48]:

$$\frac{dV_r}{V_r^2} = -C\rho_1 e^{-(h-h_1)/\text{hS}} \frac{dh}{\dot{h}}. \tag{6}$$

This equation may be integrated assuming a constant altitude rate to give the velocity loss due to atmospheric drag between two arbitrary altitudes h_1 and h_2.

$$V_{r2} = \left[1/V_{r1} - ((C\rho_1\text{hS})/\dot{h})\,\{e^{-(h_2-h_1)/\text{hS}} - e^{-(h_1-h_1)/\text{hS}}\}\right]^{-1} \tag{7}$$

and, with the scale height as previously calculated

$$V_{r2} = \left[\frac{1}{V_{r1}} - \frac{C\rho_1 (h_1 - h_2)}{\dot{h}\log(\rho_2/\rho_1)}\left(\frac{\rho_2}{\rho_1} - 1\right)\right]^{-1} \quad (8)$$

This equation gives the relative velocity at h_2 as a function of the relative velocity at h_1 and the densities and altitudes at the two locations. The method for employing this feature in the predictor step of the control algorithm is to first use the velocity, density and altitude at the current satellite location as the subscript 1 variables and to predict the velocity at the next interval where density measurements were stored during the entry using that altitude and that density multiplied by the density multiplier discussed earlier as the subscript 2 variables. Then that velocity may be used to compute the velocity at the next altitude band using the lower stored density and altitude values as subscript 1 variables and the next higher density and altitude measurements as subscript 2 variables. Notice that the density multiplier, when multiplied by each of the stored density measurements, will cancel in all but one location.

$$V_{r2} = \left[\frac{1}{V_{r1}} - \frac{CK_\rho \rho_1 (h_1 - h_2)}{\dot{h}\log(\rho_2/\rho_1)}\left(\frac{\rho_2}{\rho_1} - 1\right)\right]^{-1} \quad (9)$$

This procedure is repeated until the exit relative velocity is computed. The velocity change expected between the current location and atmospheric exit may be calculated by subtracting the current relative velocity from the predicted exit relative velocity.

$$\Delta V = V_{rx} - V_r \quad (10)$$

Polynomial Density Estimator

The second method of density estimation curve fits a sixth order polynomial in altitude to the normalized density function. This technique uses accelerometer derived density measurements at three trajectory locations to define a two phase exponential function. Derived density is recorded at one second intervals and then normalized by the exponential function in an effort to remove the underlying predominant exponential component. As the satellite reaches the bottom of the trajectory a batch estimate[42] is used to perform a weighted least squares fit of the polynomial coefficients to the resulting normalized function. After that, a sequential estimate[42] is used to continue updating the coefficients of the polynomial for the remainder of the trajectory.

Based on MARS-GRAM[35] generated data a two phase exponential function was chosen to normalize the density data. The underlying exponential component is assumed to be two exponential functions divided at 250,000 ft altitude such that the normalizing expression $\hat{\rho}$ is

$$\hat{\rho}(h) = \begin{bmatrix} \rho_I e^{-(h-250000)/hS2} \Big| (h > 250,000\text{ft}) \\ \rho_I e^{-(h-250000)/hS1} \Big| (h < 250,000\text{ft}) \end{bmatrix}. \quad (11)$$

$hS1$ and $hS2$ are the scale heights below and above 250,000 ft. ρ_I is the density at 250,000 ft, determined using accelerometer derived density which is filtered using a low pass filter like the one presented in Eq. (5). The scale height $hS1$ is found by using the filtered density measurement when the vehicle's altitude rate first becomes positive and that at 250,000 ft in Eq. (4). similarly, $hS2$ is found using the measured density at 400,000 ft and the measured filtered value from 250,000 ft. The density value chosen at 400,000 ft is not the filtered version because at this early point in the trajectory the density filter has not had sufficient data to converge to a reliable estimate.

After the altitude rate first becomes positive and the constants of Eq. (11) have been determined, the density values which were saved at one second intervals during the descent into the atmosphere may be normalized. The resulting data is fit with a sixth order polynomial in normalized altitude using a weighted least squares (batch) criterion to select the coefficients for the polynomial. A ninth order polynomial was originally chosen because the Viking 1 and Viking 2 atmospheric descent data (Fig. 7 and Fig. 8) shows six and five major density extremes respectively in the aerobraking region and the Viking 1 data shows four additional local extremes. These data suggest that at least a seventh order polynomial is required to model even the major extremes accurately. Because computational requirements for the density filter increase approximately as the square of the order of the polynomial, it was desired to use as low order polynomial as practical. After several iterations a ninth order polynomial appeared to be numerically ill-conditioned. A sixth order polynomial behaved much more consistently and was adequate for modeling the expected density function. The density function is approximated by

$$\rho(h) \approx \hat{\rho}(h)\,[c_1 + c_2 x + c_3 x^2 + c_4 x^3 + c_5 x^4 + c_6 x^5 + c_7 x^6] \tag{12}$$

where x is normalized altitude, $x = \frac{h}{h_e}$.

The coefficients c_1 through c_7 are initially determined by a weighted least squares batch estimate presented by Junkins[42]. The procedure is to begin with the batch of m normalized density measurements

$$\tilde{y}_j = \frac{\rho_j}{\hat{\rho}_j(h)} \tag{13}$$

taken at the m known altitude locations (h_j) at m one second intervals until the altitude rate becomes positive. The altitudes are normalized by the atmospheric interface altitude to determine the x_is. The batch estimator must select the coefficients c_1 through c_7 so that

$$\tilde{y}_j = c_1 + c_2 x_j + c_3 x_j^2 + c_4 x_j^3 + c_5 x_j^4 + c_6 x_j^5 + c_7 x_j^6 + e_j \tag{14}$$

where e_j is the residual errors after selection of the coefficients. This equation may be written in matrix form

$$\tilde{Y} = A\hat{C} + \tilde{E} \tag{15}$$

where $\hat{C}$ is the estimate of the coefficients c_1 through c_7 and A is the matrix

$$A = \begin{bmatrix} 1 & x_1 & x_1^2 & x_1^3 & x_1^4 & x_1^5 & x_1^6 \\ 1 & x_2 & x_2^2 & x_2^3 & x_2^4 & x_2^5 & x_2^6 \\ \vdots & \vdots & \vdots & \vdots & \vdots & \vdots & \vdots \\ 1 & x_m & x_m^2 & x_m^3 & x_m^4 & x_m^5 & x_m^6 \end{bmatrix}. \tag{16}$$

The batch estimator is tasked with selecting $\hat{C}$ to minimize the weighted quadratic function of residual errors

$$\varphi = \tilde{E}^T \overline{W} \tilde{E} \tag{17}$$

where the weighting matrix selected is a diagonal matrix of weights applied to the residual error of each measurement.

$$\overline{W} = \begin{bmatrix} w_1 & 0 & 0 \\ 0 & w_2 & 0 \\ & & \ddots & \\ 0 & 0 & w_m \end{bmatrix} \tag{18}$$

Because the vehicle is traveling into a region of higher density which has greater impact on the satellite trajectory than does the thinner atmosphere near entry and exit and because more recent data were deemed to be more representative of future density than was older data, the weights were chosen to increase with time. An exponentially increasing weighting function was chosen which doubled the weighting after 1000 seconds. This weighting function was selected through experimentation which showed that a slower increasing weighting function did not respond quickly enough to abrupt density shears to produce adequate controller performance, while weighting functions that increased faster tended to ignore data gathered early in the trajectory and produced a poor estimate of density in the upper altitude regions. This poor estimate had a distinctly negative impact on controller performance. The weights selected were

$$w_i = e^{6.9314\times10^{-4} t_i}. \tag{19}$$

Equation (15) is solved for E and the result substituted into Eq. (17). After some manipulation ϕ is expressed

$$\varphi = \tilde{Y}^T \overline{W} \tilde{Y} - 2\tilde{Y}^T \overline{W} A \hat{C} + \hat{C}^T A^T \overline{W} A \hat{C}. \tag{20}$$

To minimize ϕ it is necessary that

$$\nabla_{\hat{C}} \varphi = -2A^T \overline{W} \tilde{Y} + 2A^T \overline{W} A \hat{C} = 0. \tag{21}$$

This equation is solved to obtain the weighted least squares normal equation for $\hat{C}$

$$\hat{C} = (A^{\mathrm{T}} \overline{W} A)^{-1} A^{\mathrm{T}} \overline{W} \tilde{Y}. \tag{22}$$

After the satellite altitude rate becomes positive the estimator switches to a linear sequential estimator[42]. To facilitate this switch, the covariance matrix P is recorded from the batch estimate

$$P_k = (A_k^T \overline{W}_k A_k)^{-1}. \tag{23}$$

where for the first sequential estimation step the k subscripts are simply the matrix values from the batch estimate. For subsequent steps the k subscripts will indicate values from the previous step while k+1 will indicate updated values. A linear Kalman filter is then employed to update the estimates of $\hat{C}$. As new density measurements are made available at one second intervals the estimate of $\hat{C}$ is updated using

$$\hat{C}_{k+1} = \hat{C}_k + P_k A_{k+1}^T (\overline{W}_{k+1}^{-1} + A_{k+1} P_k A_{k+1}^T)^{-1} \{\tilde{Y}_{k+1} - A_{k+1} \hat{C}_k\}. \tag{24}$$

For the sequential estimator W is just the scalar value of w_i calculated using Eq. (19). A is only the new row of the A matrix shown in Eq. (16) calculated using the current value of h. Y is the current normalized density measurement. To prepare for the next iteration the covariance matrix is updated using

$$P_{k+1} = P_k - P_k A_{k+1}^T (\overline{W}_{k+1}^{-1} + A_{k+1} P_k A_{k+1}^T)^{-1} A_{k+1} P_k . \tag{25}$$

This process of updating the polynomials of the density estimate and then updating the covariance matrix in preparation for the next step is repeated at one second intervals until atmospheric exit. With the density estimate now in place, an estimate of the velocity loss to occur in the exit phase due to aerodynamic drag may be computed by integrating the drag equation. Begin by writing the drag equation.

$$\frac{dV_r}{dt} = -\frac{1}{2}\rho V_r^2 \frac{SC_D}{m} = -\frac{\rho V_r^2}{2M_D} \tag{26}$$

where M_D is the vehicle ballistic coefficient

$$M_D = \frac{m}{C_D S}. \tag{27}$$

Replace dt with $\frac{dh}{\dot{h}}$ in Eq. (26) and substitute the expression given in Eq. (12) for ρ and rearrange terms to obtain

$$\frac{dV_r}{V_r^2} = -\frac{0.5\hat{\rho}(h)}{M_D \dot{h}} (c_1 + c_2 x + c_3 x^2 + \ldots + c_7 x^6)\, dh. \tag{28}$$

Since $x = h/h_e$, if $\dot{h}$ is a function of h, this expression can be integrated analytically between any two altitudes to determine the change in velocity due to aerodynamic drag. Again, as was done in the APC algorithm and in Eq. (7), $\dot{h}$ is chosen to be a constant. If h is less than 250,000 ft, $\hat{\rho}$ has a discontinuity at $h_1 = 250,000$ ft; so, the integration must be performed in two steps, one from the current altitude to 250,000 ft and a second from 250,000 to the exit altitude. If we change the variable of integration from h to x, we get

$$-\frac{1}{V_r}\bigg|_{x_i}^{1} = -\frac{0.5\rho_1}{M_D \dot{h}} \left[\left(\int_{x_i}^{x_1} e^{-(x - x_1)\left[\frac{h_e}{hS1}\right]} (c_1 + c_2 x + c_3 x^2 + \ldots + c_7 x^6)\, dx \right) \right. \tag{29}$$

$$+\left(\int_{x_1}^{1} e^{-(x-x_1)\left[\frac{h_e}{hS2}\right]}(c_1+c_2x+c_3x^2+\ldots+c_7x^6)\,dx\right)\Bigg]$$

where $x_1 = h_1/h_e$ and the current altitude is expressed $x_i = h/h_e$. When h is greater than 250,000 ft this integration may be carried out in a single integration step.

$$-\frac{1}{V_r}\Bigg|_x^1 = -\frac{0.5\rho_1}{M_D\dot{h}}\left[\int_{x_i}^{1} e^{-(x-x_1)\left[\frac{h_e}{hS2}\right]}(c_1+c_2x+c_3x^2+\ldots+c_7x^6)\,dx\right] \quad (30)$$

To obtain density from this expression, integration by parts is carried out repeatedly to obtain

$$\int_a^b \rho dx = -\rho_1 e^{-(x-x_1)\frac{h_e}{hS}}\left[\left[\frac{hS}{h_e}\right]u+\left[\frac{hS}{h_e}\right]^2 u'+\left[\frac{hS}{h_e}\right]^3 u''+\ldots+\left[\frac{hS}{h_e}\right]^7\frac{d^6u}{dx^6}\right]\Bigg|_a^b \quad (31)$$

where

$$u = c_1+c_2x+c_3x^2+c_4x^3+c_5x^4+c_6x^5+c_7x^6 \quad (32)$$

and the primes indicate a derivative with respect to x so that

$$u' = c_2+2c_3x+3c_4x^2+4c_5x^3+5c_6x^4+6c_7x^5 \quad (33)$$

$$u'' = 2c_3+6c_4x+12c_5x^2+20c_6x^3+30c_7x^4 \quad (34)$$

This process is continued until all six of the required derivatives are formed using the values of c which were most recently estimated. u and all six of its derivatives are calculated for the current altitude, and the atmospheric exit altitude. Additionally, u and the six derivatives must be calculated at 250,000 ft altitude if the current altitude is below 250,000 ft. These values are inserted into Eq. (31), which is in turn inserted into Eq. (29) or (30) as required. The predicted velocity loss due to aerodynamic drag is then found by solving Eq. (29) or (30) for the predicted exit relative velocity and then subtracting the current relative velocity

$$\Delta V = V_{rx} - V_r. \tag{35}$$

If the current altitude is below 250,000 ft

$$V_{rx} = \left[\frac{1}{V_r} + \frac{0.5\rho_1}{M_D\dot{h}}\left(e^{-(x-x_1)\frac{h_e}{hS1}}\left[\frac{hS1}{h_e}u + \left[\frac{hS1}{h_e}\right]^2 u' + \ldots + \left[\frac{hS1}{h_e}\right]^7 \frac{d^6u}{dx^6}\right]\right)\Bigg|_{x_i}^{x_1}\right. \tag{36}$$

$$\left. + \frac{0.5\rho_1}{M_D\dot{h}}\left(e^{-(x-x_1)\frac{h_e}{hS2}}\left[\frac{hS2}{h_e}u + \left[\frac{hS2}{h_e}\right]^2 u' + \ldots + \left[\frac{hS2}{h_e}\right]^7 \frac{d^6u}{dx^6}\right]\right)\Bigg|_{x_1}^{1}\right]^{-1},$$

or if the current altitude is above 250,000 ft

$$V_{rx} = \left[\frac{1}{V_r} + \frac{0.5\rho_1}{M_D\dot{h}}\left(e^{-(x-x_1)\frac{h_e}{hS2}}\left[\frac{hS2}{h_e}u + \left[\frac{hS2}{h_e}\right]^2 u' + \ldots + \left[\frac{hS2}{h_e}\right]^7 \frac{d^6u}{dx^6}\right]\right)\Bigg|_{x_i}^{1}\right]^{-1}. \tag{37}$$

Improved Exit Phase

This improved exit phase, first published by the Charles Stark Draper Laboratory[43,44], is a simplified method of calculating the required altitude rate $\dot{h}$ for the APC controller. It is intended to replace the exit phase for the APC algorithm with a simpler calculation. To begin the development, the velocity loss due to aerodynamic drag is calculated starting with the differential equation for drag:

$$\frac{dV}{dt} = -\frac{\bar{q}}{M_D} \tag{38}$$

Rearrange terms in Eq. (38) to obtain

$$dV = -\frac{\bar{q}}{M_D}dt. \tag{39}$$

Replace dt with $\frac{dh}{d\dot{h}}$ and expand $\bar{q}$.

$$\frac{dV}{V^2} = -\frac{0.5\rho}{M_D\dot{h}}dh \tag{40}$$

With the assumptions of a constant altitude rate and an exponential atmosphere of known scale height the above equation may be integrated analytically to obtain the change in velocity ΔV which will occur due to aerodynamic drag. This result is slightly different from the original APC exit phase derivation which uses this equation to predict the velocity at exit instead of computing the change in velocity which will occur due to drag. The preferred form for the drag equation is

$$\Delta V = -1/\left(\frac{\dot{h}_{des}M_D}{hS\bar{q}} + \frac{1}{V_R}\right). \tag{41}$$

To use the hybrid density estimator replace the expression for ΔV given in Eq. (41) with the expression given in Eq. (10). Likewise, to use the polynomial density estimator replace the results of Eq. (41) with those of Eq. (35).

The desired velocity for a vehicle in a purely Keplerian (no aerodynamic forces) orbit at the current radius with the desired altitude rate $\dot{h}$ to attain the targeted apocenter radius may be computed

$$V_{des} = \sqrt{\frac{2\mu R_{target}}{R(R+R_{target})} - \frac{\dot{h}_{des}^2}{\left(\frac{R_{target}}{R}\right)^2 - 1}} \tag{42}$$

The first term under the radical is the velocity at pericenter for an elliptical orbit with pericenter radius R and apocenter at R_{target}

$$V_{per} = \sqrt{\frac{2\mu R_{target}}{R(R+R_{target})}}. \tag{43}$$

A new variable $\dot{r}_{factor}$ was introduced

$$\dot{r}_{factor} = -\frac{0.5}{V_{per}\left(\left(\frac{R_{target}}{R}\right)^2 - 1\right)} \tag{44}$$

Therefore V_{des} may be written

$$V_{des} = V_{per}\sqrt{1 + 2\left(\frac{\dot{r}_{factor}}{V_{per}}\right)\dot{r}_{des}^2}. \tag{45}$$

To avoid the square root in Eq. (45) a small term is added under the radical to complete the square

$$V_{des} \approx V_{per}\sqrt{1 + 2\left(\frac{\dot{r}_{factor}}{V_{per}}\right)\dot{r}_{des}^2 + \left[\left(\frac{\dot{r}_{factor}}{V_{per}}\right)\dot{r}_{des}^2\right]^2}. \tag{46}$$

V_{des} may now be approximated

$$V_{des} \approx V_{per}\left(1 + \left(\frac{\dot{r}_{factor}}{V_{per}}\right)\dot{r}_{des}^2\right) + O(\varepsilon^2) = V_{per} + \dot{r}_{factor}\dot{r}_{des}^2 + O(\varepsilon^2) \tag{47}$$

The corrector step to update altitude rate is a single step Newton iteration. The difference between the current inertial velocity minus the velocity loss expected from aerodynamic drag and the desired velocity computed above is called the velocity miss or V_{miss}.

$$V_{miss} = (V_I - \Delta V) - (V_{per} + \dot{r}_{factor}\dot{r}_{des}^2) \tag{48}$$

The negative of V_{miss} is then divided by $\frac{dV_{miss}}{d\dot{h}_{des}}$ to produce an update for $\dot{h}_{des}$.

$$\dot{h}_{des\,update} = \dot{h}_{des} + \frac{(V_{per} + \dot{r}_{factor}\dot{r}^2_{des}) - (V_I - \Delta V)}{\frac{M_D \Delta V^2}{hs\bar{q}} - 2\dot{r}_{factor}\dot{r}_{des}}. \tag{49}$$

Equilibrium Glide to Exit Phase Transition Velocity

To minimize total ΔV required to transition from the intermediate orbit to the desired orbit it is sufficient to minimize the exit flight path angle provided the vehicle exits in the desired orbit plane and the apocenter of the intermediate orbit equals the desired apocenter. This approach will maximize the pericenter of the post-aero braking orbit. If the controller is able to properly target the apocenter altitude, then minimizing γ_x will produce a maximum exit velocity, a maximum pericenter for the intermediate orbit and a minimum ΔV. Fig. 11 shows how selecting a higher transition velocity for the APC controller to switch to the exit phase control algorithm will tend to minimize γ_x and the ΔV required to attain the desired final orbit provided the vehicle can properly target the desired apocenter. When the transition velocity is increased the predictor/corrector step will calculate a lower $\dot{h}$ to target the desired apocenter. The drawback to minimizing γ_x by increasing the transition velocity and using a shallower flight path for the exit phase is that by doing so the exit phase will be flown using a higher percentage of the available lift to follow the desired trajectory. In the limit the minimum ΔV path flies the entire exit trajectory with a bank angle of 180°. When the transition velocity becomes too great the vehicle can no longer maintain the required shallow flight path, even in a relatively smooth atmosphere, and may overshoot the desired apocenter altitude, as seen in Fig. 12. Following this type of shallow flight path angle trajectory severely limits the robustness to density dispersions. If in the initial phases of the exit phase, the control system calculates a shallow exit trajectory, one which requires almost full lift down to maintain, any decrease in atmospheric density from that modeled in the predictor step will result in less control authority and an inability to fly the shallow tra-

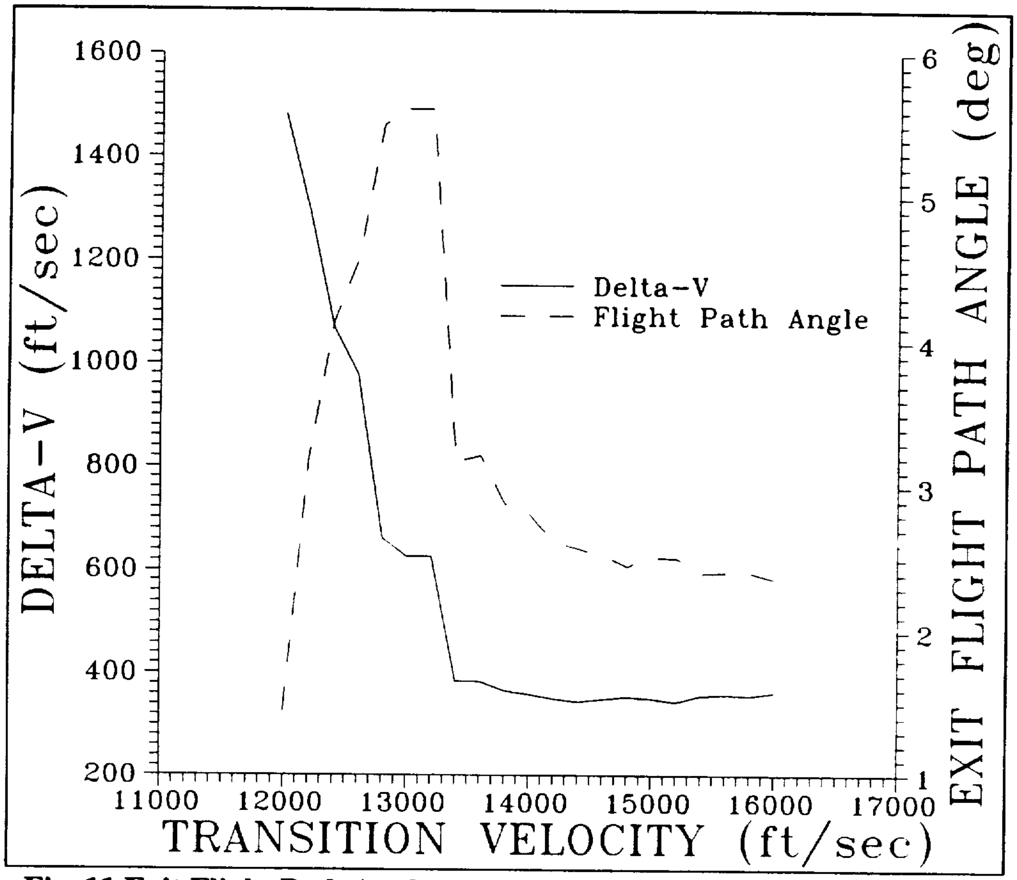

Fig. 11 Exit Flight Path Angle and ΔV Required vs. Transition Velocity

jectory, less velocity loss than predicted resulting in a faster exit speed than desired and a post-aerobraking apocenter higher than desired. An increase in ΔV results. On the other hand, transitioning to the exit phase at a velocity which is too slow guarantees an increase in ΔV by requiring a steep $\dot{h}$ to target apocenter which produces large exit flight path angles. The best trajectory is one which strikes a desirable balance between minimizing ΔV while retaining enough control to be robust under the influence of off-nominal density variations. It would seem to be a simple matter to pick a transition velocity which produces the desired balance, but the "correct" transition velocity varies with the state of the atmosphere, the initial conditions, and the vehicle configuration.

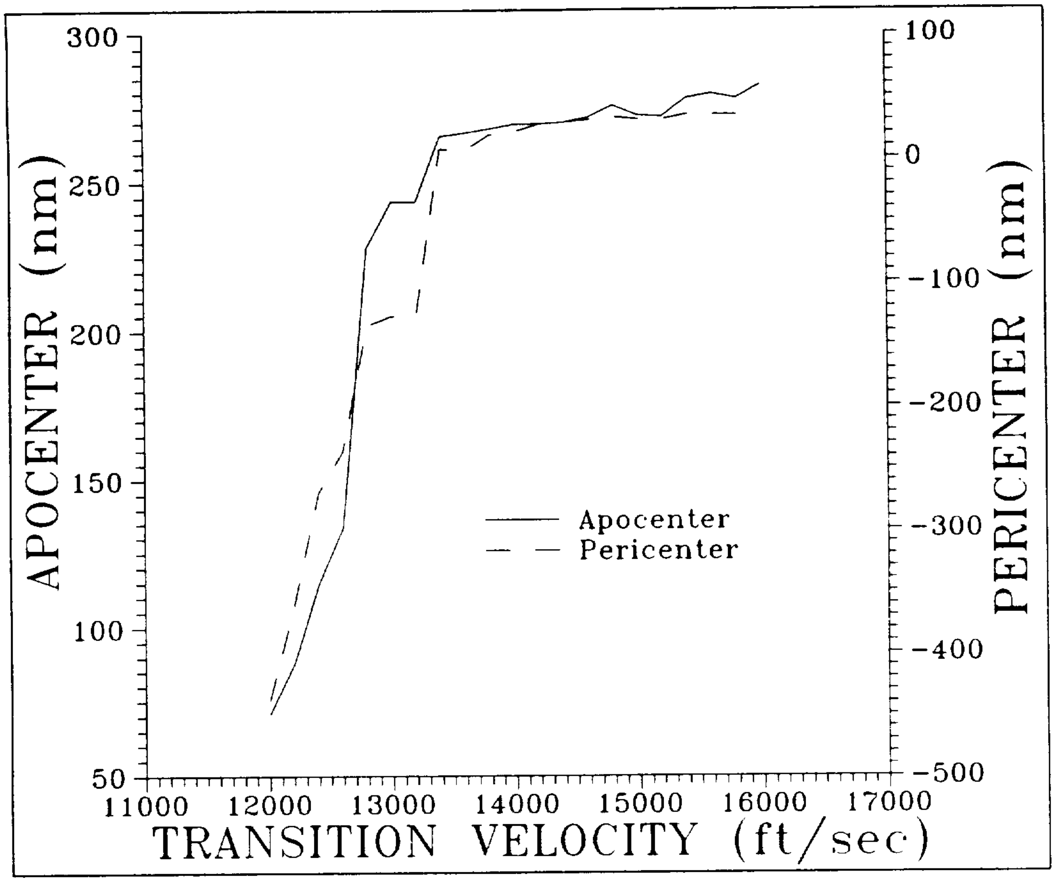

Fig. 12 Apocenter and Pericenter Altitudes vs. Transition Velocity

The two most important parameters used to select an appropriate transition velocity are the drag coefficient of the vehicle and the atmosphere yet to be traversed. These two parameters and $\dot{h}$ define the velocity loss that will occur. After considerable testing a desired altitude rate, $\dot{h}_c$, of 450 ft/sec was found to yield a good trade off between minimizing ΔV and producing robustness. The simulations depicted in Fig. 11 and Fig. 12 require a transition velocity of 14,922 ft/sec to produce an exit phase altitude rate of 450 ft/sec. As seen in Fig. 11, this transition velocity (and hence this altitude rate) are slightly removed from the region where exit flight path angle and ΔV increase dramatically. Yet this altitude rate was still steep enough to provide a measure of robustness against density variations. Armed with this choice for altitude rate, a better way to calculate transition velocity may be formulated.

The desired velocity V_{des} for a vehicle in a purely Keplerian (no aerodynamic forces) orbit at the current radius with the desired altitude rate $\dot{h}$ to attain the targeted apocenter radius was computed in Eq. (47). By adding the velocity loss expected due to aerodynamic drag the current velocity required to target the desired apocenter altitude by following a 450 ft/sec path may be computed. The chosen method of density estimation may be used to compute the velocity loss due to aerodynamic drag, by inserting the desired 450 ft/sec altitude rate into the appropriate derivation. Equation (10) is used if the hybrid density estimator is the selected method of density estimation, whereas, Eq. (35) is used for the polynomial density estimator or Eq. (41) for the simple estimate of a constant scale height exponential atmosphere. One additional term is added to allow for the velocity loss between initiation of the exit phase and achievement of the desired altitude rate. The appropriate velocity to transition from the equilibrium glide phase to the exit phase may now be expressed

$$V_{trig\,I} = V_{des} + \Delta V_{(drag)} + \dot{V}\delta t \tag{50}$$

δt in this equation is the time required from initiation of the exit phase until the desired altitude rate is attained. The vehicle modeled in this study has a limit of 5°/sec^2 on roll acceleration and 20°/sec on roll rate. A value of 20 seconds was selected for δt because with these current limits on roll rate and roll acceleration the vehicle requires thirteen seconds to perform a 180° rest to rest maneuver. After rolling to the lift up configuration there is still an additional delay of five to ten seconds before the vehicle's altitude rate matches the desired value. With δt set to 20 seconds the transition velocity calculation performed extremely well. The methodology for employing a variable transition velocity is to compute $V_{\mathrm{trig}\,I}$ using eq. (50). When the inertial velocity decreases below the calculated $V_{trig\,I}$ the controller initiates the exit phase.

CHAPTER III

LYAPUNOV CONTROLLERS

Lee and Grantham present a Lyapunov Steepest Descent controller[7] which is robust to at least some atmospheric perturbations. Their controller is for a vehicle which modulates angle of attack while the MRSR vehicle under study flies at a constant angle of attack and varies the bank angle to control the trajectory. A similar controller is developed to control the MRSR vehicle. A desired target state is defined for the vehicle at atmospheric exit which will minimize the ΔV required to transition to the desired final orbit. A positive definite Lyapunov function is defined such that the vehicle's state is at the target when the Lyapunov function is zero. The control variable is then selected so that the Lyapunov function is driven, in a steepest descent fashion, toward the origin. When this method failed to be as robust as hoped, a new Lyapunov Tracking controller was developed.

The Lyapunov Tracking controller permits the introduction of a preferred path leading the vehicle to an exit state which gives an acceptable ΔV to transition to the desired final orbit. In the particular case studied here, the preferred path is recomputed for each trajectory based on accelerometer data fed back to the controller early in the flight and a "best guess" of the density function for the remainder of the trajectory. Again, a positive definite Lyapunov function is defined such that, if the vehicle is on the preferred path, the Lyapunov function is zero. The control variable is again selected in a "Lyapunov Optimal" fashion to drive the Lyapunov function toward the origin as quickly as possible. A gain scheduling scheme defines an optimal descent function for each phase of the trajectory. Finally, because of high trajectory loads generated by this control scheme and difficulty in acquiring the desired path, this Lyapunov tracking controller was employed only during the exit phase following the modified equilibrium glide[9, 34] phase of the MPC controller presented in Chapter 2. The equilibrium glide phase was developed to minimize trajectory loads and is very good at doing just that. With the modifications suggested in Chapter 2 the equilibrium glide phase control algorithm is very robust to perturbations in atmospheric density. The transition velocity from the equilibrium glide phase to this exit phase is chosen using the methods presented in Chapter 2 so the trajectory is at the base of the preferred path when transition occurs. The Lyapunov Tracking exit phase then follows the computed path to exit the atmosphere with exit state very near the minimum ΔV exit state.

Lyapunov Steepest Descent Controller

Equations of Motion

Derivation of the Lyapunov Steepest Descent control algorithm begins with the equations of motion for planar flight

$$\frac{dr}{dt} = \frac{dh}{dt} = V\sin\gamma \tag{51}$$

$$\frac{dV}{dt} = \frac{-C_D \rho S V_r^2}{2m} - \frac{\mu}{r^2}\sin\gamma \tag{52}$$

$$\frac{d\gamma}{dt} = \frac{-C_L \rho S V_r^2}{2mV}\cos\Phi - \left(\frac{\mu}{Vr^2} - \frac{V}{r}\right)\cos\gamma \tag{53}$$

Eq. (51) is simply the radial velocity in terms of the inertial velocity and flight path angle. Eq. (52) gives the time rate of change in velocity composed of two parts: 1) the velocity loss due to aerodynamic drag and 2) the change in velocity due to gravitational acceleration, often referred to as the inertial component. Similarly, Eq. (53) is the time rate of change in the flight path angle, also composed of two parts: 1) the change in flight path angle due to the component of aerodynamic lift in the vertical plane and 2) the change in flight path angle due to gravitational acceleration (the inertial component). The control variable Φ, the bank angle, determines the amount of lift exerted in the vertical plane to bend the trajectory and change the flight path angle.

Nondimensional State Variables

Dimensionless state variables are introduced:

$$\bar{x} = \begin{bmatrix} x_1 \\ x_2 \\ x_3 \end{bmatrix} = \begin{bmatrix} h/h_e \\ V/(\sqrt{\mu/R}) \\ \gamma \end{bmatrix} \tag{54}$$

along with a dimensionless time variable τ

$$\tau = (t/h_e)\sqrt{\mu/R}. \tag{55}$$

The equations of motion may now be written:

$$\dot{x}_1 = x_2 \sin x_3 \tag{56}$$

$$\dot{x}_2 = -B\sigma x_{2_r}^2 - \frac{c}{(c-1+x_1)^2}\sin x_3 \tag{57}$$

$$\dot{x}_3 = \frac{A\sigma x_{2_r}^2}{x_2}\cos\Phi + \frac{\cos x_3}{c-1+x_1}\left[x_2 - \frac{c}{(c-1+x_1)x_2}\right] \tag{58}$$

where $\sigma = \rho/\rho_0 = exp\,[(-(h-h_0))/hS]$, $A = (\rho_0 S h_e C_L)/(2m)$, $B = (\rho_0 S h_e C_D)/(2m)$ and $c = R/h_e$. It has been found that a good approximation is to assume that the relative and inertial velocity differ by a constant, so that

$$V_r = V - \delta V \tag{59}$$

and similarly

$$x_{2_r} = x_2 - \delta x_2. \tag{60}$$

For this controller it is more convenient to replace $\cos\Phi$ in Eq. (58) with the control variable u where $u = \cos\Phi$ and is thus bounded between ± 1. Eq. (58) is therefore replaced with

$$\dot{x}_3 = \frac{A\sigma x_{2_r}^2 u}{x_2} + \frac{\cos x_3}{c - 1 + x_1}\left[x_2 - \frac{c}{(c - 1 + x_1)x_2}\right]. \tag{61}$$

Target State

The minimum ΔV aerobraking maneuver is one which exits the atmosphere on a trajectory with the correct apocenter altitude and a maximum vacuum pericenter altitude. This goal is attained by exiting the atmosphere with the minimum possible flight path angle and the correct velocity to attain the desired apocenter. The goal, therefore, is to guide the vehicle along an aerobraking trajectory which reaches the atmospheric interface altitude with the correct velocity to attain the desired apocenter altitude while maintaining a minimum positive flight path angle at exit. The flight path angle must remain positive for the vehicle to exit the atmosphere. This design objective is established by setting the targeted flight path angle at atmospheric exit to zero and establishing a target exit velocity. The target state may be presented in non-dimensional form as[7]

$$\hat{x} = \begin{bmatrix} 1 \\ \hat{x}_2 \\ 0 \end{bmatrix}. \tag{62}$$

The target exit velocity, and hence $\hat{x}_2$ may be derived assuming a Keplerian orbit from atmospheric exit to apocenter. This desired exit velocity is a function of the exit flight path angle, and several constants for the problem including the atmospheric interface radius (R) and target apocenter radius (r_a). The desired exit velocity is

$$\hat{x}_2 = \sqrt{\left(\left(2\frac{r_a}{R}\left[1 - \frac{r_a}{R}\right]\right) / \left((\cos x_{3x})^2 - \left(\frac{r_a}{R}\right)^2 \right) \right)}. \tag{63}$$

Descent Function

A function is a descent function if, and only if, it is a positive definite differentiable function. That is:[45]

$$W(x) > 0 \text{ for all } x \neq \hat{x} \tag{64}$$

$$W(\hat{x}) = 0 \tag{65}$$

$$\frac{\partial W(x)}{\partial x} \neq 0 \text{ for all } x \neq \hat{x} \tag{66}$$

Any candidate Lyapunov function may be chosen as the descent function $W[x(t)]$. However, the most logical choice, and the one recommended by Lee and Grantham[7], is a weighted quadratic measure of distance to the target. This function is expressed

$$W(x) = \begin{bmatrix} x_1 - 1 & x_2 - \hat{x}_2 & x_3 \end{bmatrix} \begin{bmatrix} p_{11} & 0 & p_{12} \\ 0 & 1 & 0 \\ p_{12} & 0 & p_{22} \end{bmatrix} \begin{bmatrix} x_1 - 1 \\ x_2 - \hat{x}_2 \\ x_3 \end{bmatrix} \tag{67}$$

where the constant weighting terms p_{xx} are chosen to define a preferred direction toward the target in the x_1 - x_3 state space. The preferred direction for the states is presented in Fig. 13. An ellipsoid is chosen, oriented so that, while the vehicle is deep in the atmosphere, the preferred direction (opposite the descent function gradient) in the x_1 - x_3 state space gives positive lift to climb out of the atmosphere, but as the vehicle approaches atmospheric exit the preferred direction uses negative lift to minimize the exit flight path angle. The weights must be scaled so the velocity reaches the target velocity as the vehicle

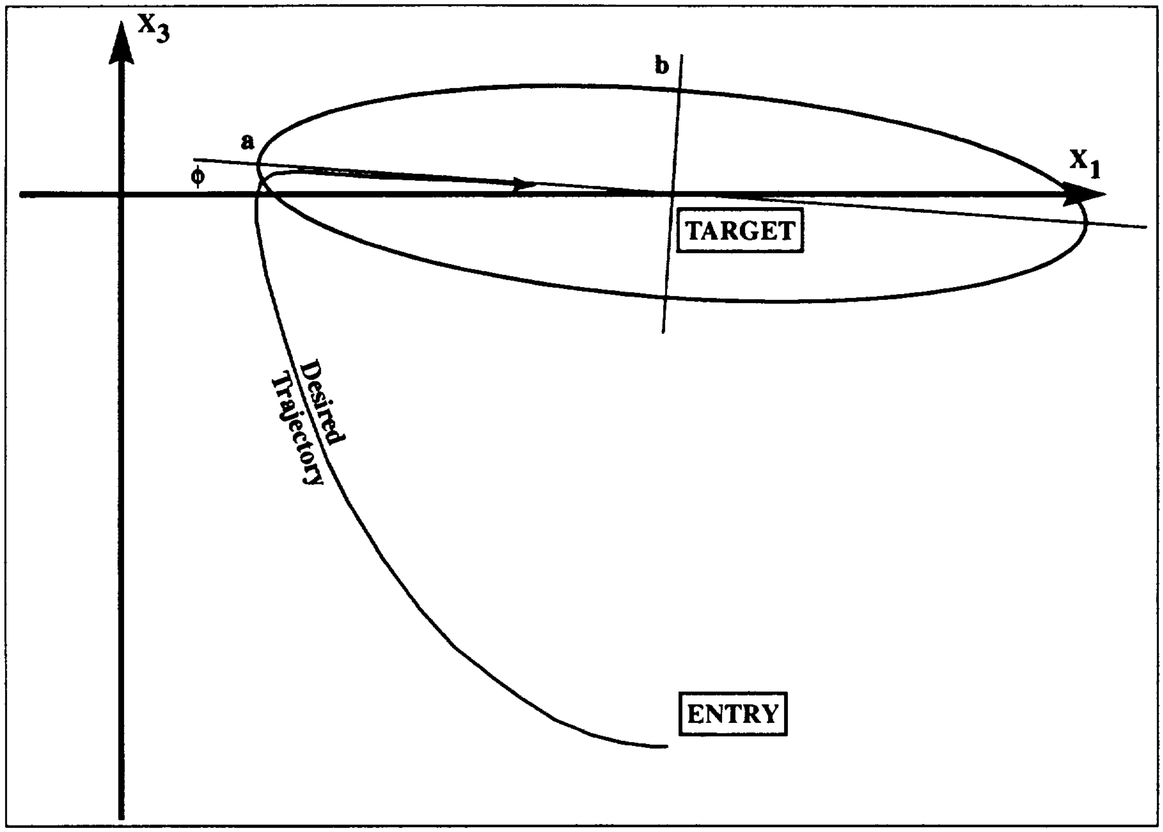

Fig. 13 Preferred x_1 - x_3 Direction of Motion
(Adapted from Reference 7)

reaches the atmospheric interface altitude. For the elliptical descent function shown in Fig. 13, p_{xx} may be calculated as follows[7].

$$p_{11} = a^2 sin^2\phi + b^2 cos^2\phi \tag{68}$$

$$p_{12} = \sin\phi\cos\phi\,(a^2 - b^2) \tag{69}$$

$$p_{22} = b^2\sin^2\phi + a^2\cos^2\phi \tag{70}$$

The angle between the gradient of the descent function and the state space velocity vector $f(x, u)$ is expressed

$$H(x, u) = \frac{(\partial W(x))/(\partial x)}{\|(\partial W(x))/(\partial x)\|}\frac{f(x, u)}{\|f(x, u)\|} = \cos\beta \tag{71}$$

where β is the angle between the gradient of the descent function and $f(x, u)$.

Lyapunov Steepest Descent Optimal Control

For the control to be Lyapunov steepest descent optimal, $u^* (x)$ must make[7]

$$H [x, u^* (x)] \leq H [x, u (x)] \tag{72}$$

for all $u \in U$ where U is the allowable set of controls bounded by ± 1. Furthermore, for the control to be Lyapunov steepest descent optimal, $f [x, u^* (x)] \neq 0$. If it were possible to make $H [x, u^* (x)] < 0$ everywhere, then global stability with respect to the target could be guaranteed. Even if $H [x, u^* (x)] \leq 0$, asymptotic stability with respect to the target could be guaranteed. Unfortunately, with u bounded between ± 1 neither of these outcomes is always possible. Even so, $u^* (x)$ tries to move the system state variables as nearly opposite the gradient of the descent function as possible, given the dynamics of the system and the limits on the control.

To determine $u^* (x)$ set $\frac{\partial H}{\partial u} = 0$ and solve for u. If this value of u lies between ± 1, then $u^* (x)$ is either this value or ± 1, whichever minimizes H. If the value of u which solves $\frac{\partial H}{\partial u} = 0$ is not between ± 1, then $u^* (x)$ is selected from ± 1 to minimize H[47].

Performance Results

The Lyapunov Steepest Descent feedback control algorithm will guide the vehicle to very near the minimum ΔV exit state provided the p_{xx} weights, and hence, $W (x)$ is properly selected. Unfortunately, these p_{xx} weights must be readjusted to attain acceptable performance for each perturbed entry condition, vehicle lift and drag perturbation, or atmospheric density perturbation. No acceptable method, other than a manual search, was found to determine the appropriate weighting for each perturbed run. Clearly, this lack of asymptotic stability is not compatible with the objectives of this research.

An appropriate descent function is found for this controller to perform acceptably for the nominal case of a vehicle targeting a 270 nm circular orbit after entering the Martian standard atmosphere with 6.0 km/sec velocity relative to the planet, -12° entry flight path angle, and a lift to drag ratio of 1. The same vehicle and the same entry conditions are also simulated, assuming both a high and a low density Martian atmosphere. The ellipse which determines the descent function is chosen to have a semimajor axis of 1.65, a semiminor axis of 0.41, and a rotation angle ϕ of 4.2°, measured as shown in Fig. 13. A few perturbations from the nominal case are then simulated and the somewhat disastrous results are presented in Table 1 along with the optimal results for the same perturbations generated using the method of Appendix A.

This controller is simply not very robust, given density, navigation or vehicle perturbations expected for the Martian aerobraking problem. The controller may be fine tuned for one rate of energy depletion, but if anything alters the rate of energy loss the controller must be readjusted, by altering the relative weights between the states, to bring the velocity to the targeted velocity exactly as the vehicle passes through the atmospheric interface altitude. A steeper entry flight path angle thrusts the vehicle deeper into the atmosphere, thereby increasing the rate of energy loss. Likewise, an atmosphere which is more dense than expected, or a drag coefficient higher than expected, causes the vehicle to lose energy at a higher rate than planned. The resulting exit conditions are too slow and at too low an apocenter altitude. In the worst trajecories the vehicle fails to exit the atmosphere at all. Similarly, a shallower entry flight path angle, less dense atmosphere or lower drag coefficient results in less velocity loss than intended and apocenter altitudes higher than desired. To reduce the sensitivities to perturbations which change the rate of energy loss the Lyapunov controller is therefore reformulated as a tracking controller designed to follow a chosen path to atmospheric exit.

Table 1 Lyapunov Steepest Descent Controller Performance Results

Atmosphere Model	Entry γ (deg)	L/D	Apocenter Altitude (nm)	Pericenter Altitude (nm)	Delta-V (ft/sec)	Minimum Delta-V (ft/sec)
Nominal	-12.0	.99	279.86	30.22	345.86	325.
Low Density	-12.0	.99	295.80	31.73	363.28	331.
High Density	-12.0	.99	253.94	24.61	363.57	316.
Nominal	-11.5	.99	1416.49	34.33	1388.48	325.
Nominal	-11.75	.99	1005.64	34.89	1076.92	325.
Nominal	-12.25	.99	25.81	-906.00	2819.01	325.
Low Density	-11.5	.99	1882.06	30.70	1682.49	331.
Low Density	-12.25	.99	29.96	-467.00	1603.49	331.
High Density	-11.5	.99	1685.92	38.07	1558.47	316.
High Density	-12.25	.99	76.92	-80.50	783.42	316.
All Atmospheres	-12.5	.99	Failed to Exit Atmosphere			
Nominal	-12.0	1.31	2205.1	34.16	1849.33	324.
Low Density	-12.0	1.31	2329.21	30.95	1913.19	329.
High Density	-12.0	1.31	2584.82	37.94	2021.28	316.
All Atmospheres	All	.66	Failed to Exit Atmosphere			

Lyapunov Tracking Controller

To gain acceptable robustness for this controller, the methodology is changed from a steepest descent controller which targets the optimal terminal state to a steepest descent controller which targets a preferred path. That path then is selected to lead the vehicle to a desirable exit state with enough robustness to prevent minor density upsets from being catastrophic.

The Preferred Path

Derivation of this controller begins with definition of the preferred path. As with the predictor corrector algorithms a constant altitude rate path leading to the desired atmospheric exit state is selected. The difference between this Lyapunov Tracking Controller (LTC) and the predictor correctors is in how the controller computes the constant altitude rate path. The predictor corrector algorithms use various methods to select a constant altitude rate which will give the desired apocenter altitude and then use altitude rate error to select the appropriate bank angle. The LTC, on the other hand, assumes that it is desirable to always fly the same altitude rate to atmospheric exit and arrive there with the appropriate velocity to achieve the proper apocenter altitude. The LTC then chooses the in-plane portion of lift to approach the path in a steepest descent fashion. The altitude rate is selected to produce the desired trade-off between robustness to density perturbations while still minimizing the total ΔV required.

A constant altitude rate of 450 ft/sec is again selected (as on page 37) to define the desired path leading to atmospheric exit with the appropriate velocity to target the desired apocenter altitude. This altitude rate produces trajectories which require within 20 to 30 ft/sec of the minimum ΔV values for the various expected perturbations without short period density upsets, yet is still robust to density variations of ±50% over small altitude intervals. The equations used to derive the improved exit phase for the Mars Predictor Corrector are employed again here to define this path. The velocity required at a given altitude flying a specified altitude rate assuming a Keplerian orbit (no aerodynamic drag effects) was given in Eq. (47) but is repeated here for completeness.

$$V_{des} \approx V_{per}\left(1 + \left(\frac{\dot{r}_{factor}}{V_{per}}\right)\dot{r}_{des}^2\right) = V_{per} + \dot{r}_{factor}\dot{r}_{des}^2 \tag{73}$$

The velocity loss expected due to aerodynamic drag is added to this velocity to determine the current velocity for the desired path. Note that this desired velocity is a function of the dynamics of the Martian orbit, the current altitude, the selected altitude rate (450 ft/sec) and the expected velocity loss (which is a function of the expected atmospheric density function and the vehicle coefficient of drag). The velocity loss expected due to aerodynamic drag is calculated assuming the 450 ft/sec altitude rate path will be flown using Eq. (10) of the hybrid density estimator, or with Eq. (35) of the polynomial density estimator, or with Eq. (41) using the simplification of a constant scale height exponential atmosphere. The desired current velocity defining the preferred path is

$$\hat{V} = V_{des} + \Delta V. \tag{74}$$

This velocity may be converted to non-dimensional form

$$\hat{x}_2 = \hat{V}/(\sqrt{\mu/R}) \tag{75}$$

The desired flight path angle $\hat{x}_3$ is computed

$$\hat{x}_3 = \operatorname{asin}(\dot{h}_{des}/V). \tag{76}$$

Together, $\hat{x}_2$ and $\hat{x}_3$ define the preferred path which leads the vehicle along a robust corridor to a desirable exit state. Now, a Lyapunov function must be formulated and a control found which will drive the vehicle onto and then along the chosen path.

The Lyapunov Descent Function

The selected positive definite Lyapunov function is

$$W(x) = \begin{bmatrix} x_2 - \hat{x}_2 & x_3 - \hat{x}_3 \end{bmatrix} \begin{bmatrix} p_{11} & p_{12} \\ p_{12} & p_{22} \end{bmatrix} \begin{bmatrix} x_2 - \hat{x}_2 \\ x_3 - \hat{x}_3 \end{bmatrix}. \tag{77}$$

This function is analogous to distance from the target path and is zero whenever the vehicle is on the target path and positive otherwise. Again, the p_{xx} values are chosen to form an ellipsoid, the negative gradient of which defines the preferred approach to the target path. This ellipsoid is shown in Fig. 14. The p_{xx} values are computed from the semima-

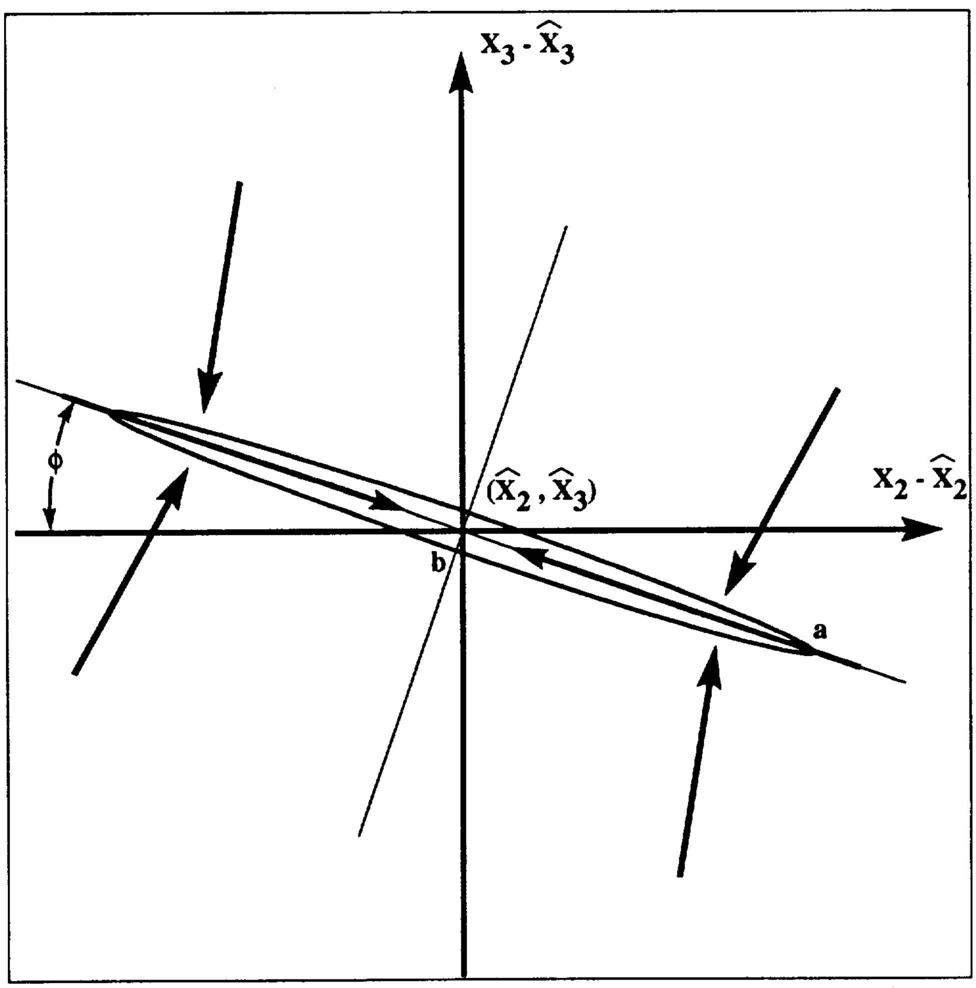

Fig. 14 Lyapunov Tracking Controller x_2 - x_3 Descent Function

jor axis a, the semiminor axis b, and the angle of rotation ϕ of the ellipse defining the preferred gradient[7] onto the chosen path as in Eqs. (68) through (70). They are repeated here for completeness

$$p_{11} = a^2 sin^2\phi + b^2 cos^2\phi \tag{78}$$

$$p_{12} = sin\phi cos\phi (a^2 - b^2) \tag{79}$$

$$p_{22} = b^2 sin^2\phi + a^2 cos^2\phi \tag{80}$$

Again, the angle between the gradient of the descent function and $f(x, u)$ is expressed

$$H(x, u) = \frac{(\partial W(x))/(\partial x)}{\|(\partial W(x))/(\partial x)\|} \frac{f(x, u)}{\|f(x, u)\|} = \cos\beta \tag{81}$$

where β is the angle between the gradient of the descent function and the state space velocity vector $f(x, u)$.

Selection of the Control

As was done earlier in the report for the Lyapunov Steepest Descent Controller, a control $u^*(x)$ is sought which will move the system state variables as nearly opposite the gradient of the descent function as possible, given the dynamics of the system and the limits on the control.

As before, to determine $u^*(x)$ set $\frac{\partial H}{\partial u} = 0$ and solve for u. Note however, that H in this discussion is not the same function as H in the LSDC discussion. If the value of u lies between ± 1 then $u^*(x)$ is either this value or ± 1, whichever minimizes H. If the value of u which solves $\frac{\partial H}{\partial u} = 0$ is not between ± 1, then $u^*(x)$ is selected from ± 1 to minimize H.

Performance Results

An acceptable descent function for this algorithm has not been found. Fig. 15 shows the x_2 and $\hat{x}_2$ time histories while Fig. 16 shows the x_3 and $\hat{x}_3$ time histories for a trajectory guided by this LTC. The elliptical descent function used in these simulations has a semimajor axis of 40, a semiminor axis of 1, and a rotation angle ϕ of 19°, measured as shown in Fig. 14. This descent function produces an apocenter altitude following the aerobraking maneuver of 356 nautical miles which is as close to the 270 nm target as could be obtained while keeping the flight path angle near the optimal. But as Fig. 15 shows, as the vehicle neared the target path, the LTC did not make the final correction necessary to converge on the desired velocity. A second descent function is formed which guides the vehicle closer to the target apocenter altitude. This descent function uses an elliptical function with the same semi-major axis of 40, a semi-minor axis of 1, but the rotation angle is changed to 55°. As Fig. 17 and Fig. 18 plainly show, the desired apocenter altitude is not achieved by following the desired path to exit but rather by reducing the velocity (x_2) more than desired and then climbing with a steeper flight path angle (x_3) than preferred. Almost by accident, the desired apocenter altitude is attained in this one case. No fixed configuration for the elliptical descent function was found which consistently allows this algorithm to acquire the target path and follow it to an acceptable exit state.

Intuitively, it is easy to see that, if the velocity is slower than $\hat{V}$ and the flight path angle is less than $\hat{x}_3$, the logical choice is to use positive lift to get closer to the path. Likewise, if V is greater than $\hat{V}$ and the flight path angle is greater than $\hat{x}_3$ a lift down orientation is required to approach the path. The ambiguous areas are in the other two quadrants, where either the velocity is too fast but the flight path angle is too shallow, or where the velocity is too slow but the flight path angle is greater than desired. It is desirable to define a line passing through the target state at each instant in time separating the regions. The

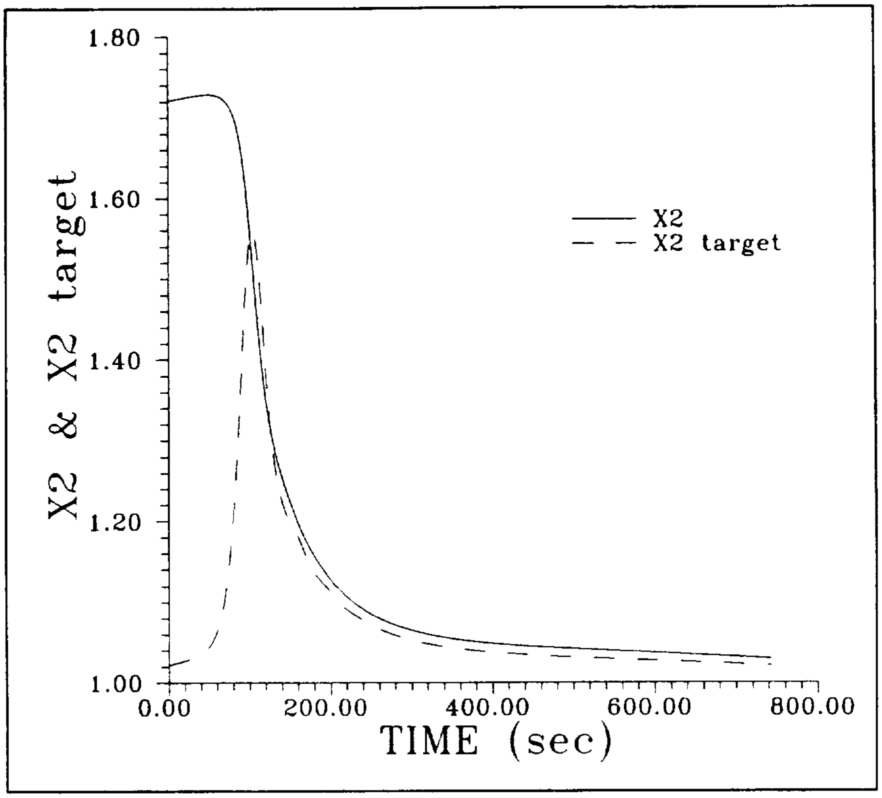

Fig. 15 x_2 and $\hat{x}_2$ - Sample Lyapunov Tracking Controller Trajectory

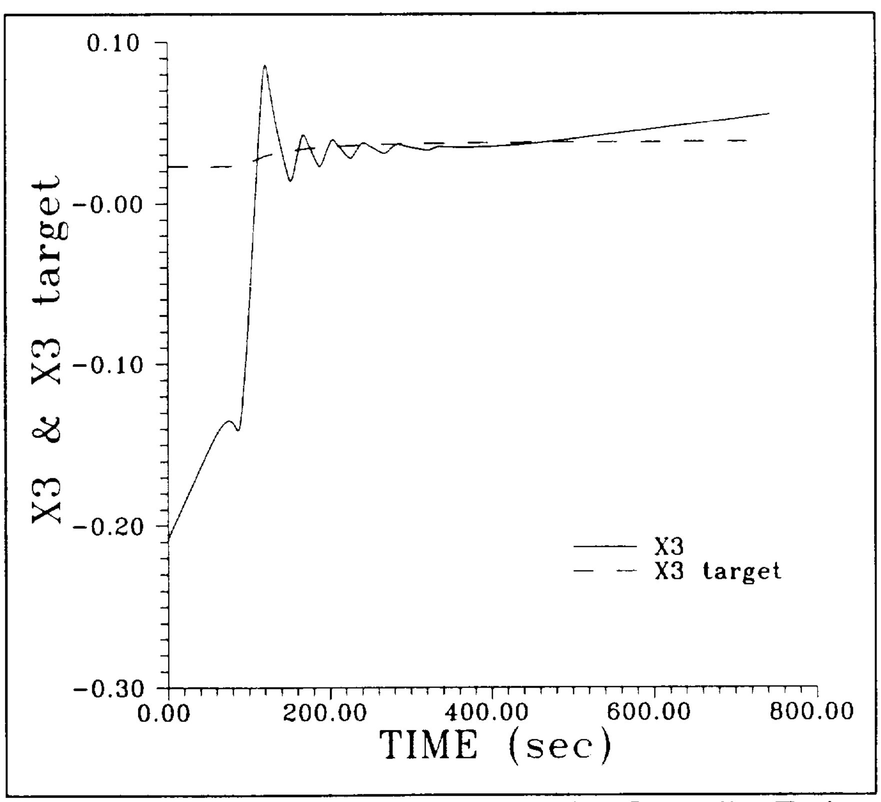

Fig. 16 x_3 and $\hat{x}_3$ - Sample Lyapunov Tracking Controller Trajectory

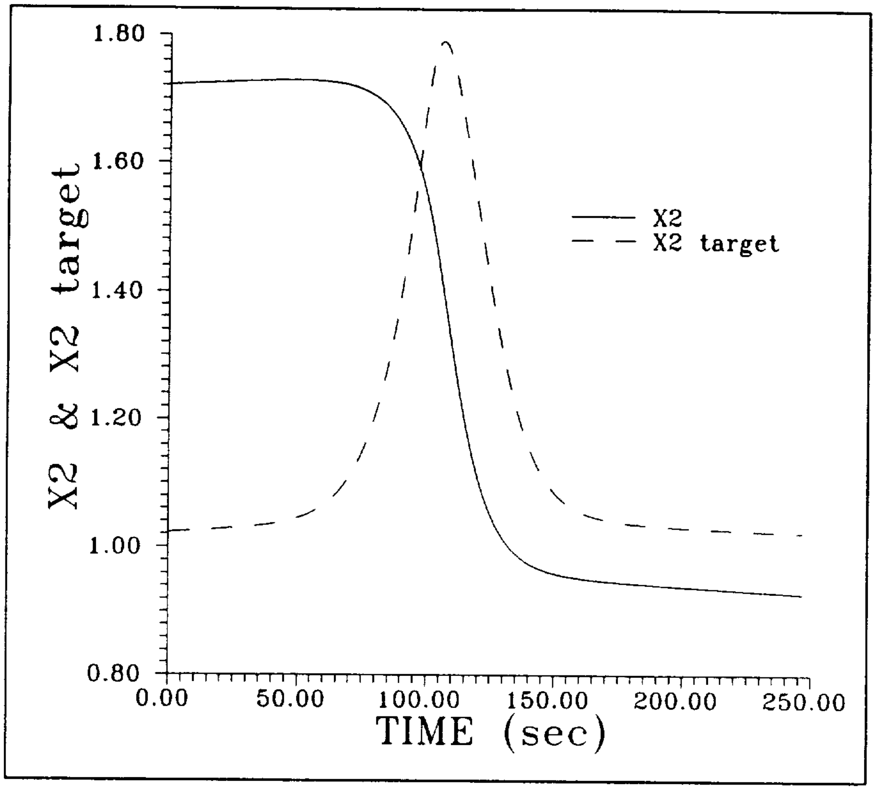

Fig. 17 x_2 **and** $\hat{x}_2$ **- Alternate Lyapunov Tracking Controller Trajectory**

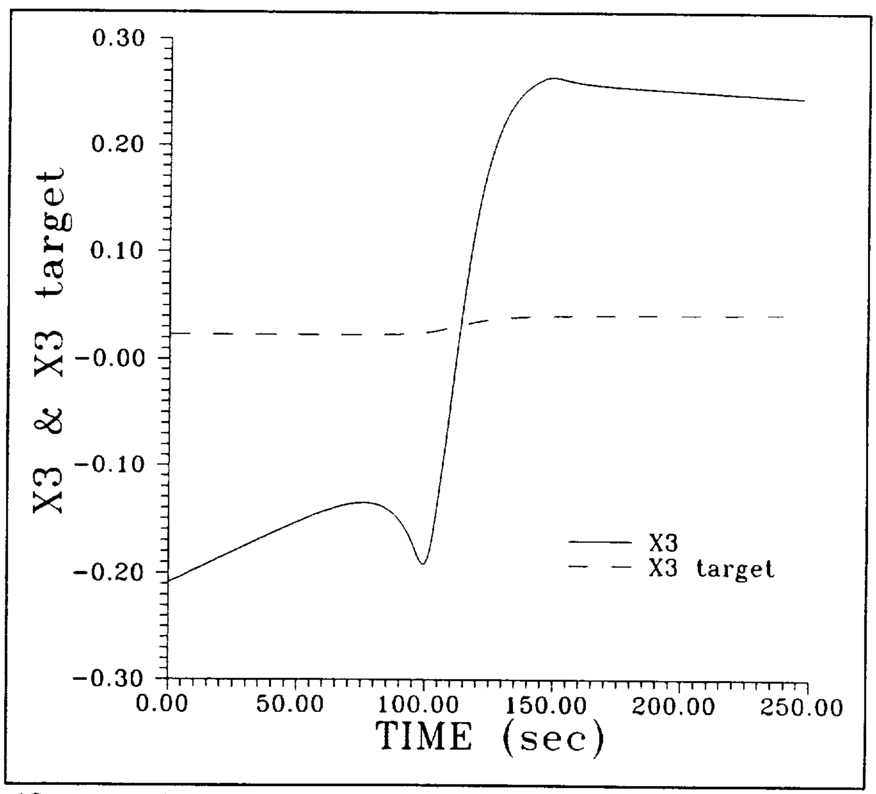

Fig. 18 x_3 **and** $\hat{x}_3$ **- Alternate Lyapunov Tracking Controller Trajectory**

slightly different altitude rate. Though the 450 ft/sec altitude rate that was chosen gives excellent results, it should still be acceptable to fly a 425 or a 475 ft/sec altitude rate path which would lead the vehicle to the desired apocenter orbit.

To define this switching line, the angle of rotation ϕ (Fig. 14) of the descent function is varied during the trajectory such that

$$\phi = \operatorname{atan}\left[-\frac{\frac{d\hat{x}_3}{d\dot{h}}}{\frac{d\hat{x}_2}{d\dot{h}}}\right]. \tag{82}$$

In effect this expression defines a switching line formed by linearizing about the current target state and varying altitude rate. Though

$$\left[\frac{\partial W(x,t)}{\partial x}\right](f(x,u)) \neq \frac{dW}{dt}, \tag{83}$$

because of the missing $\frac{\partial W}{\partial \phi}\frac{d\phi}{dt}$ component. But, since $\frac{\partial W}{\partial \phi}$ is small compared to the elements of $\frac{\partial W}{\partial x}$ and since ϕ varies slowly, increasing monotonically from about 15° to about 75° during the exit phase, this component is assumed to be insignificant. The commanded bank angle is still determined as before by selecting the value of u which minimizes $H(x,u)$ with $H(x,u)$ defined as Eq. (81).

Though this method of varying the weighting matrix gives improved performance, the algorithm still has problems acquiring the target path. The vehicle still uses lift down too early and plunges deeply into the atmosphere, creating extremely high vehicle accelerations and heat rates in the process. To cure this problem the Lyapunov Tracking Algorithm (LTA) developed here is incorporated as an exit phase following the equilibrium glide phase of the MPC algorithm outlined in Chapter 2.

Lyapunov Tracking Controller Exit Phase

The equilibrium glide phase was developed to guide the vehicle into the atmosphere and hold it in equilibrium until the velocity has been appropriately reduced. It must perform this task while keeping the maximum trajectory loads and peak heat rates within bounds. It performs this task very well. On the other hand the LTC just described does a good job of holding the desired path to exit if somehow it is started near that path. If we break up the trajectory so that the LTC has responsibility for control when these conditions exist, its strong points are likely to improve overall performance. With this idea in mind the marriage of the LTA as an exit phase with an equilibrium glide phase controlled with one the controllers developed earlier is a natural implementation. Such a concept is implemented next. The method of computing transition velocity from the equilibrium glide phase to the exit phase presented in Chapter 2 placed the vehicle very near the desired path. This combination of equilibrium glide phase and LTA proved to be the best controller examined.

The two density estimation techniques presented in Chapter 2 are also tested. The complete control algorithm with the hybrid density estimator included will be referred to as the Hybrid Lyapunov Tracking Controller (HLTC) while this controller with the polynomial density estimator will be called the Lyapunov Tracking Controller (LTC).

CHAPTER IV

CONTROLLER SENSITIVITY ANALYSIS

The performance of the MPC and MHPC control algorithms developed in Chapter 2 and of the LTC and LHTC control algorithms developed Chapter 3 was determined along with the performance of the APC and Energy Controllers which are derived and discussed in detail in the literature[9,10,12,13,48]. All the algorithms are tested using a six degree of freedom computer simulation based on the Program to Optimize Simulated Trajectories[36] (POST), which utilizes a fourth order Runge-Kutta numerical integration scheme to continuously integrate both the force and the moment equations of the vehicle. The control algorithms are tested to determine the effect of large scale density variations such as those caused by the seasonal sublimation and condensation of the Martian atmosphere or by a global dust storm. They are also run to determine the effect on the performance of short period atmospheric variations by injecting square wave density pulses, similar to those used by Fitzgerald[10, 11], of various magnitudes and durations into the density function at various altitudes. Entry flight path angles are varied within the current predicted error band[46]. Perturbations in the vehicle lift and drag characteristics are also simulated. Finally, combinations of these perturbations in the atmospheric density function, entry flight path angle and vehicle lift and drag characteristics are examined and the performance of each controller is analyzed.

Following a brief description of the vehicle and trajectory simulation program used, the data from this test program are presented graphically utilizing three dimensional mesh plots. The primary thrust of this simulation effort is to select the best controller(s) from those studied. A fuller performance evaluation of the selected controllers, aimed at determining their robustness limits, is presented in Chapter 5.

Vehicle and Trajectory Simulation Inputs

The vehicle used in the study is a biconic aeroshell design with a fifteen foot base diameter and a weight of 11,023 lbs. The base surface area of 176.1 ft^2 is used as the reference surface area. The vehicle is designed with a five foot center of gravity offset resulting in a trim angle of attack of 27° which is maintained throughout the maneuver via a simple proportional feedback controller. Control is attained through bank maneuvers which reorient the direction of the lift vector. These bank maneuvers are commanded as body axis rolls with coordinating body axis yaw maneuvers. The nominal lift coefficient is 0.68892 while the drag coefficient is 0.69819, producing a nominal L/D of 0.99.

The Mars Global Reference Atmosphere Model[35] (MARS-GRAM) is used to produce realistic atmospheres for the study. Three different atmospheres representing a nominal, a low density and a high density Martian atmosphere are considered (Fig. 19). The nominal atmosphere is the COSPARV Model Atmosphere For Mars[18], while the high density and low density atmospheres are derived using MARS-GRAM. The low density atmosphere is a MARS-GRAM simulation of the lowest density Martian atmosphere predicted for April 10, 1999 assuming no dust storms and a 10.7 cm solar flux of 50 (nominal value = 150). The high density atmosphere represents the highest density atmosphere predicted on December 27, 1997, again with no dust storms but this time with a 10.7 cm solar flux of 300. Although MARS-GRAM was originally incorporated as a subroutine to POST which could be called to generate atmospheric data on line, MARS-GRAM is not utilized in this manner because of the added computational time. MARS-GRAM generates atmospheric data which is stored in tabular form. These tables of atmospheric data are then included in the POST input namelist.

In addition to the large scale density variations introduced by using the low, nominal or high density atmosphere models described above, short period variations in the atmo-

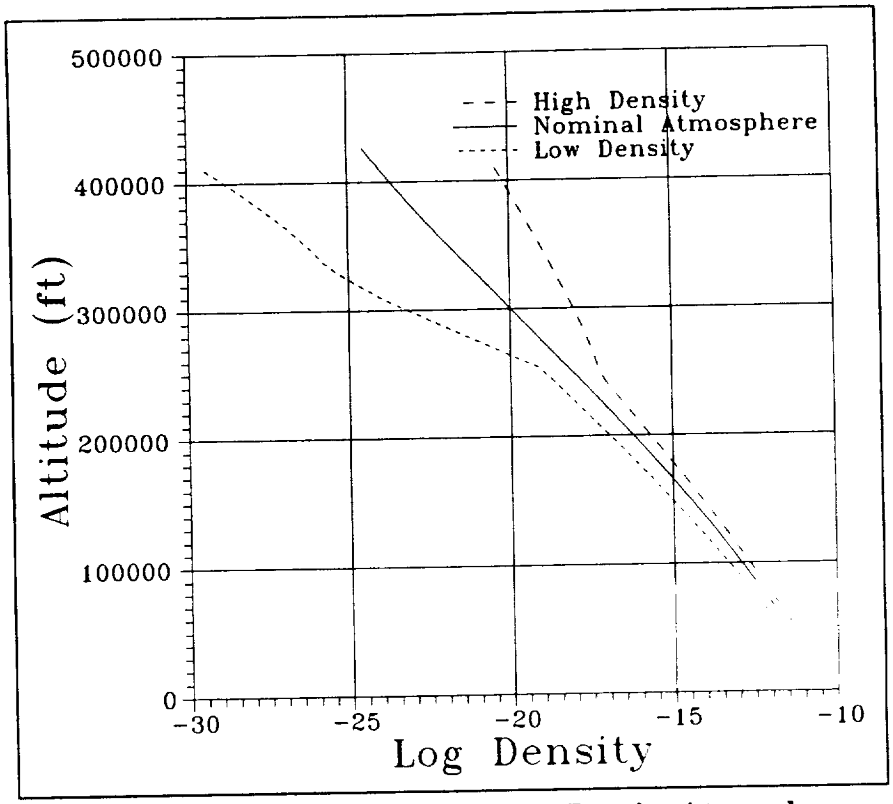

Fig. 19 Mars Nominal, Low and High Density Atmospheres

spheric density function are investigated by introducing square wave density pulses, similar to those used by Fitzgerald[10, 11]. These pulses perturb the local atmosphere within a 10,000 or 20,000 ft altitude band by multiplying the expected density by a constant magnitude density multiplier. The magnitudes of the density multipliers used include 0.5, 0.75, 1.25, 1.5, 1.75 and 2.0. The lower edge of the density pulses are varied in 10,000 ft steps from 100,000 to 290,000 ft

The atmospheric interface altitude is taken to be 125 km (410,105 ft) and the initial conditions are defined at this altitude. The entry velocity is 6 km/sec (19,685 ft/sec) and the nominal entry flight path angle is -12°. The targeted orbit is a 270 nm circular orbit. In addition to the atmospheric perturbations mentioned above, perturbations are introduced in the vehicle lift and drag coefficients representing variations of ±33% from the nominal L/D ratio of 0.99. The +33% L/D perturbation is introduced by multiplying the nominal lift coefficient by 1.14, while the drag coefficient is multiplied by 0.86. The −33% L/D perturbation is introduced by multiplying the nominal lift coefficient by 0.8, while the drag coefficient is multiplied by 1.2. This method of varying L/D also perturbed the ballistic coefficient of the vehicle. Navigation errors in the form of variations in the entry flight-path-angle of ±0.25° and ±0.5° from the nominal -12° are considered. The performance for each perturbed run is presented as total ΔV required to achieve the desired final orbit. ΔV is a measure of the controllers overall success in meeting the desired exit conditions. The ΔV is calculated assuming one burn at atmospheric exit oriented along the velocity vector to correct any apocenter error, a second at apocenter to raise pericenter, and a final burn to correct any orbit plane error.

Analytic Predictor Corrector Performance Results

The original APC controller[9, 10, 12, 13, 48] did not fare very well when challenged with the postulated perturbations used in this study. Figures 20, 21, 22, and 23 present the performance of this controller when faced with these perturbations. These charts summarize the performance of a nominal vehicle which enters the atmosphere with an $\gamma_e = -12°$ and then encounters a square wave density pulse. The ΔV required to circularize is plotted on the vertical axis. Figure 20 presents the results of encountering square wave density pulses in a nominal Martian atmosphere, while Fig. 21 shows similar data for a low density atmosphere and Fig. 22 then illustrates the results for a high density atmosphere. In the first diagram of each figure the density pulse perturbs a 10,000 ft altitude band while in the second diagram the pulse affects a 20,000 ft band. Magnitudes for these pulses range from -50% to +100% in 25% increments. The location of the lower edge of the pulse was moved from 100,000 ft to 290,000 ft in 10,000 ft increments. The magnitude of the pulse

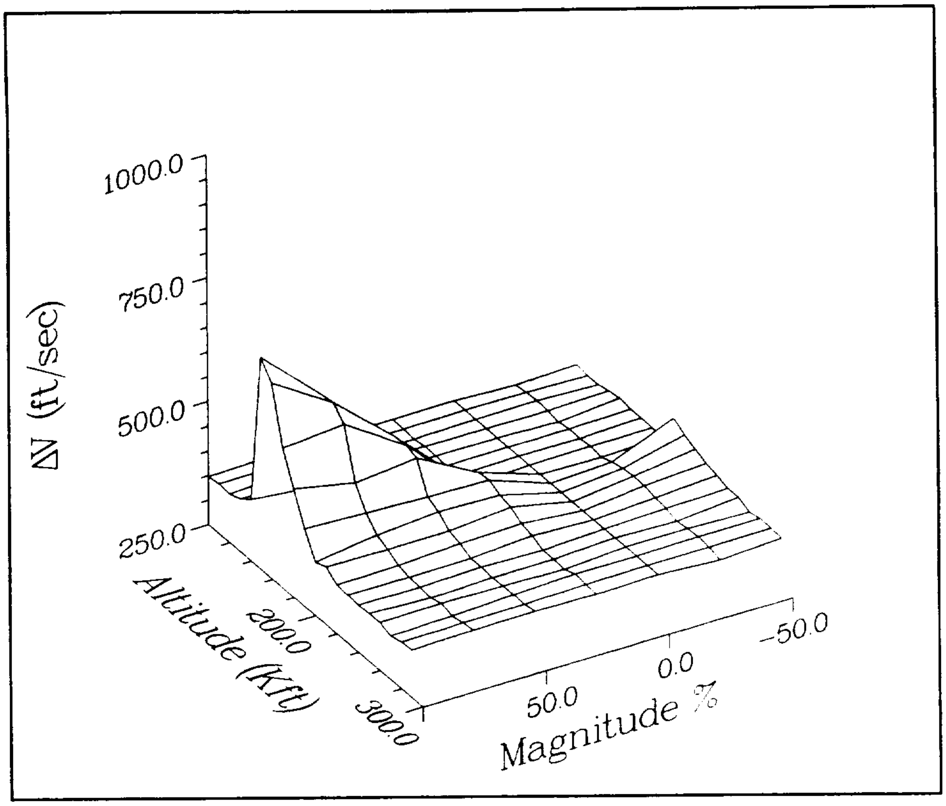

a)

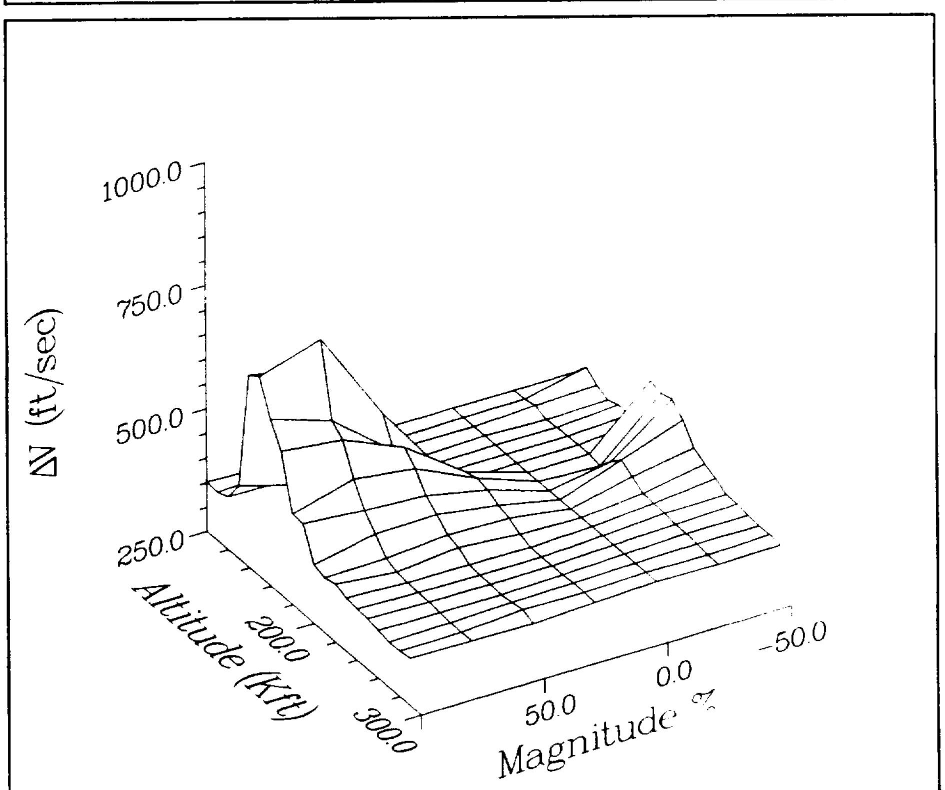

b)

Fig. 20 Analytic Predictor Corrector Sensitivity to Square Wave Density Pulses in Nominal Atmosphere. a) 10000 feet Duration; b) 20000 feet Duration

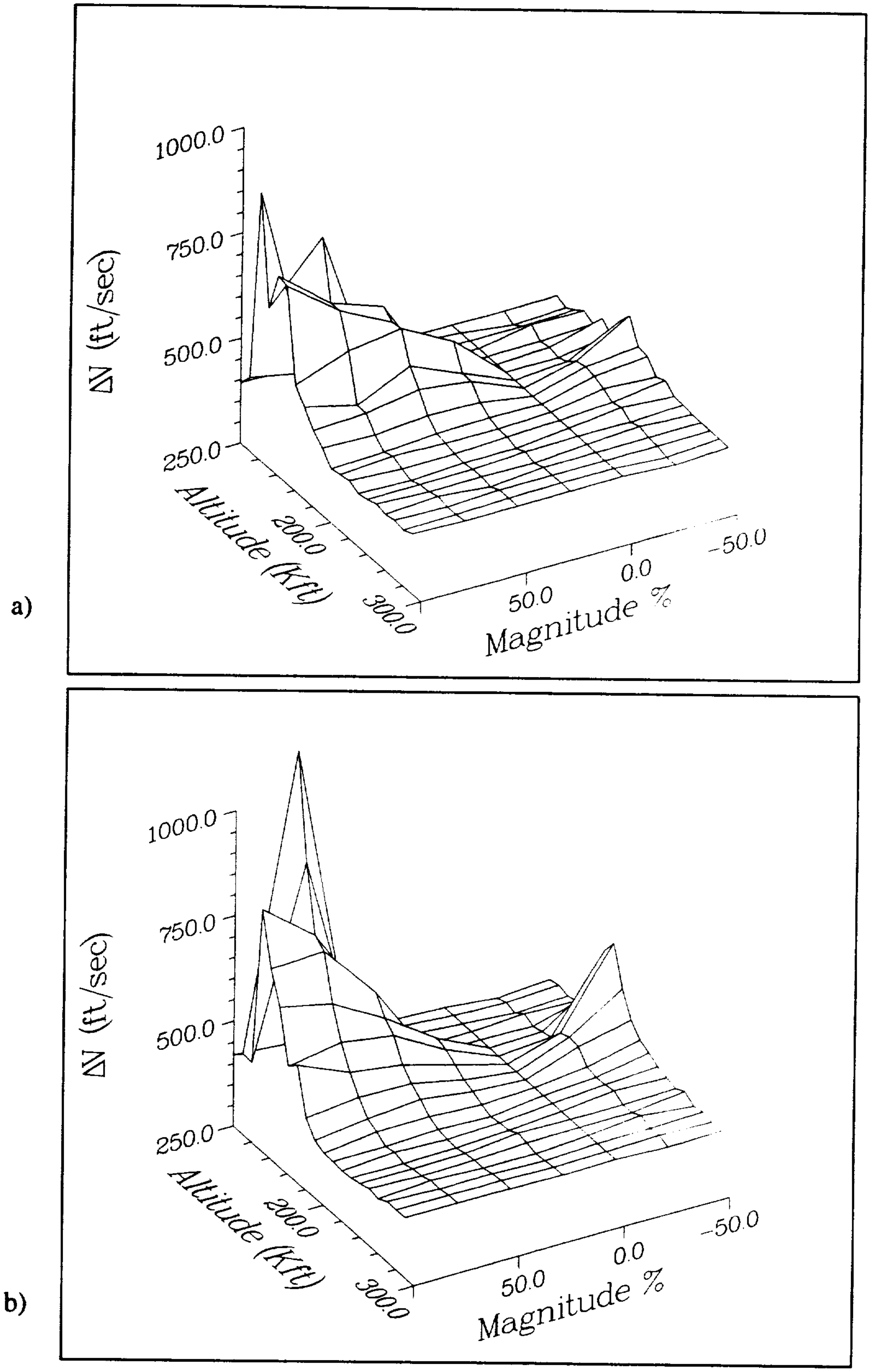

Fig. 21 Analytic Predictor Corrector Sensitivity to Square Wave Density Pulses in Low Density Atmosphere. a) 10000 feet Duration; b) 20000 feet Duration

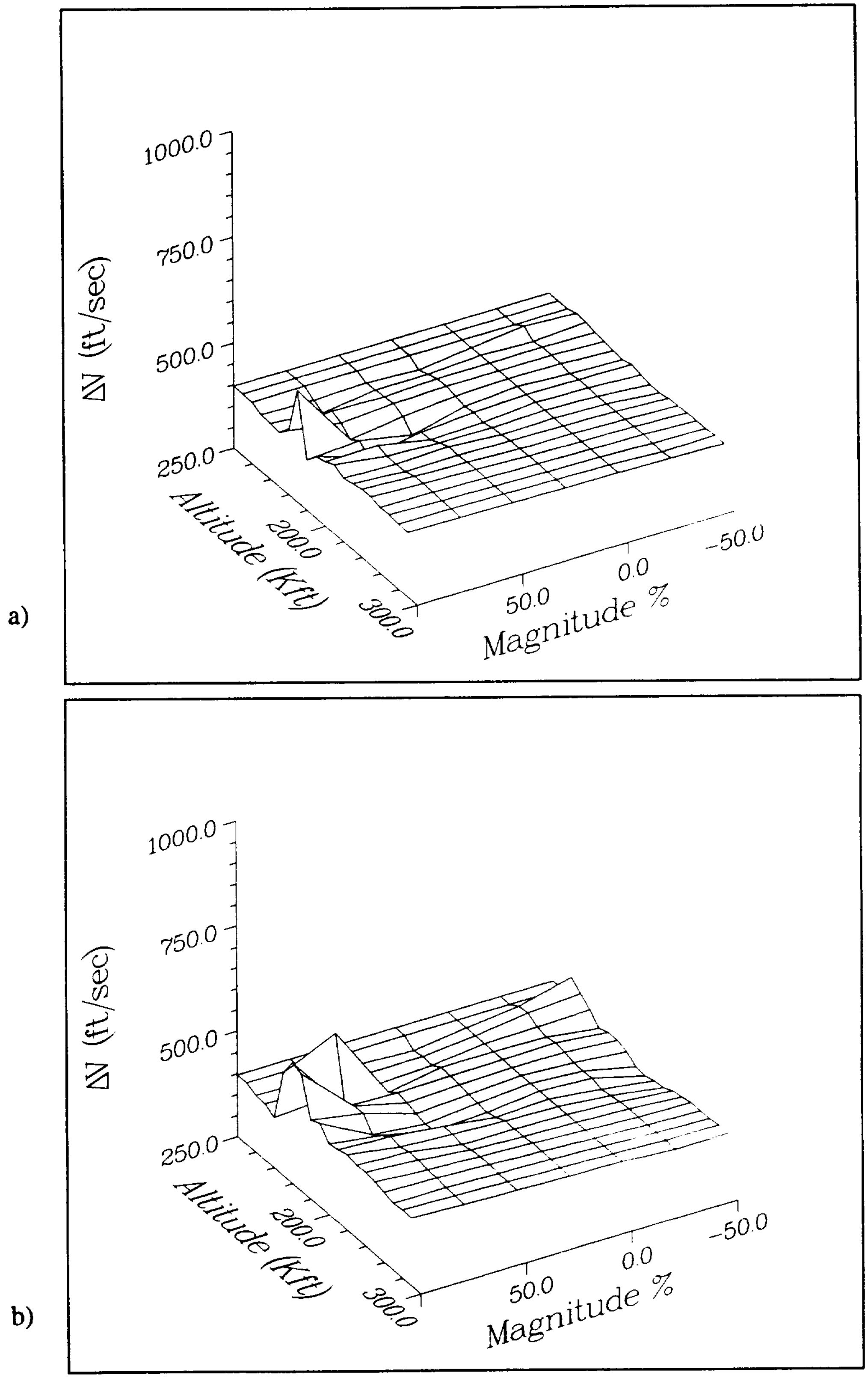

Fig. 22 Analytic Predictor Corrector Sensitivity to Square Wave Density Pulses in High Density Atmosphere. a) 10000 feet Duration; b) 20000 feet Duration

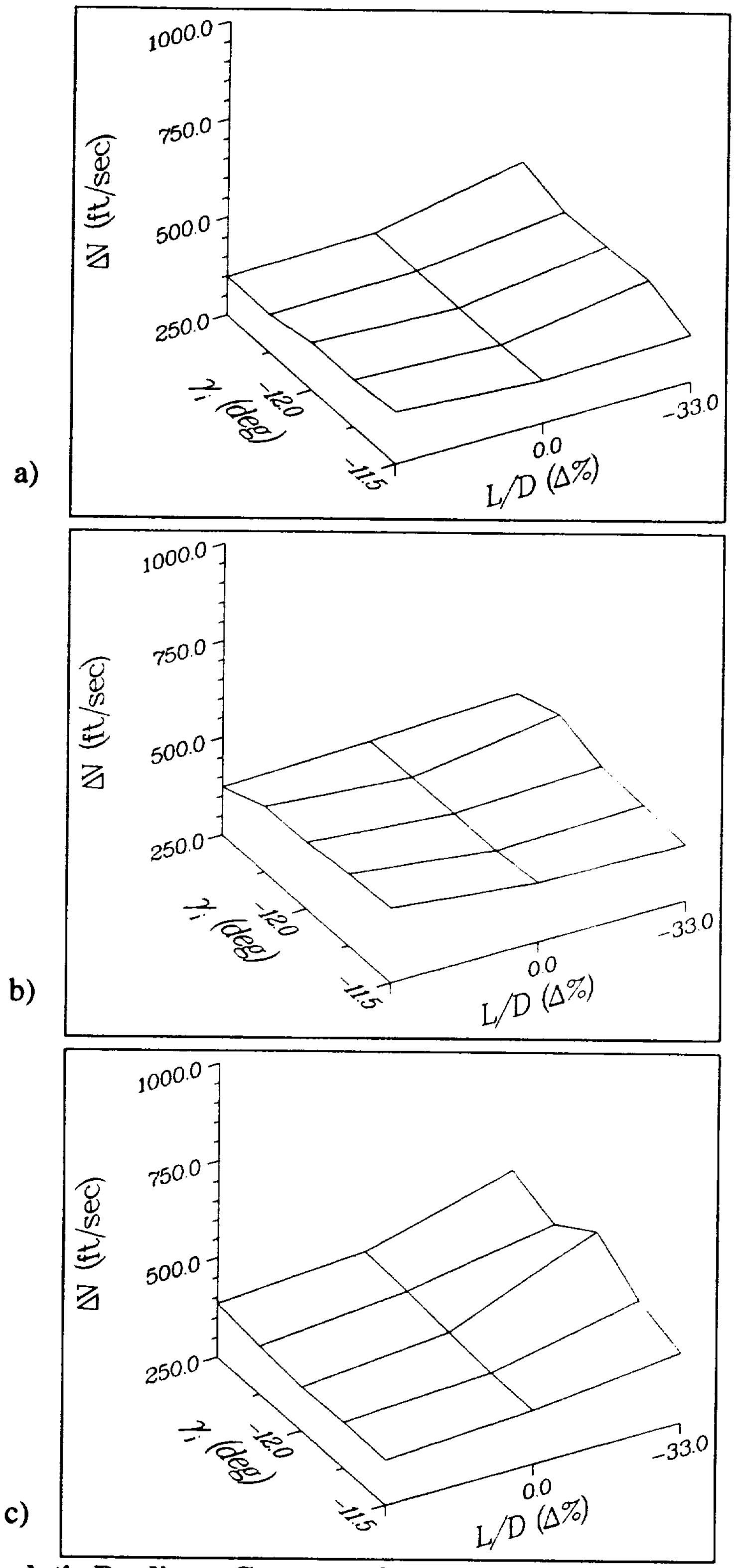

Fig. 23 Analytic Predictor Corrector Sensitivity to Variations in Lift to Drag Ratio and Entry Flight Path Angle. a) Nominal Atmosphere; b) Low Density Atmosphere; c) High Density Atmosphere

and the altitude of the lower edge are shown on the diagrams. Figure 23 shows the ΔV required to circularize as L/D and γ_e are varied. Figure 23a shows the results of these variations in a nominal atmosphere, while Fig. 23b presents the same perturbations in a low density atmosphere and Fig. 23c in a high density atmosphere.

Figure 23 indicates that the APC controller exhibits a considerable sensitivity to off nominal vehicle aerodynamics and to navigation errors. This controller also shows a marked decrease in performance in the high density atmosphere with no density steps when compared to its performance in the low density and nominal atmospheres. The ΔV required to circularize following the aerobraking maneuver in a high density atmosphere even with no density step (0% magnitude density step) is over 400 ft/sec while the optimal results presented in Table 1 show that it should require less ΔV to circularize after aerobraking in a high density atmosphere (optimally about 316 ft/sec) than in a nominal or low density atmosphere. Additionally, the variations in ΔV shown in Fig. 23c are considerably worse than those in Fig. 23a or b. Part of this sensitivity comes from using a specified transition velocity to switch to the exit phase, ignoring the actual energy loss to occur during the exit phase. The other reason for this sensitivity is a rather simplistic density model. Also, the APC controller is less sensitive to density steps in the high density atmosphere than in the low or nominal atmosphere. This sensitivity can again be explained by the choice of a specified transition velocity for the switch from entry to exit phase.

The transition velocity selected for this controller was 14,922 ft/sec. This transition velocity is appropriate for a nominal vehicle which enters the nominal atmosphere with a nominal flight path angle of -12°. Also, if the initial flight path angle is steeper than -12° or the atmosphere is more dense than expected, the vehicle will plunge into the atmosphere deeper than expected, and consequently, will have more atmosphere to traverse during the exit phase and will lose more energy to aerodynamic drag. Similarly, if the vehicle's drag coefficient is higher than estimated, the vehicle will lose more energy during exit than planned. Forcing the vehicle to decelerate to a predetermined velocity before initiating the exit phase requires the exit phase to be flown at a larger altitude rate than desired to reach the nominal apocenter altitude. This approach results in higher ΔV values and tends to amplify the effect of off nominal entry conditions or drag coefficient. The steeper exit path flown by this controller in the high density atmospheres is, however, more robust to density variations, as is suggested in Fig. 22. This result is due to the fact that a trajectory which flies a steeper exit phase has reduced more of the velocity deep in the atmosphere and is not requiring as much velocity loss during the exit phase. Density variations which perturb the amount of velocity loss during the exit phase have less effect when more of the velocity is reduced deep in the atmosphere. Later in the report the value of making this transition velocity an adaptive parameter will be shown.

The second concern with the APC controller is the density estimation technique. The density estimator built into this algorithm assumes the density function is a fixed scale height exponential function. The density derived onboard from accelerometer measurements is filtered using a low pass filter to remove high frequency noise. The result is then used to bias the exponential function used to estimate density. This technique works well as long as the density function does not vary much from a smooth exponential function and, more critically, the scale height of the atmosphere is fairly constant and does not vary appreciably from the assumed scale height. Unfortunately, the scale height of the Martian atmosphere does vary considerably

Fig. 19 shows the range in the density function predicted by MARS-GRAM. This figure presents altitude versus log density. The scale height may be determined by taking the negative of the slope of the density function from this graph. The scale height does not vary considerably below 250,000 ft, but above 250,000 ft there is considerable variation.

This variation does not affect the trajectories flown in the low density atmosphere very much because, in a low density atmosphere above 250,000 ft, aerodynamic forces have negligible effect on the vehicle. But, for those trajectories flown in the high density atmosphere, failure to properly model the atmosphere has considerable effect. The estimated density falls well short of the actual values above 250,000 ft. Consequently, there is more aerodynamic drag than predicted. Typically, this density modeling error leads to a final apocenter altitude ten to twenty nautical miles lower than targeted. This problem, compounded by the steep altitude rate in the exit phase (brought on by the constant transition velocity) reduces the controller's ability to correct for density upsets which occur after the exit phase is initiated. A noticeable sensitivity to square wave density pulses (Fig. 20, Fig. 21 and Fig. 22) results.

Overall, the APC is still a good controller. It guides the vehicle through the aerobraking maneuver with minimal heat, acceleration, and dynamic pressure loads. It exits with a state near the optimal one when the density function encountered is near the nominal value, when navigation is good enough to allow precise control over the entry state, and when the hypersonic lift and drag characteristics of the vehicle are close to the design values. As part of the modification of this controller to meet the Martian requirements the value of $K_{\bar{q}}$ was changed to 4.5 as recommended in Chapter 2. This change kept the vehicle from exiting the atmosphere before slowing enough to transition to the exit phase (skipping out) for all of the test cases examined. However, the APC just is not quite robust enough to adequately handle expected perturbations in the Martian atmosphere, vehicle entry conditions, or vehicle lift and drag variations.

Energy Controller Performance Results

Figures 24, 25, 26, and 27 show the performance of the Energy Controller. Again, the results are presented in the same format as before with Fig. 24 showing results for den-

a)

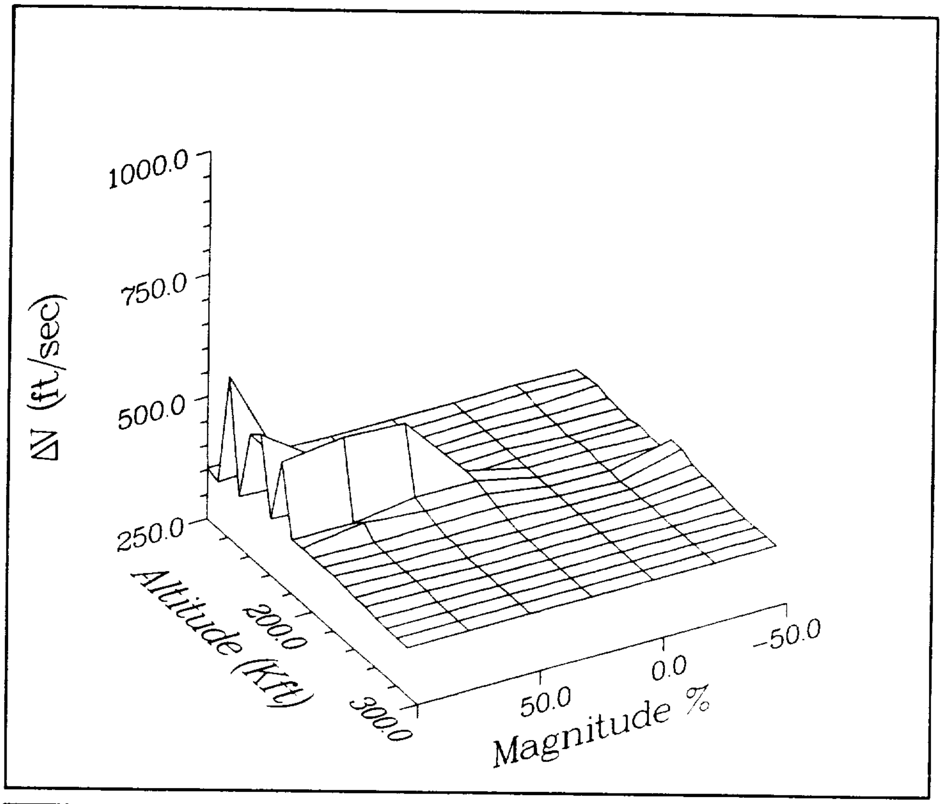

b)

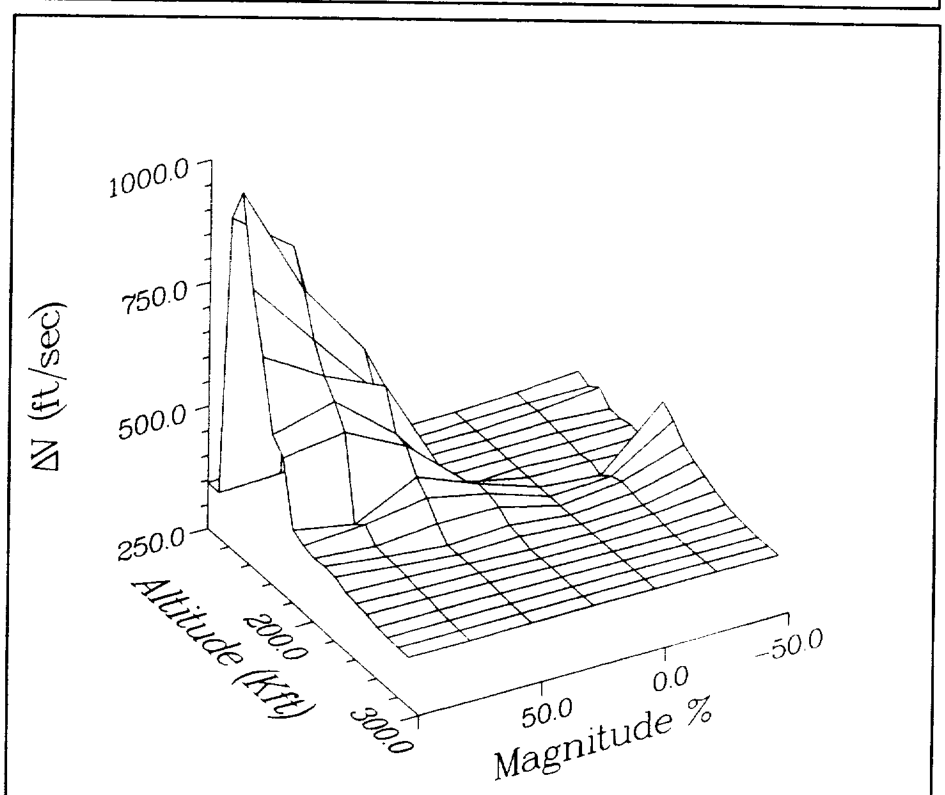

Fig. 24 Energy Controller Sensitivity to Square Wave Density Pulses in Nominal Atmosphere. a) 10000 feet Duration; b) 20000 feet Duration

a)

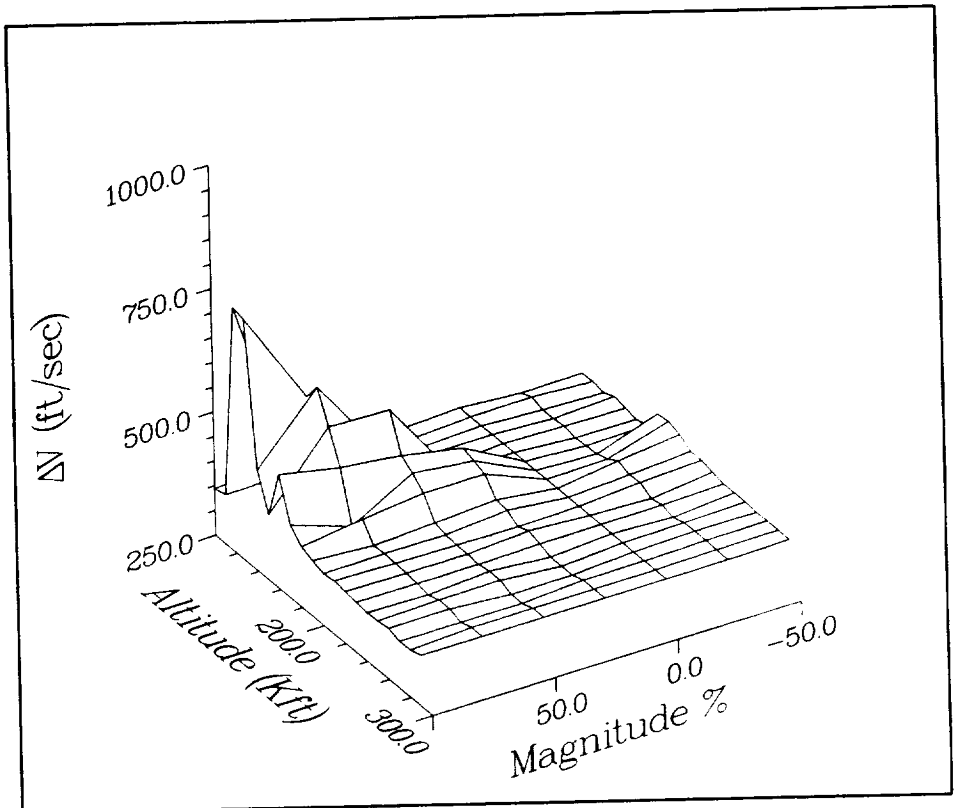

b)

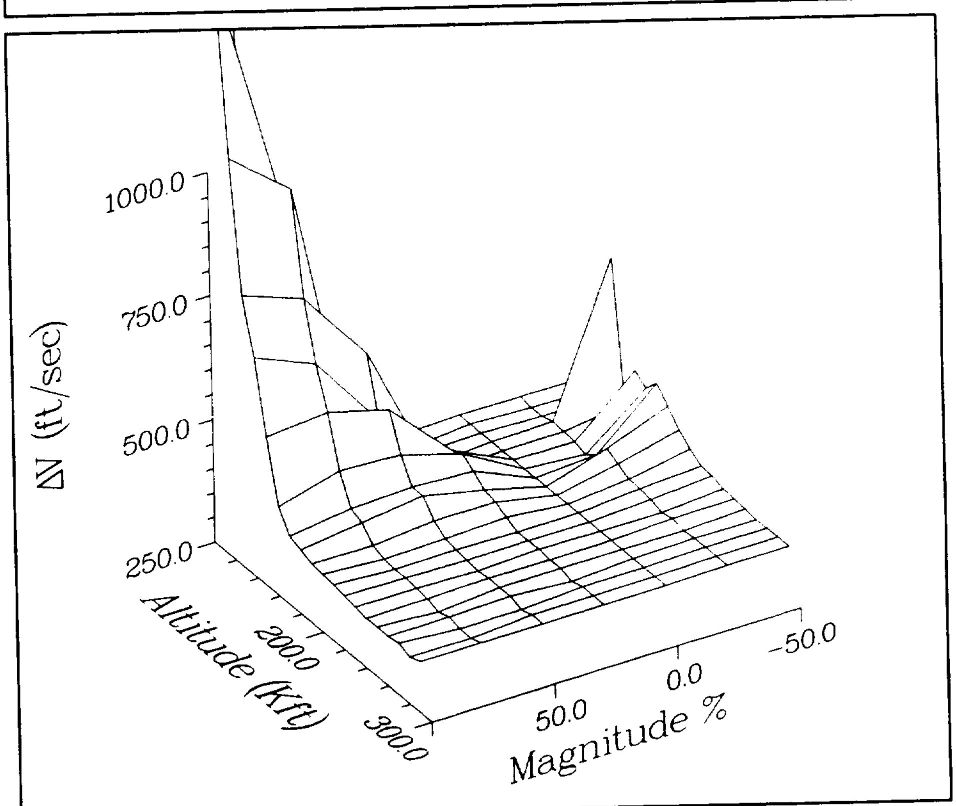

Fig. 25 Energy Controller Sensitivity to Square Wave Density Pulses in Low Density Atmosphere. a) 10000 feet Duration; b) 20000 feet Duration

a)

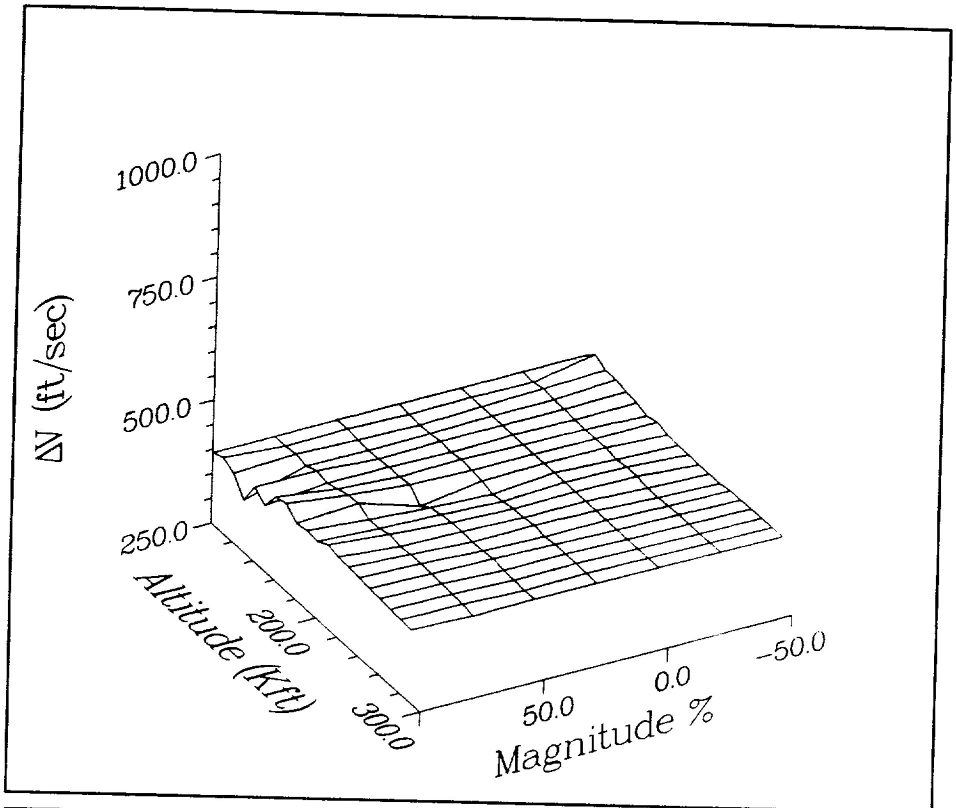

b)

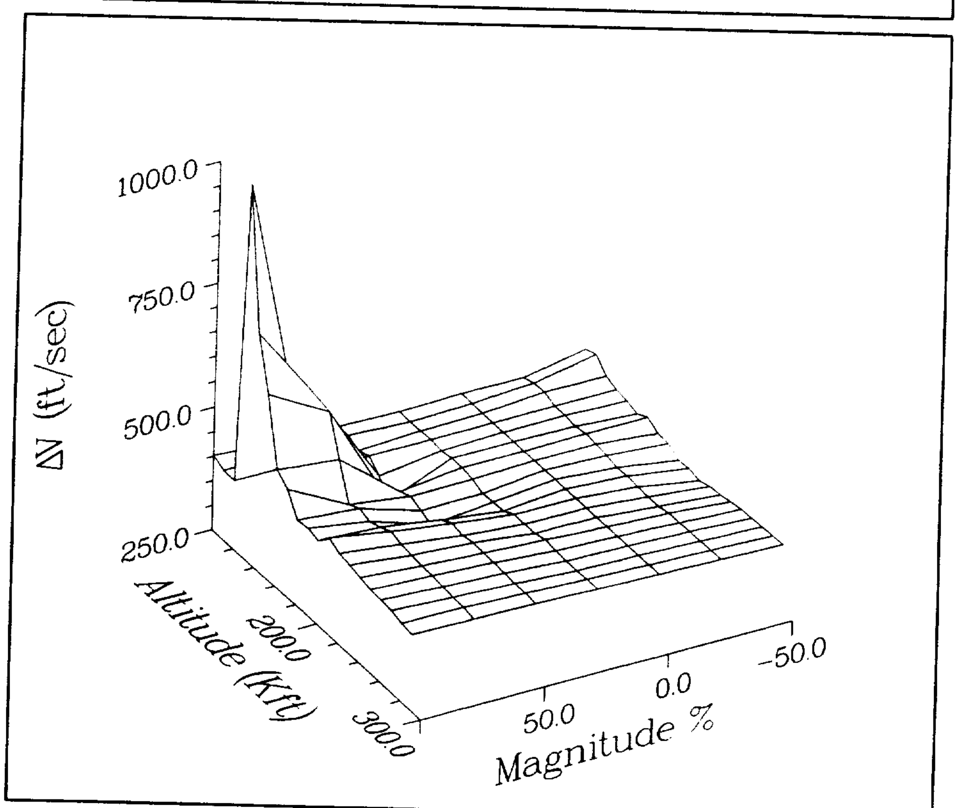

Fig. 26 Energy Controller Sensitivity to Square Wave Density Pulses in High Density Atmosphere. a) 10000 feet Duration; b) 20000 feet Duration

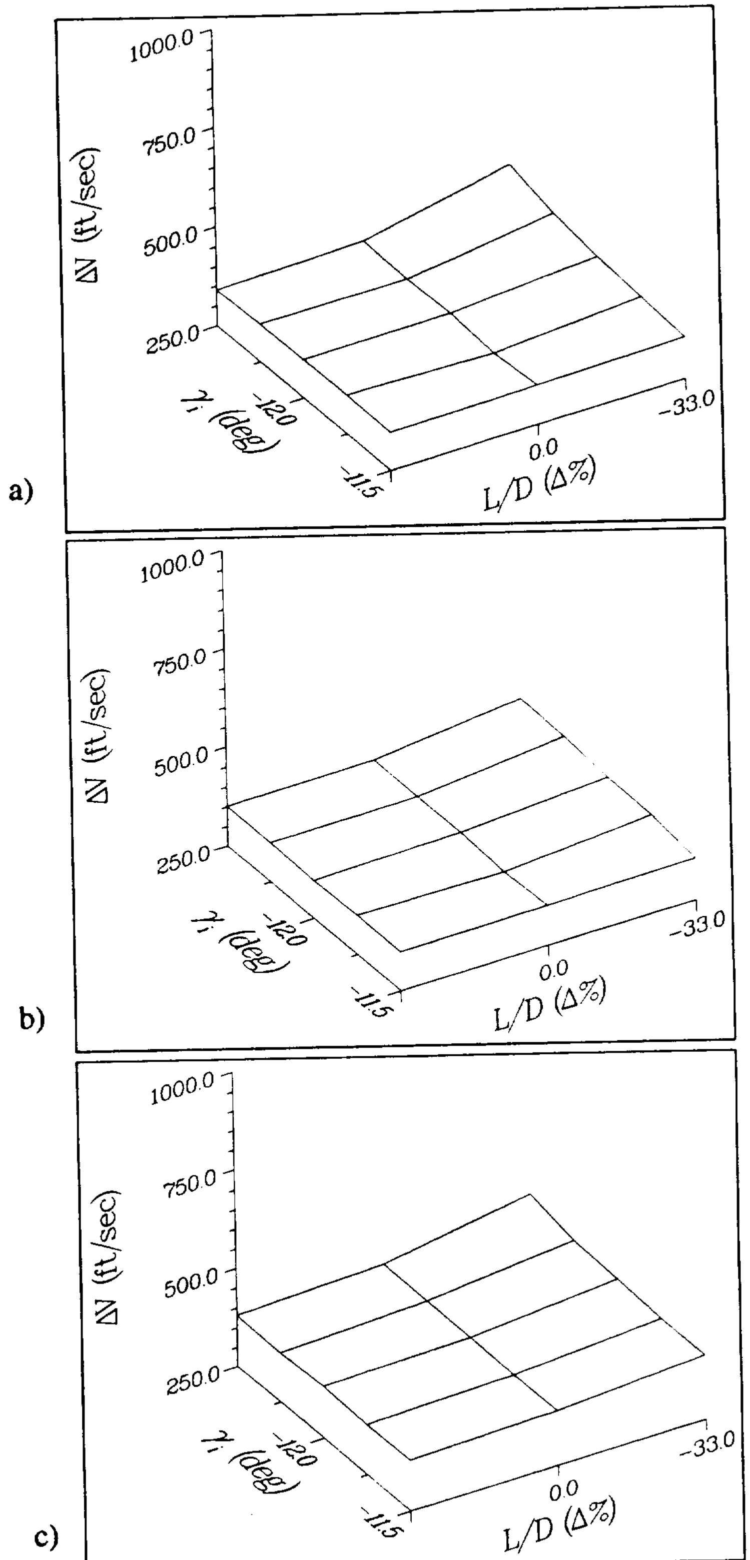

Fig. 27 Energy Controller Sensitivity to Variations in Lift to Drag Ratio and Entry Flight Path Angle. a) Nominal Atmosphere; b) Low Density Atmosphere; c) High Density Atmosphere

sity steps in a nominal atmosphere while Fig. 25 shows the results for a low density atmosphere and Fig. 26 shows the performance results in a high density Martian atmosphere. Fig. 27 shows the effect of varying lift-to-drag ratio and entry flight path angle with Fig. 27a being in a nominal atmosphere, Fig. 27b showing these results in a low density atmosphere, and Fig. 27c showing the results in a high density atmosphere.

The Energy Controller is substantially more robust than the APC controller with respect to vehicle lift and drag variations and to navigational errors. Figure 27 shows practically no variation in ΔV required to circularize. Furthermore, these results all fall below 400 ft/sec to circularize. This insensitivity may be attributed to the fact that the Energy Controller does not assume a density function, though an exponential function is expected; instead, it relies on the current energy rate and energy error to determine which path should be pursued. Variations in the vehicle's drag coefficient simply change the energy rate and the controller compensates . Likewise, variations in the overall state of the atmosphere (low, nominal, or high density atmosphere), or variations in the entry flight path angle which force the vehicle deeper or shallower into the atmosphere are seen by the controller as changes in the energy rate. Since the controller seeks to make energy rate approach zero as energy error approaches zero, variations of this type are handled well.

This method works well as long as the density function is a smooth exponential but, as the 10,000 and 20,000 ft density pulse diagrams illustrate, the Energy Controller shows definite sensitivity to density functions which are not smooth. The large magnitude 20,000 ft duration density steps are more than this controller can tolerate. Figure 25b shows that in a low density atmosphere, 20,000 ft duration density steps of +75 and +100% magnitude with lower edges between 100,000 ft and 120,000 ft, cause a catastrophic failure requiring more than 1000 ft/sec of propulsive maneuvering to circularize the desired orbit. These failures occur because the vehicle enters the high density region near the bottom of the trajectory. When the onboard accelerometers sense the rapid deceleration caused by the high density pocket and feed this information to the controller, the control system responds by applying lift up to decrease the energy rate. As the vehicle exits the high density pocket the control system responds by commanding a lift down configuration. But the vehicle's response time is too slow, requiring thirteen seconds to perform a 180° rest to rest roll maneuver. By the time the maneuver is complete the vehicle has moved higher in the atmosphere and no longer is able to control the trajectory using aerodynamic forces. The vehicle exits the atmosphere without properly depleting the kinetic energy. This behavior could also be called a skipout. The same phenomena is observed for the high magnitude density pulses in the nominal and high density atmospheres, though the effect is less disastrous.

The locations of the density pulses which cause the problems are higher in the nominal atmosphere than in the low density atmosphere, and even higher still in the high density atmosphere than in the nominal atmosphere. These higher critical locations occur because the vehicle's initial configuration is lift up. Higher density atmospheres exert more aerodynamic force at higher altitudes, tending to decrease the vehicle's negative altitude rate earlier. They also increase the altitude at which the vehicle bottoms out. A density pulse which perturbs the trajectory near its minimum altitude must be located higher in a high density atmosphere than in a low density atmosphere.

One additional drawback to the Energy Controller is higher trajectory loads than the algorithms which use an equilibrium glide phase. The equilibrium glide phase holds the lift up configuration until the trajectory bottoms out in almost all cases. The Energy Controller will roll the vehicle from lift up before the vehicle bottoms out, allowing the vehicle to sink to a lower minimum altitude, producing higher peak aerodynamic heating loads, higher maximum dynamic pressures, and higher maximum acceleration loads. These higher trajectory loads may reduce somewhat the advantages of aerobraking, especially if they require the vehicle to be more rigid to withstand the acceleration forces, or if they require additional heat shields or ablative materials. Though this study is concerned primarily with control system robustness, the effect of a control system on trajectory loads must also be considered.

The Energy Controller has shortcomings, especially with respect to short period density variations and trajectory loads, which make it unsatisfactory for controlling an aerobraking vehicle operating in the Martian atmosphere.

Mars Hybrid Predictor Corrector Performance Results

The Mars Hybrid Predictor Corrector (MHPC) was one of the two best performing algorithms tested for this series of perturbations. As discussed in Chapter 2, this algorithm employs a variable transition velocity for the switch from the equilibrium glide phase to the predictor corrector exit phase. Equally important is the density estimation technique which measures and records density at discrete altitude locations during the entry into the atmosphere. Density during the exit from the atmosphere is measured and compared against that predicted using the stored entry data. The result is filtered to remove high frequency noise and used to bias the density estimate developed during entry. This biased density estimate is then used to predict velocity loss for the remainder of the trajectory. As may be suspected, this method is extremely effective whenever the density profiles for the inbound and outbound legs of the trajectory are the same.

The performance of this controller is presented in Figures 28, 29, 30, and 31. Again, the first three figures summarize the performance when the density function is perturbed with 10,000 and 20,000 ft duration square wave density steps. Also, Fig. 28 presents these results when perturbing waves are injected into a nominal atmosphere. Figure 29 shows

a)

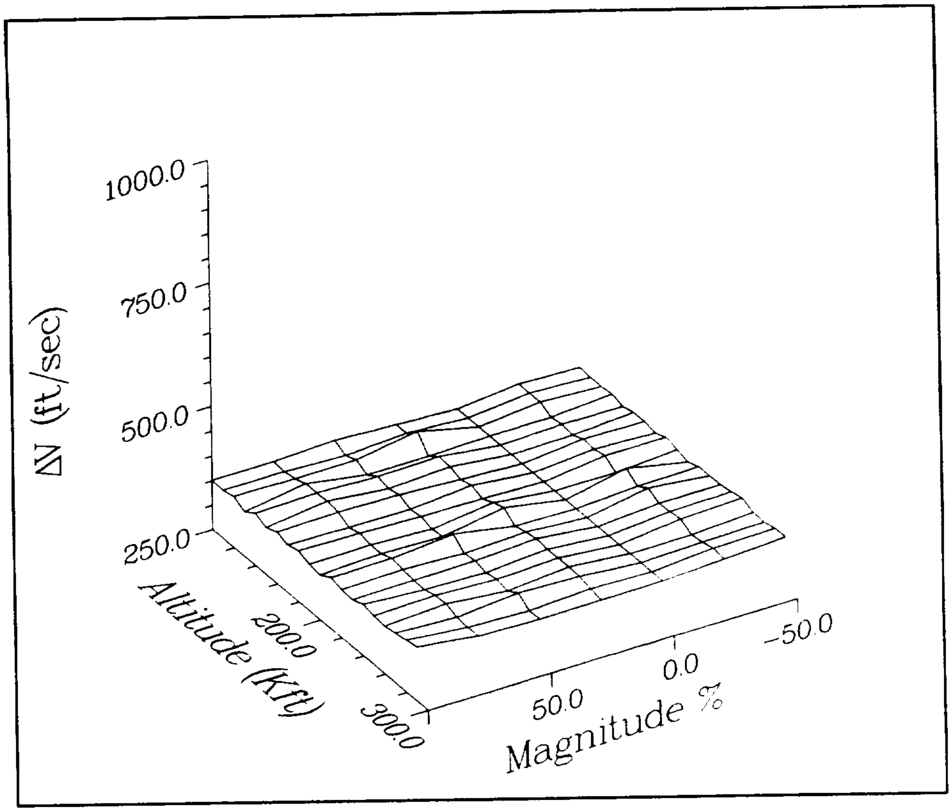

b)

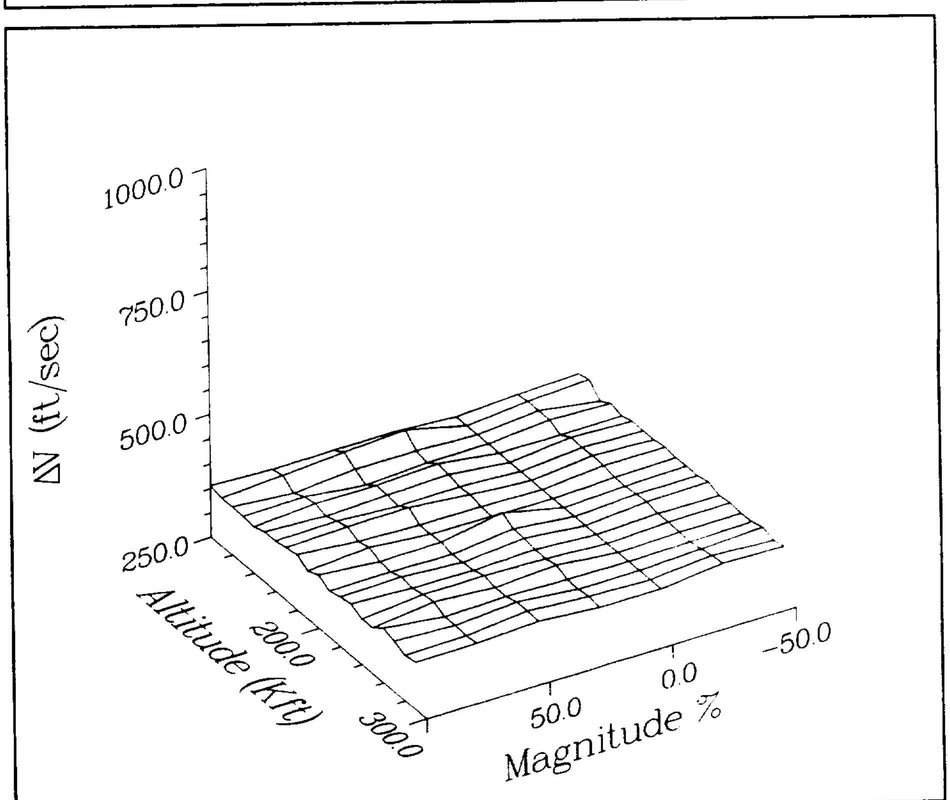

Fig. 28 Mars Hybrid Predictor Corrector Sensitivity to Square Wave Density Pulses in Nominal Atmosphere. a) 10000 feet Duration; b) 20000 feet Duration

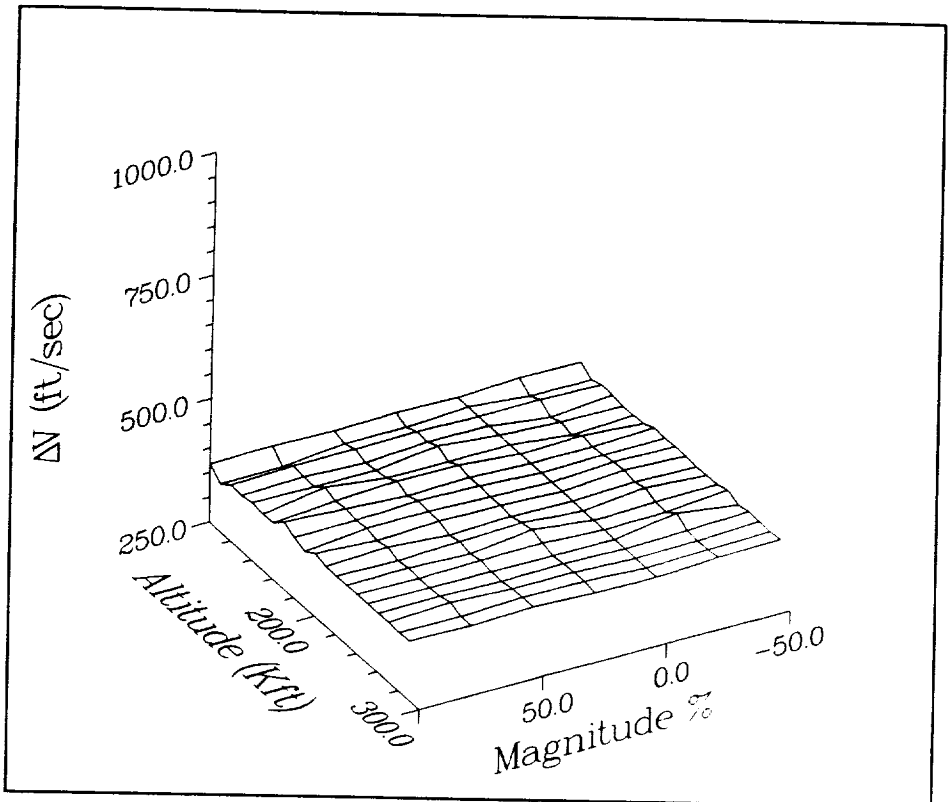

a)

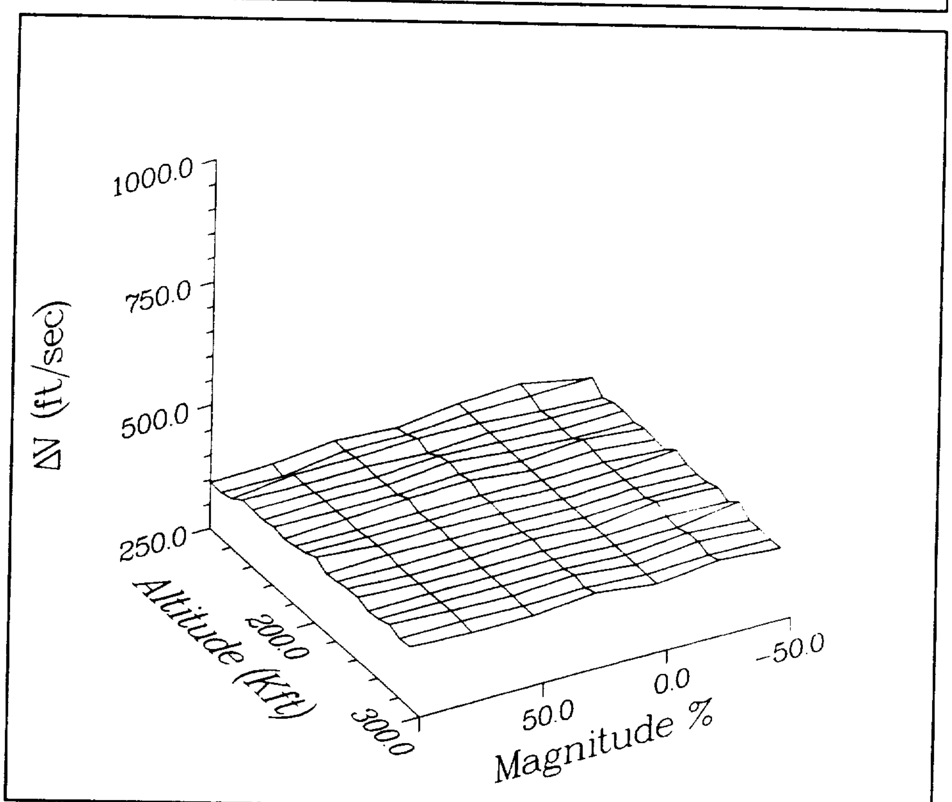

b)

Fig. 29 Mars Hybrid Predictor Corrector Sensitivity to Square Wave Density Pulses in Low Density Atmosphere. a) 10000 ft Duration; b) 20000 ft Duration

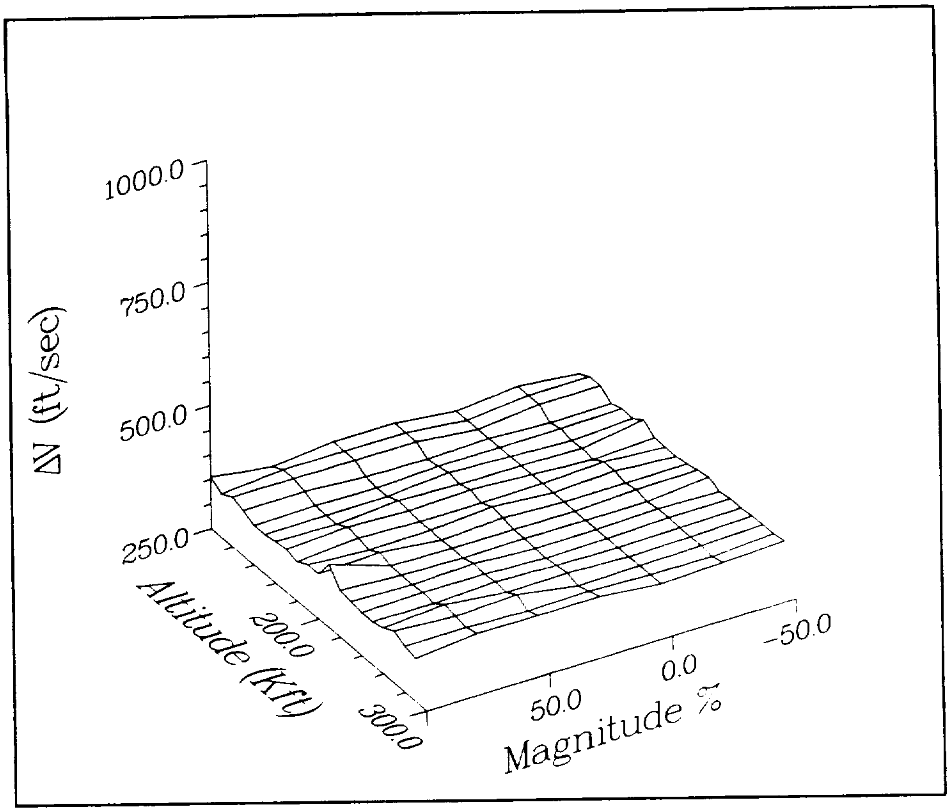

a)

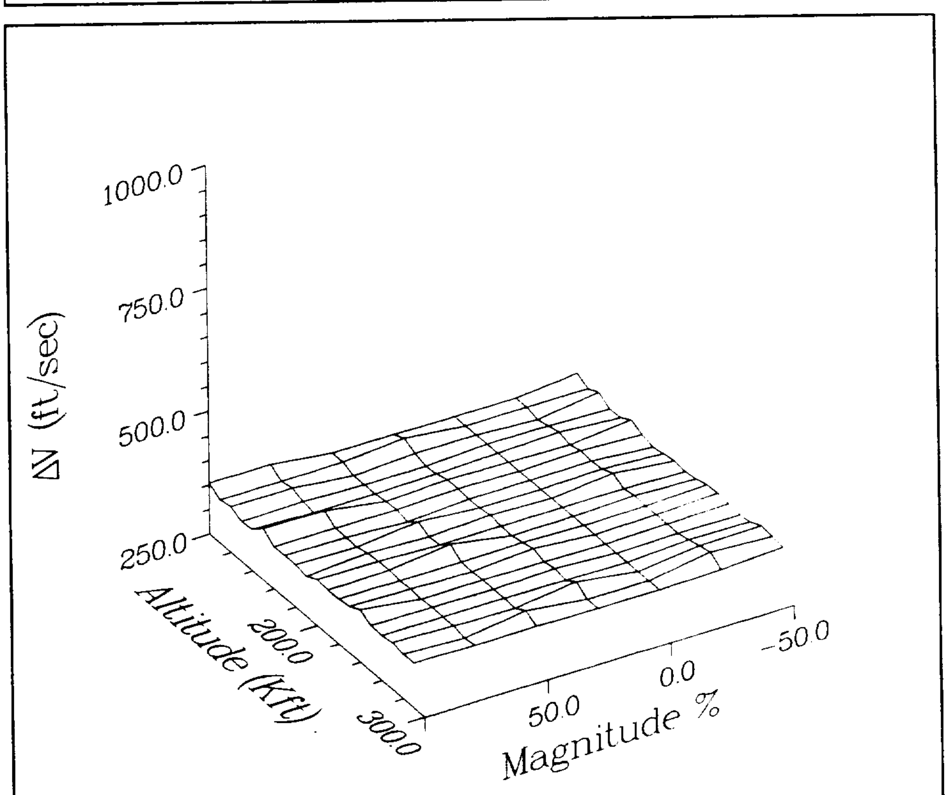

b)

Fig. 30 Mars Hybrid Predictor Corrector Sensitivity to Square Wave Density Pulses in High Density Atmosphere. a) 10000 ft Duration; b) 20000 ft Duration

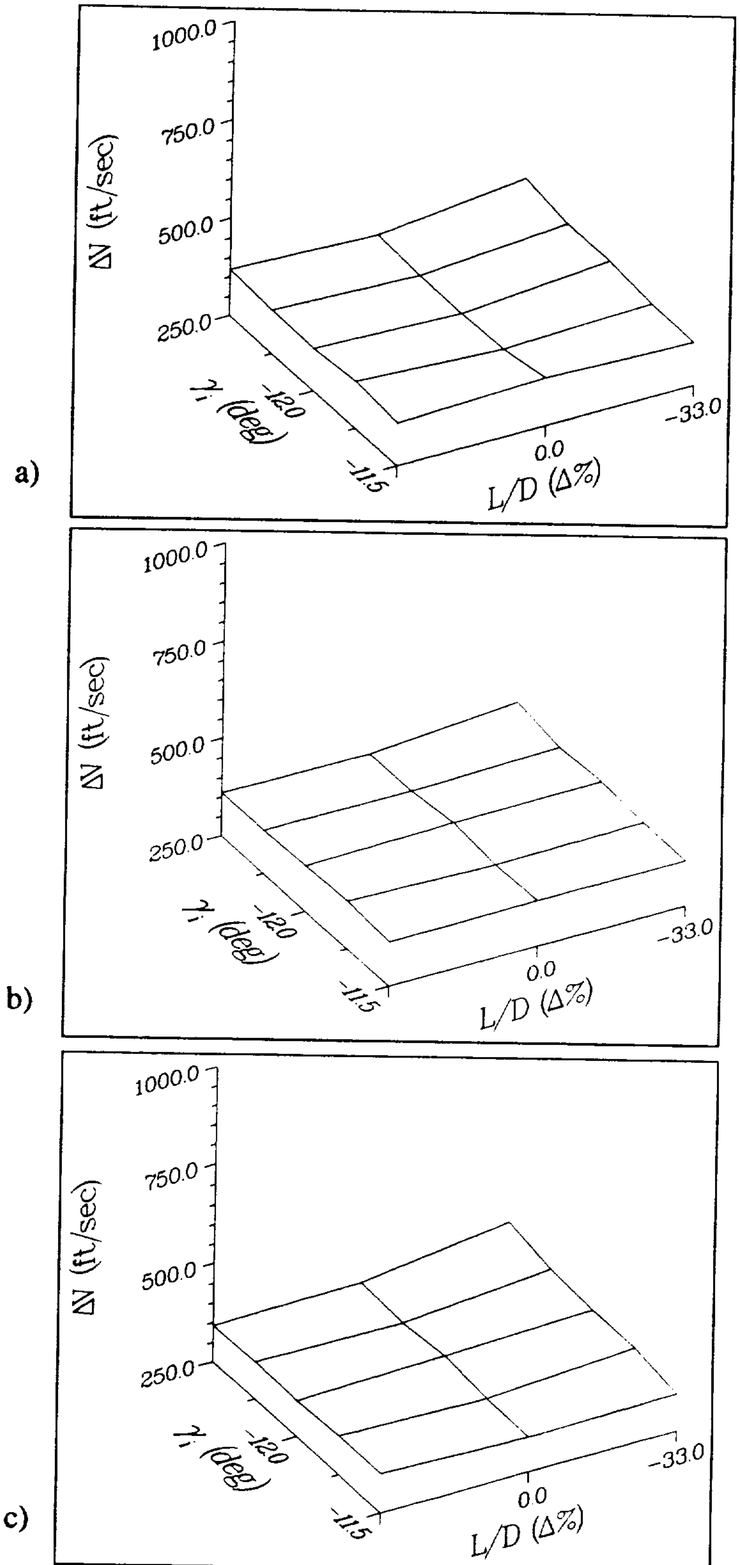

Fig. 31 Mars Hybrid Predictor Corrector Sensitivity to Variations in Lift to Drag Ratio and Entry Flight Path Angle. a) Nominal Atmosphere; b) Low Density Atmosphere; c) High Density Atmosphere

the results in a low density atmosphere and Fig. 30 in a high density atmosphere. In all of these cases the controller is able to guide the vehicle to the targeted exit state almost perfectly. With this controller the required ΔV following a maneuver in a high density atmosphere is slightly less than that in a nominal atmosphere, which is in turn slightly less than that in a low density atmosphere. These results are in agreement with those found using the Conjugate Gradient optimization technique outlined in Appendix A.

The performance when the vehicle lift and drag characteristics are varied and when the entry flight path angle is varied (Fig. 31) are equally promising. The reader is cautioned that the results presented here were all generated with density functions which are simply functions of altitude. The density function for the outbound leg of the trajectory is identical to the density on the inbound leg. The density estimator in this control algorithm gives excellent results when the outbound density function matches that measured while inbound, and the control algorithm is able to guide the vehicle to near perfect exit state whenever it is supplied with a good density function estimate. Later, in Chapter 5 the performance will be evaluated whenever the inbound and outbound density functions differ.

Mars Predictor Corrector Performance Results

The Mars Predictor Corrector (MPC) Control Algorithm differs from the MHPC of the previous section only in the density estimation technique employed. The MPC measures and stores density every second during the descent into the atmosphere. These density measurements are then normalized using a two stage exponential function. The resulting normalized data are fit with a sixth order polynomial in altitude. This polynomial is continually updated throughout the trajectory after each density measurement is taken. Again, the resulting density estimate is used to compute the velocity loss yet to occur due to aerodynamic drag.

The data generated during the simulations of this phase of the evaluation of the MPC were not as good as those from the MHPC. This density estimation technique might be expected to perform slightly worse, certainly no better, than the hybrid density estimation technique whenever the inbound and outbound density functions are the same. The strength of this density estimation technique is expected to be for those cases to be studied later when the inbound and outbound density functions are different (Again, such simulations are analyzed in Chapter 5).

The performance of this algorithm is presented in Figs. 32, 33, 34, and 35. The first three of these figures present the results when square wave density pulses are imbedded in the Martian atmosphere, while the last figure shows the results of varying lift-to- drag ratios and the entry flight path angle.

The performance of this algorithm as depicted in the following four figures, though not as good as that of the MHPC, is still quite acceptable. The worst performance noted here, caused by a 20,000 ft duration, +75% density pulse in the high density atmosphere located between 180,000 and 200,000 ft, required 457 ft/sec to attain the desired orbit. This algorithm, when faced with variations in entry flight path angle and L/D, produces practically flat performance maps that are very near the idealized near-optimal values calculated using the method of Appendix A.

a)

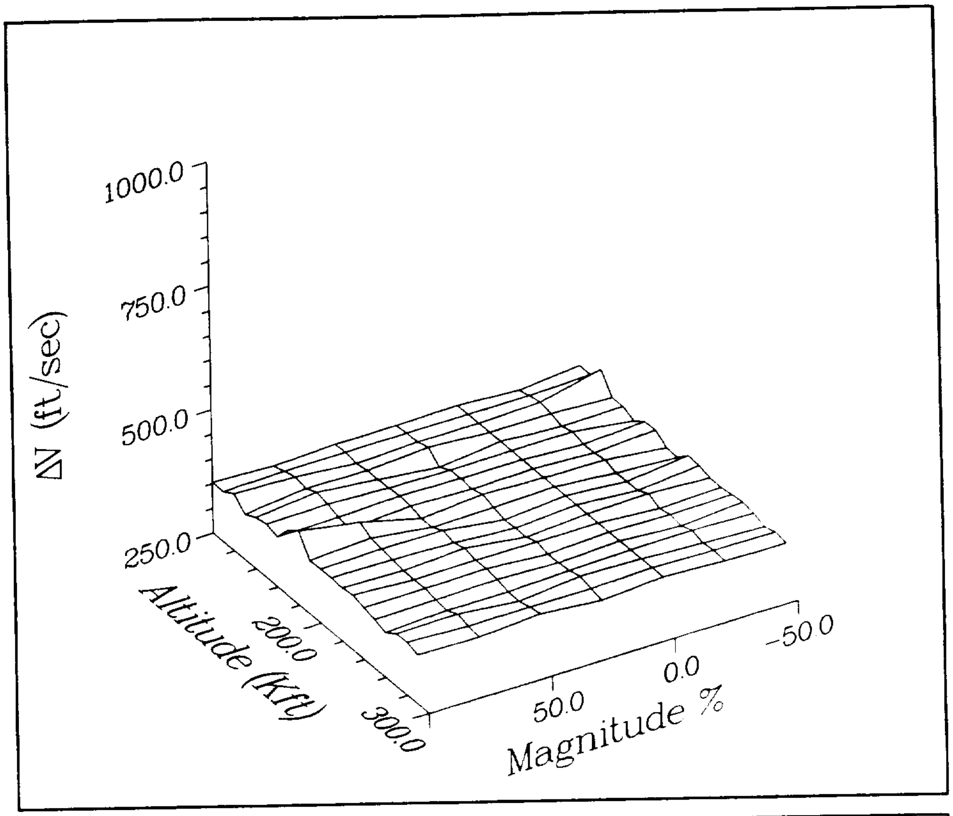

b)

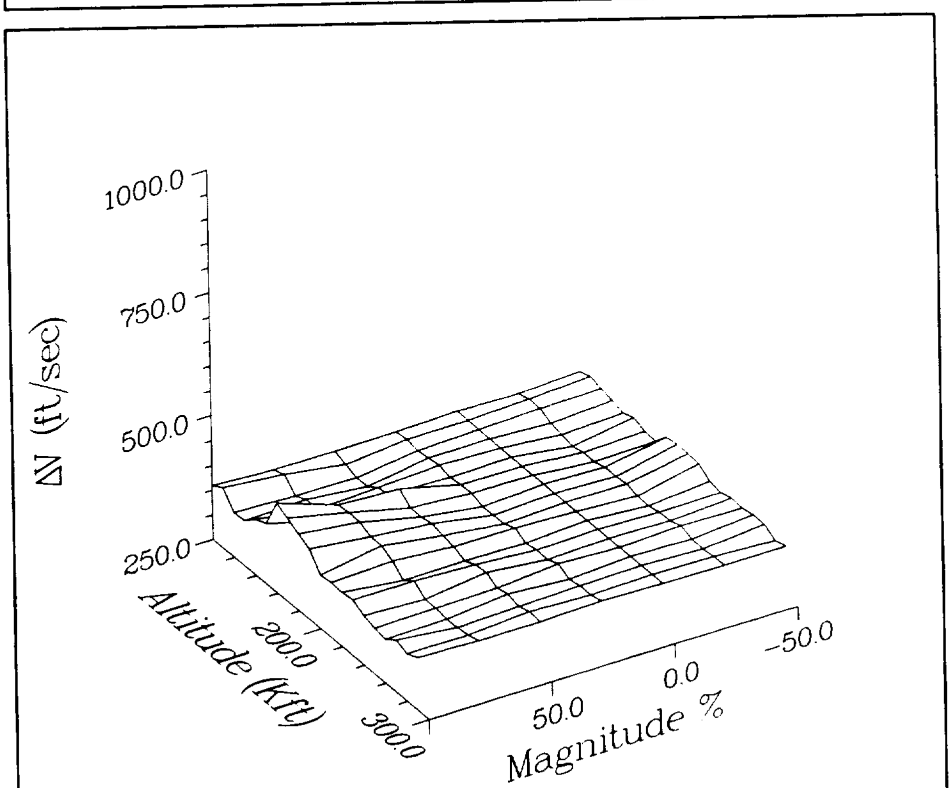

Fig. 32 Mars Predictor Corrector Sensitivity to Square Wave Density Pulses in Nominal Atmosphere. a) 10000 feet Duration; b) 20000 feet Duration

a)

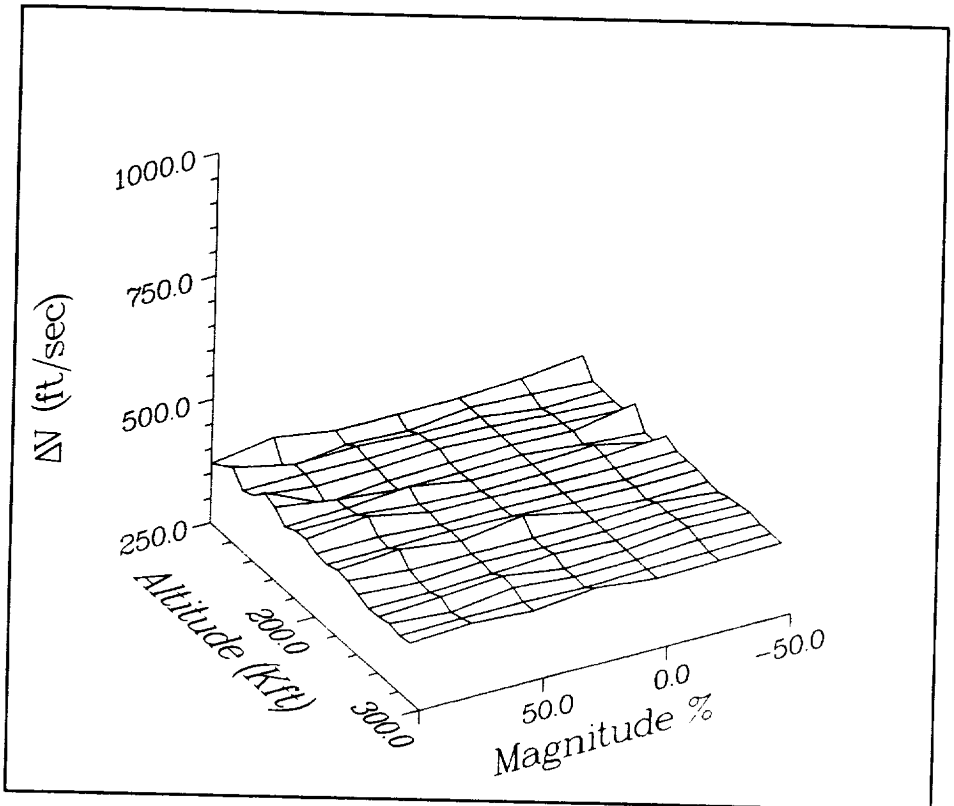

b)

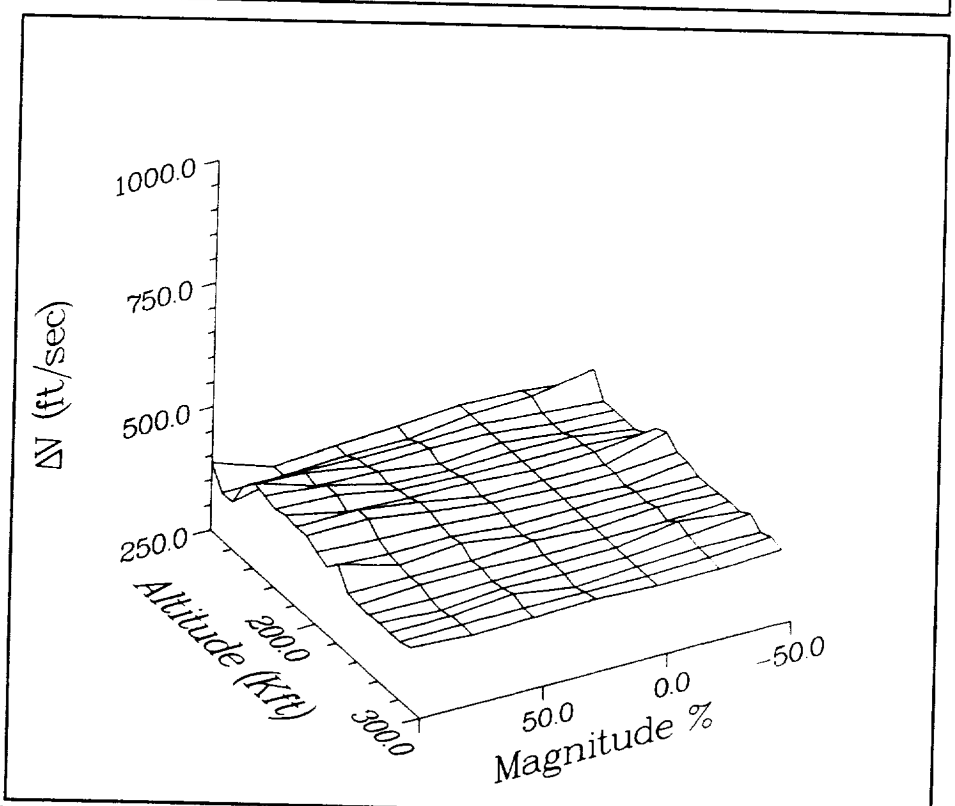

Fig. 33 Mars Predictor Corrector Sensitivity to Square Wave Density Pulses in Low Density Atmosphere. a) 10000 ft Duration; b) 20000 ft Duration

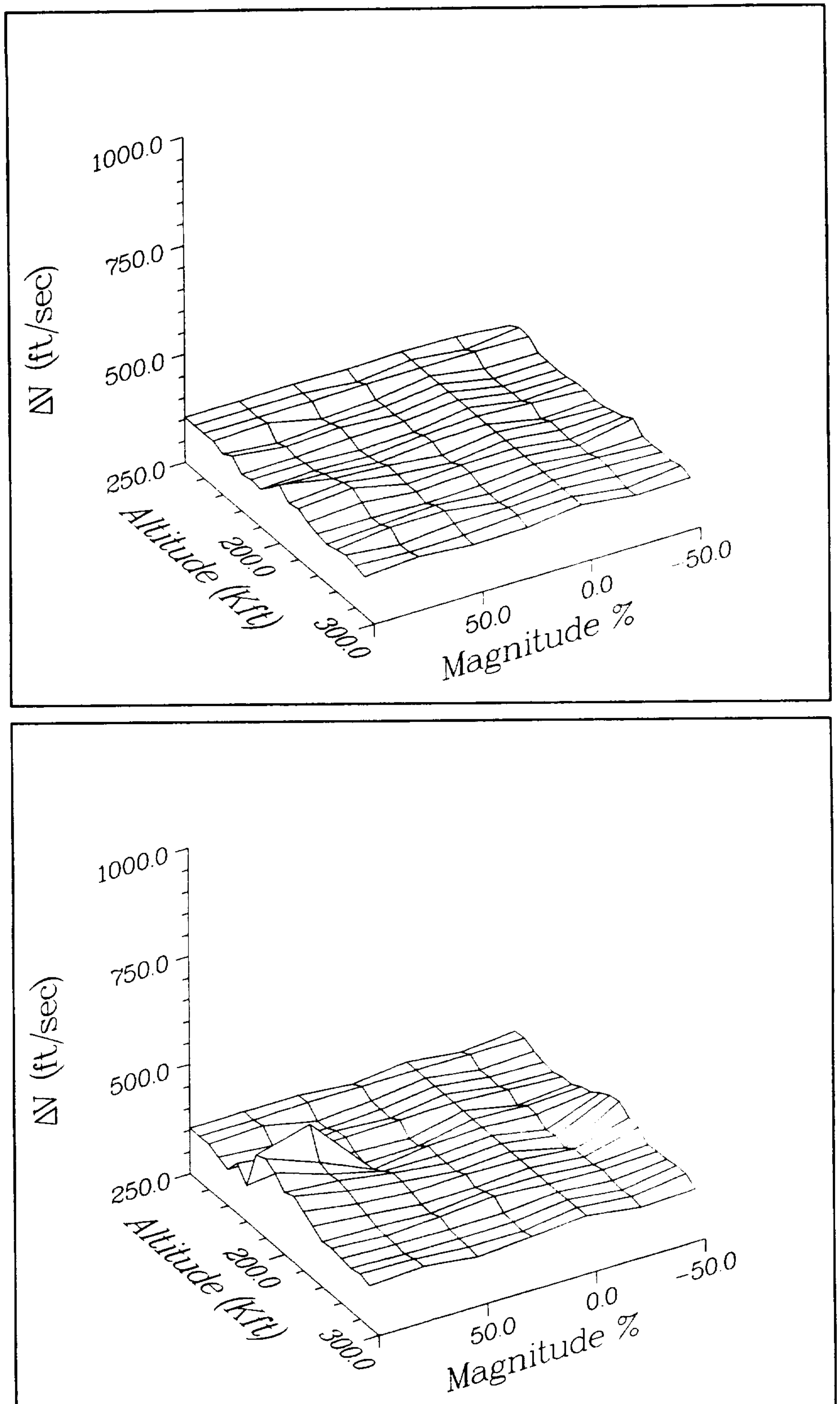

a)

b)

Fig. 34 Mars Predictor Corrector Sensitivity to Square Wave Density Pulses in High Density Atmosphere. a) 10000 ft Duration; b) 20000 ft Duration

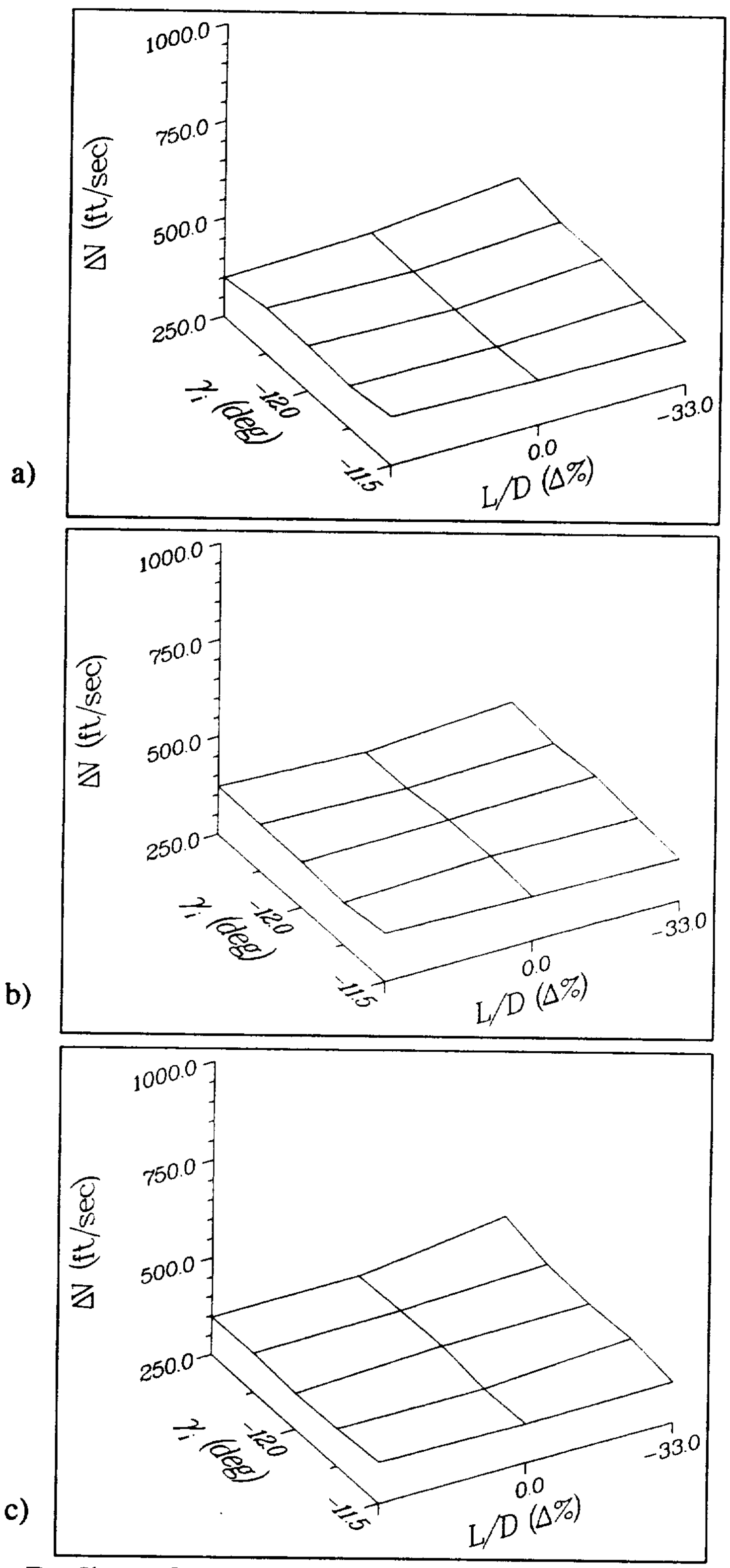

Fig. 35 Mars Predictor Corrector Sensitivity to Variations in Lift to Drag Ratio and Entry Flight Path Angle. a) Nominal Atmosphere; b) Low Density Atmosphere; c) High Density Atmosphere

Lyapunov Hybrid Tracking Controller Performance Results

The Lyapunov Hybrid Tracking Controller (LHPC), derived in Chapter 3, tied with the MHPC as the two best control algorithms for this phase of simulations. This controller uses an equilibrium glide phase for the first part of the trajectory and a Lyapunov Tracking exit phase using Lyapunov steepest descent techniques to steer the trajectory onto a target path. The target path selected is a 450 ft/sec constant altitude rate path which will lead the vehicle to the desired apocenter altitude.The transition velocity for switching from the equilibrium glide phase to the LHTC exit phase is varied using the technique of Chapter 2. The hybrid density estimation technique presented in Chapter 2 is used to define the desired path and to select the appropriate transition velocity.

Testing this controller against the same perturbations considered earlier in this chapter produced excellent results. The results of injecting square wave density pulses into the nominal atmosphere, low density atmosphere, and high density atmosphere are summarized in Figs. 37 and 38, respectively. The results of varying L/D and entry flight path angle are illustrated in Fig. 39.

This controller showed outstanding results for the density variations postulated for this set of simulations, showing practically no sensitivity to any of the perturbations. Again, however, the same caution presented in the MHPC performance results section should be repeated here: this simulated density is simply a function of altitude. The density function for the outbound leg of the trajectory is identical to the density on the inbound leg. The density estimation technique employed in this controller should excel under this condition. The robustness with respect to horizontal density variations must be evaluated to fairly generalize the evaluation of this (or any other) guidance scheme.

a)

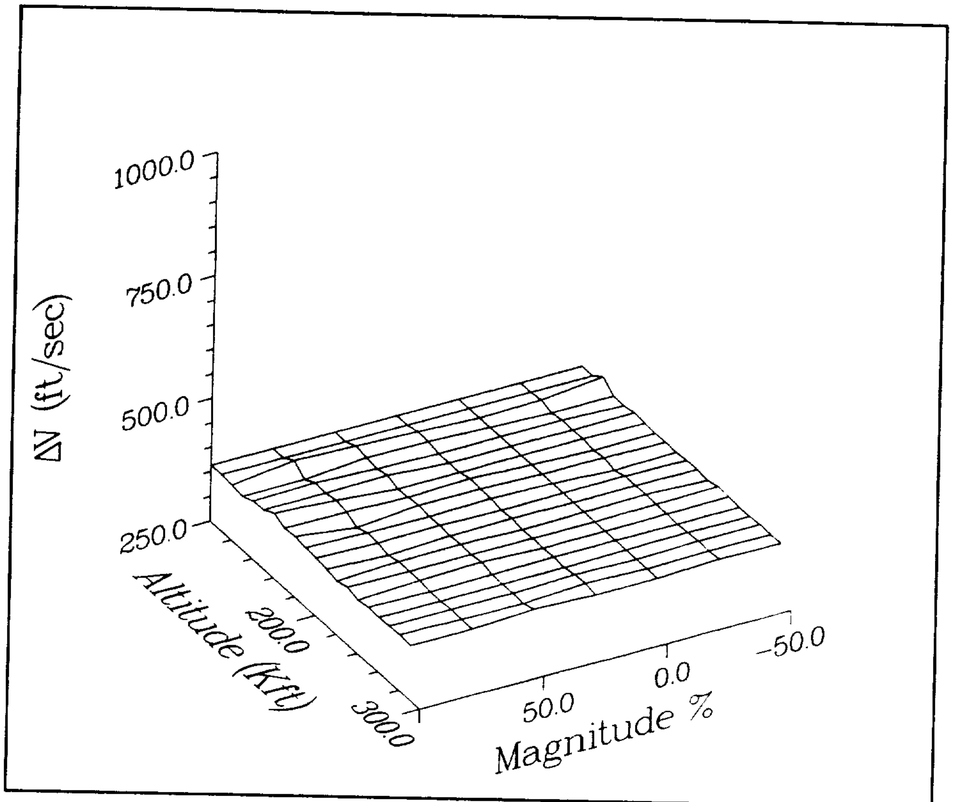

b)

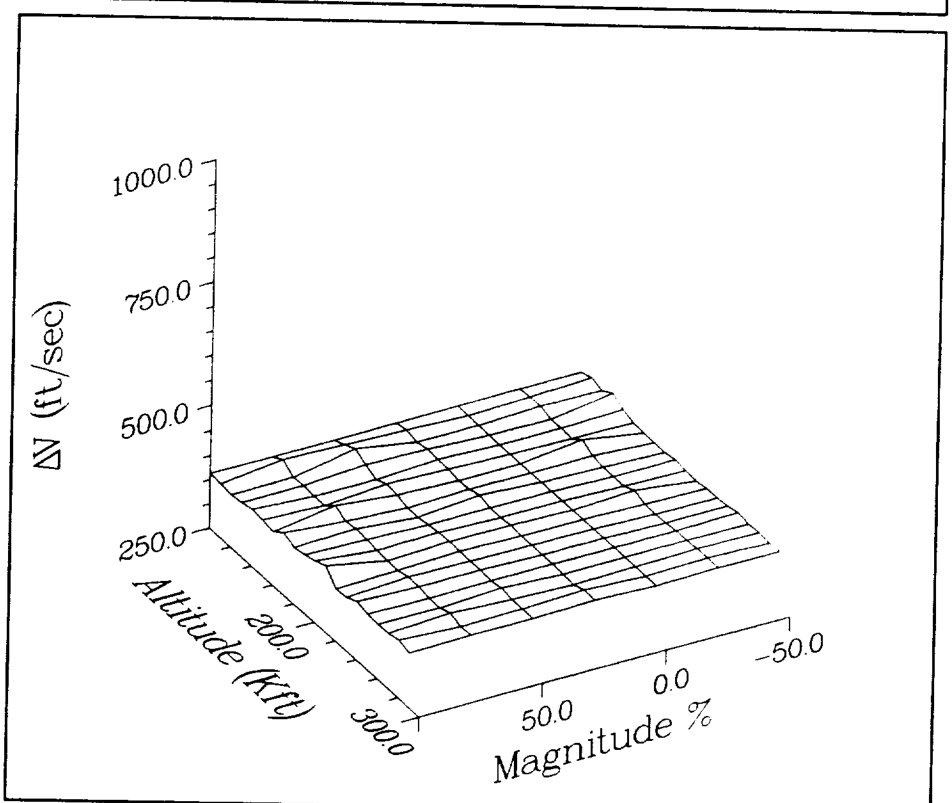

Fig. 36 Lyapunov Hybrid Tracking Controller Sensitivity to Square Wave Density Pulses in Nominal Atmosphere. a) 10000 feet Duration; b) 20000 feet Duration

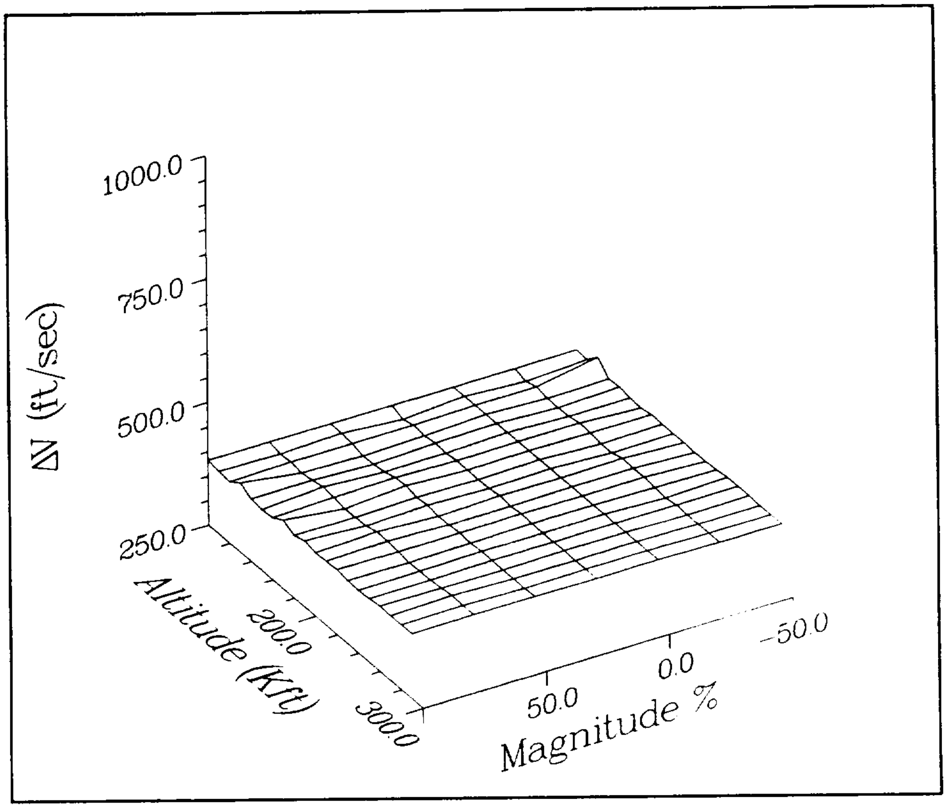

a)

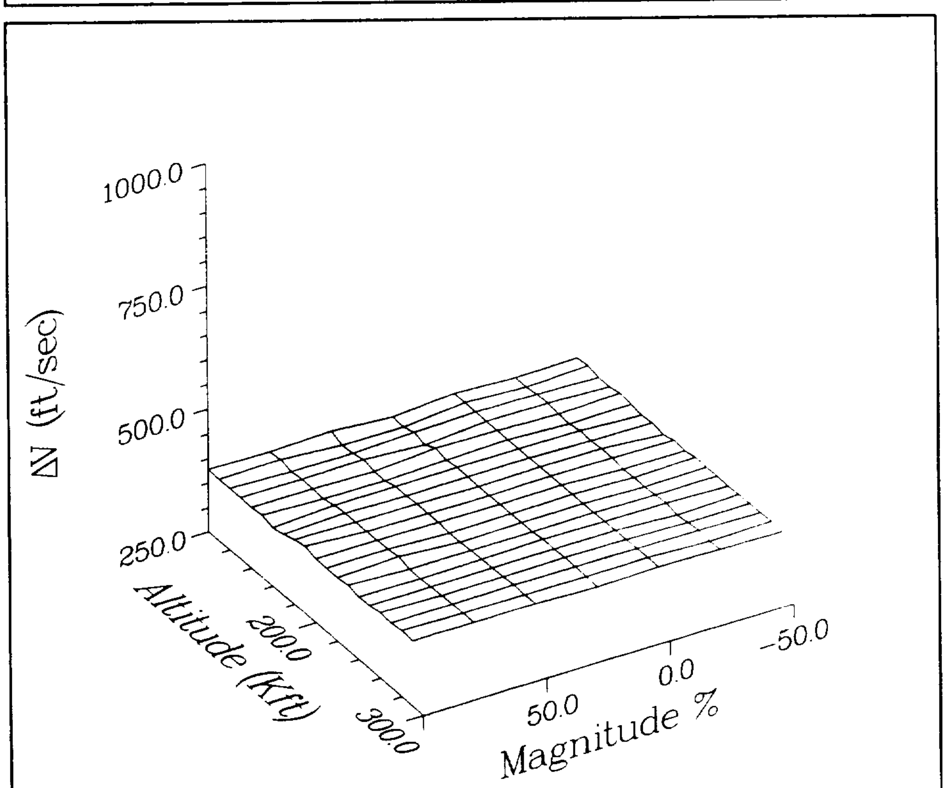

b)

Fig. 37 Lyapunov Hybrid Tracking Controller Sensitivity to Square Wave Density Pulses in Low Density Atmosphere. a) 10000 feet Duration; b) 20000 feet Duration

a)

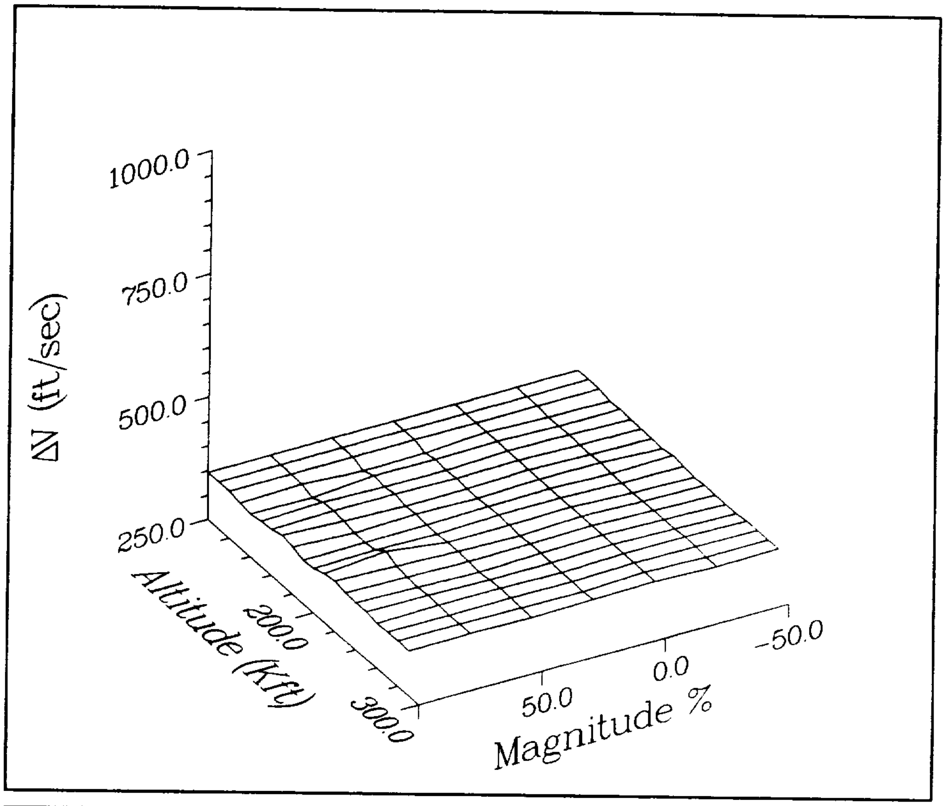

b)

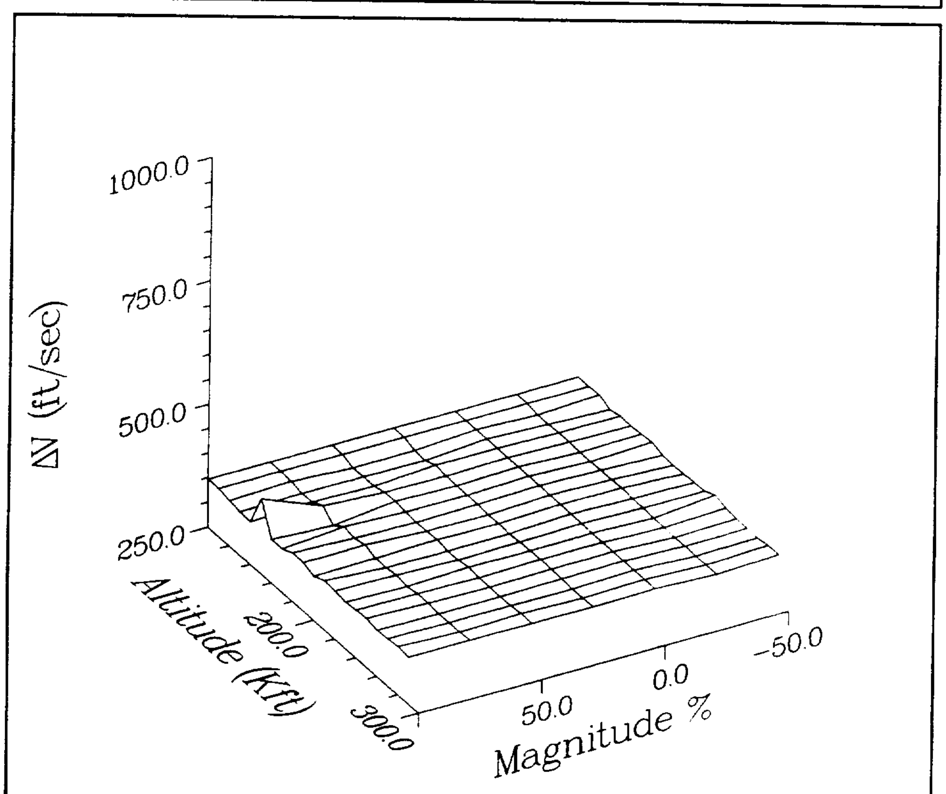

Fig. 38 Lyapunov Hybrid Tracking Controller Sensitivity to Square Wave Density Pulses in High Density Atmosphere. a) 10000 feet Duration; b) 20000 feet Duration

a)

b)

c)

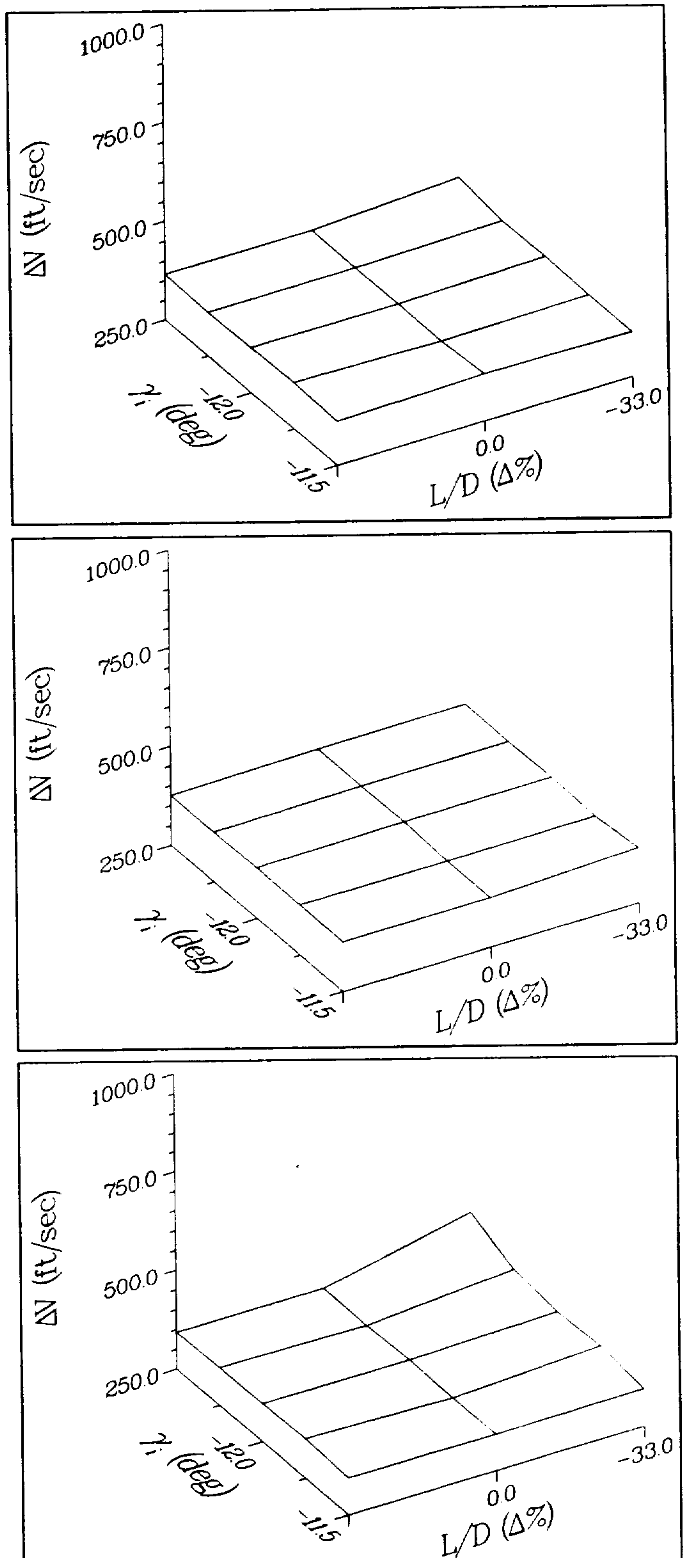

Fig. 39 Lyapunov Hybrid Tracking Controller Sensitivity to Variations in Lift to Drag Ratio and Entry Flight Path Angle. a) Nominal Atmosphere; b) Low Density Atmosphere; c) High Density Atmosphere

Lyapunov Tracking Controller Performance Results

The LTC differs from the LHTC algorithm only in the density estimation technique. The LHTC employs the polynomial density estimator described in Chapter 2, while the LHTC uses the hybrid density estimation technique. The performance of this controller appears to be slightly degraded from the performance of the LHTC at about the same level that the performance of the MPC was worse than that of the MHPC. The performance is still acceptable and, as was stated in the analysis of the MPC's performance, the strength of this density estimation technique is expected to surface when the outbound and inbound density functions differ.

Figures 40, 41, and 42 illustrate the results of the square wave density pulses which perturb the nominal, low and high density atmosphere, respectively. Varying L/D and entry flight path angle is depicted in Fig. 43. The worst performance noted during these simulations using the LTC required 464 ft/sec to attain the desired orbit. This peak was caused by a +75% density pulse perturbing the high density atmosphere between 180,000 and 200,000 ft. But again, even this worst case is considered to be acceptable.

Selection of Controllers to Proceed

The next stage of simulation was very intensive, requiring approximately sixty hours of computer time to fully test each controller. In an effort to limit this test matrix, only those controllers which showed promise of being able to handle the perturbations used in this chapter were to proceed to the next phase. The original plan was to select the two most promising controllers, and validate them. But, after analyzing the data presented in this chapter four controllers were selected for the next phase of testing. The four selected were the MHPC, the MPC, the LHTC and the LTC. The four selected are actually two

a)

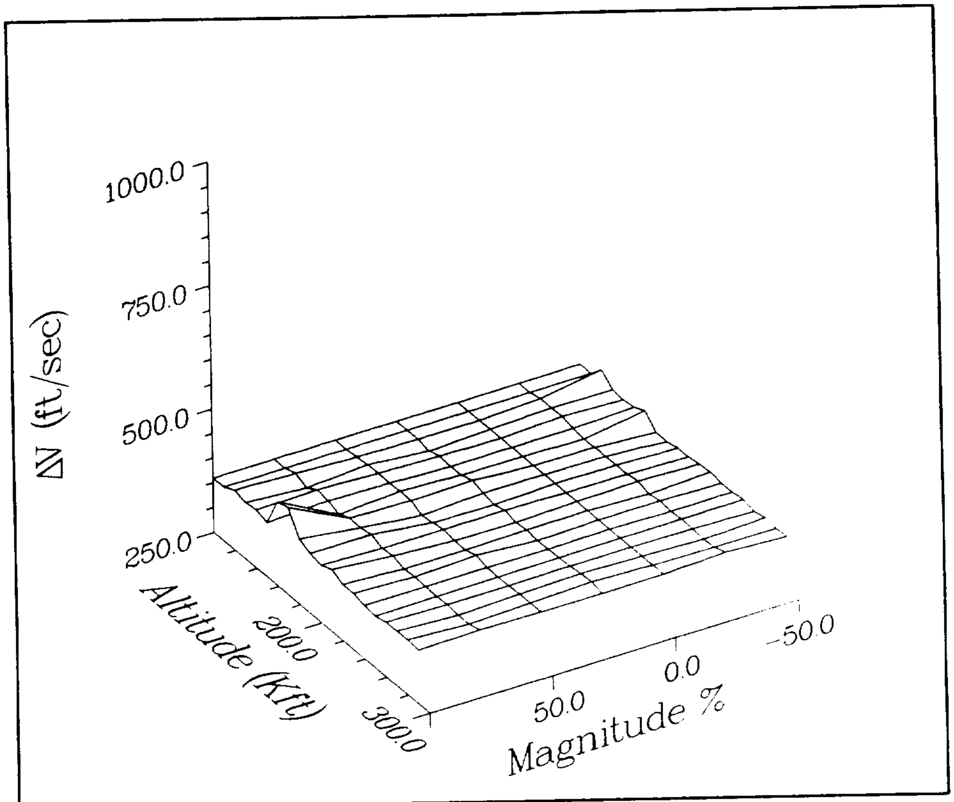

b)

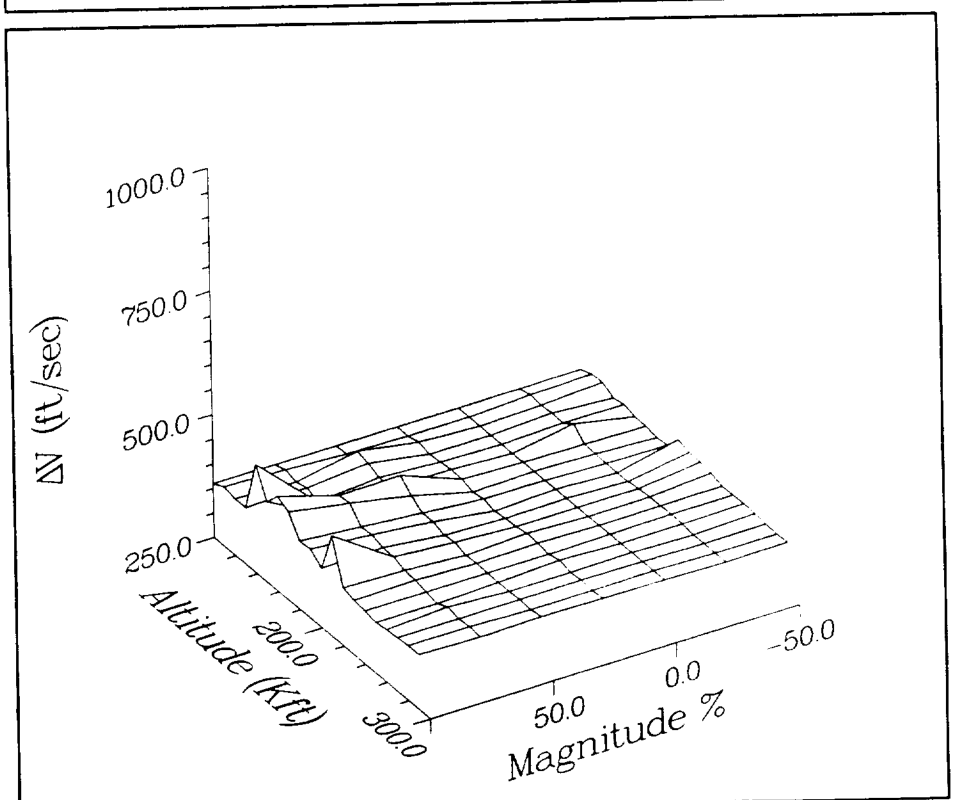

Fig. 40 Lyapunov Tracking Controller Sensitivity to Square Wave Density Pulses in Nominal Atmosphere. a) 10000 feet Duration; b) 20000 feet Duration

a)

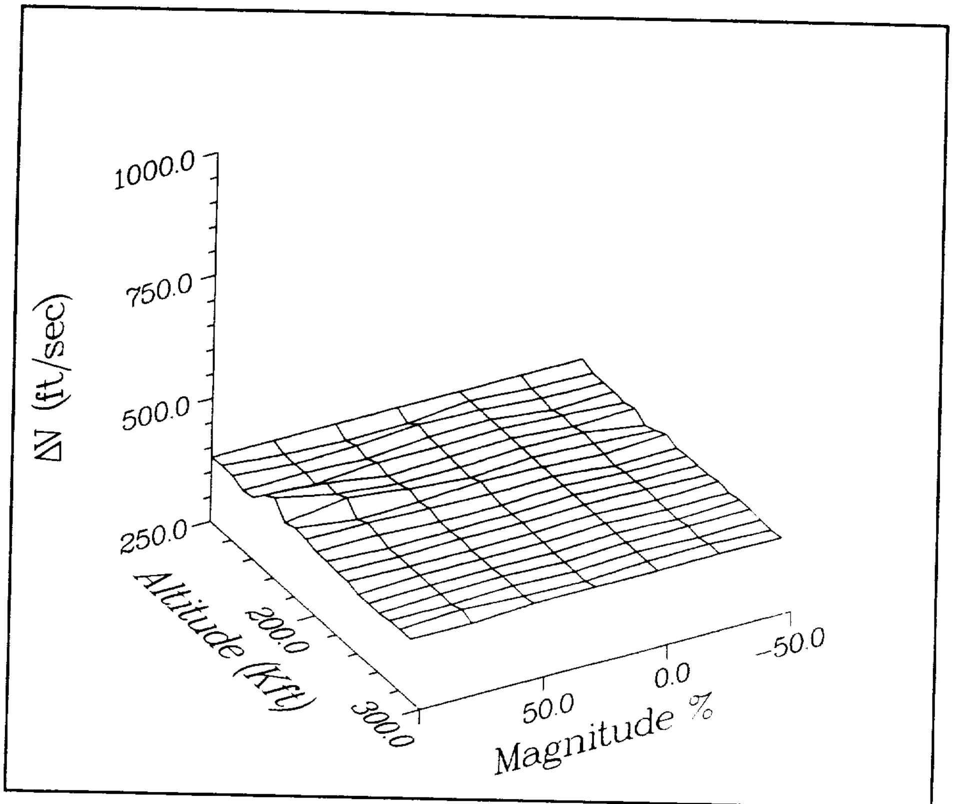

b)

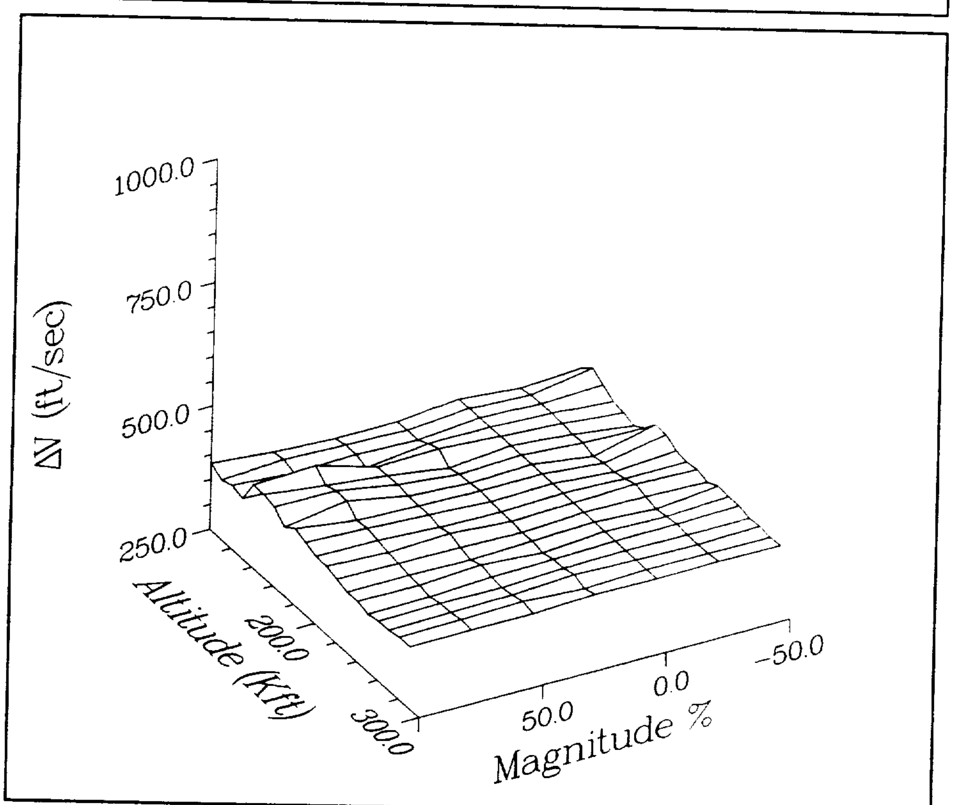

Fig. 41 Lyapunov Tracking Controller Sensitivity to Square Wave Density Pulses in Low Density Atmosphere. a) 10000 feet Duration; b) 20000 feet Duration

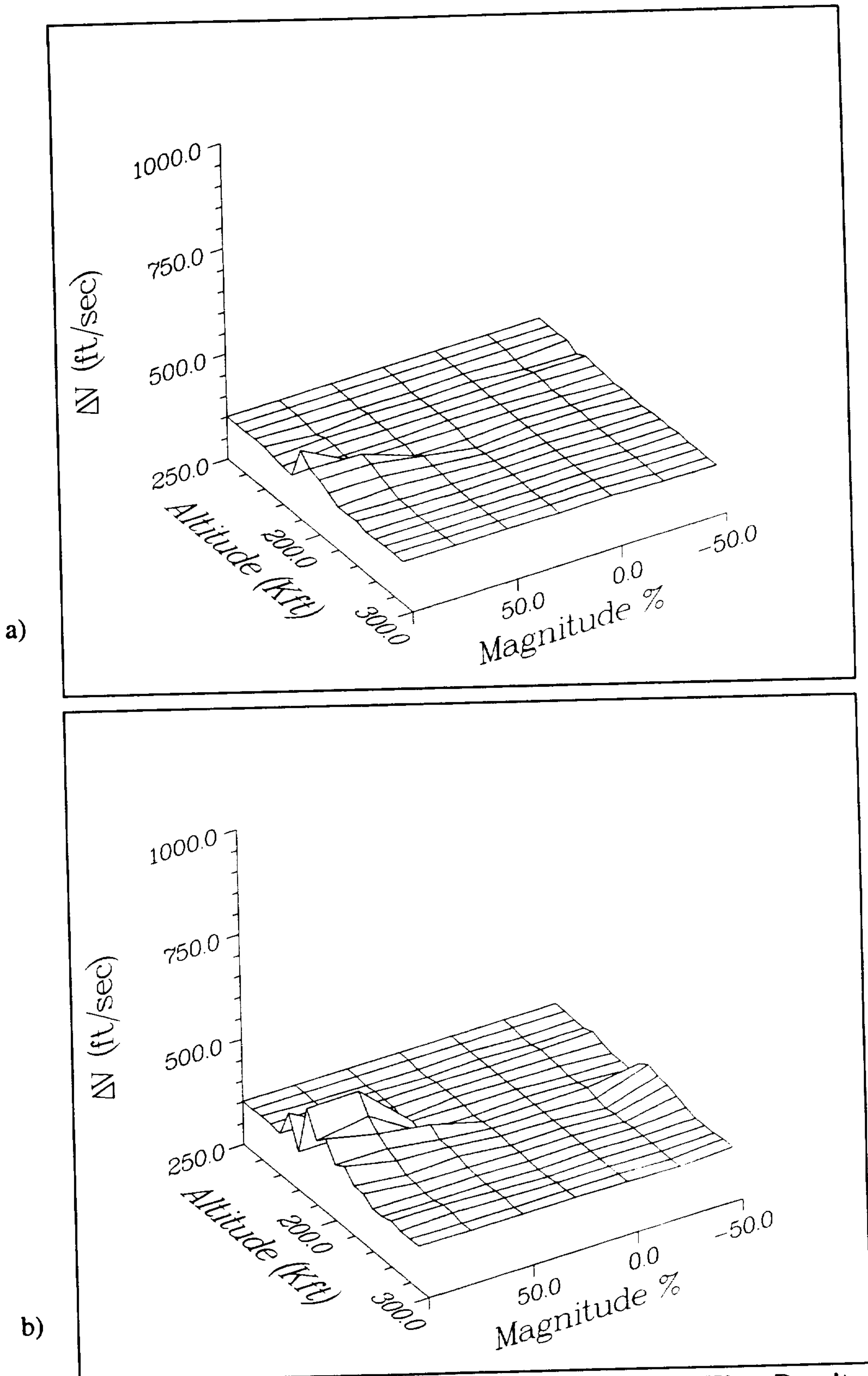

Fig. 42 Lyapunov Tracking Controller Sensitivity to Square Wave Density Pulses in High Density Atmosphere. a) 10000 feet Duration; b) 20000 feet Duration

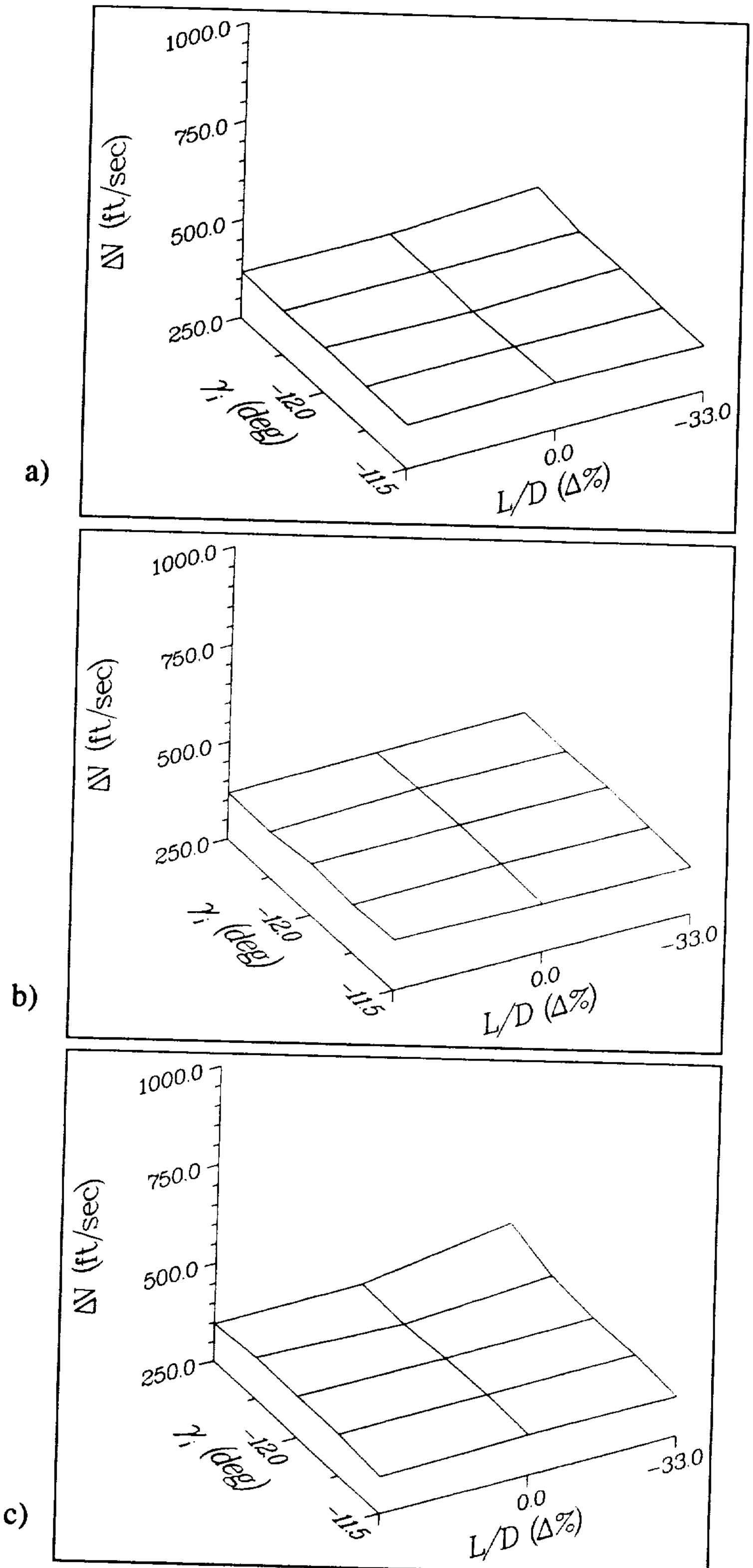

Fig. 43 Lyapunov Tracking Controller Sensitivity to Variations in Lift to Drag Ratio and Entry Flight Path Angle. a) Nominal Atmosphere; b) Low Density Atmosphere; c) High Density Atmosphere

control techniques, each employing two different methods of density estimation. All four of these controllers were able to handle the full range of testing performed during this phase without requiring more than 500 ft/sec to attain the desired orbit for any perturbation. The limitation of this set of simulations is that the inbound and outbound density functions are always the same. In the next chapter the performance of these four control algorithms will be investigated with different inbound and outbound density functions.

CHAPTER V

DETERMINATION OF ROBUSTNESS LIMITS

Determination of the robustness limits of the MHPC, MPC, LHTC and LTC, and selection of the most robust algorithm of these four is the goal of this chapter. Chapter 4 showed that these four algorithms are all capable of handling extreme variations in the vehicle L/D, entry flight path angle and in the density function, provided the density function is a simple function of altitude. This chapter will examine the effect of more realistic density functions which differ for the inbound and outbound legs of the trajectory. This will be accomplished by again injecting square wave density pulses into the density function, but this time the pulses will only perturb the outbound leg of the trajectory. In addition sinusoidal variations in altitude and in vehicle range will be used to perturb the density function. The control algorithms will also be tested using the actual density profiles measured by the Viking 1 and Viking 2 landers.

To determine the robustness limits success and failure must first be defined. Because the vehicle has not been designed yet, the fuel budget for maneuvering the vehicle has not been defined. The definition of success and failure used here is somewhat arbitrary, though it is believed to be close to the actual definition. Success is defined as any aerobraking trajectory which requires 500 ft/sec or less of propulsive maneuvering (ΔV) to attain the desired final orbit. As in Chapter 4, ΔV is computed with three components, one propulsive maneuver applied at the atmospheric interface in the direction of the velocity vector to correct the apocenter altitude, a second at apocenter to raise pericenter and a third to correct any plane error. Because of the lack of a firm definition of vehicle characteristics a grey area has been defined. The grey area is any trajectory which requires between 500 and 1,000 ft/sec. Any trajectory which requires between 500 and 1000 ft/sec to attain the desired orbit will be referred to as a soft failure. Any vehicle design should certainly carry enough fuel to perform 500 ft/sec of maneuvering to attain the desired orbit. Carrying additional fuel, however, to correct for a soft failure of the aerobraking control system reduces the advantage of aerobraking. The trajectories which terminate with soft failures would still be able to attain orbit, though not the desired orbit, using 500 ft/sec of propulsive maneuvering. This anomaly may result in some mission degradation, but not a complete mission failure. A hard failure is defined to be any trajectory which requires 1,000 ft/sec or more of ΔV to attain the desired orbit. It includes any trajectories which fail to exit the atmosphere. By this definition, all four controllers considered in this chapter succeeded in all of the simulations performed in Chapter 4.

Outbound Leg Square Wave Density Pulses

The robustness test procedure begins by using square wave density pulses which perturb the density function of the outbound leg only. The density during the descent into the atmosphere is either the nominal or a MARS-GRAM generated low or high density atmosphere model. After the altitude rate becomes positive, a square wave density pulse, similar to those employed in Chapter 4 is used to perturb either a 10,000 or a 20,000 ft altitude band of the atmosphere. These pulses multiply the density predicted by the atmosphere model by 0.5, 0.75, 1.25, 1.5, 1.75 or 2.0 within the perturbed altitude band. The pulses are again referred to as -50%, -25%, +25%, +50%, +75% and +100% magnitude density pulses, respectively. As in Chapter 4, the pulses are moved in 10,000 ft altitude intervals, with the lower edge of the density pulse located between 100,000 and 290,000 ft. The performance is presented in Figs. 44 through 55 with ΔV plotted along the vertical axis while the magnitude of the pulse and the location of the lower edge are plotted on the other two axes.

MHPC Performance

Performance of the MHPC in the nominal, low and high density atmospheres when the density of the outbound leg of the trajectory is perturbed by square wave density pulses is presented in Figs. 44, 45, and 46, respectively. In the first plot of each figure the pulse perturbs a 10,000 ft altitude band, while in the second plot the pulse perturbs a 20,000 ft altitude band.

The MHPC produced many soft failures during this test sequence but no hard failures were recorded. The 20,000 ft duration pulses produce worse performance than the 10,000 ft duration pulses in almost all cases. The MHPC is very sensitive to large magnitude (+50% and +75%) density pulses located below 180,000 ft in the nominal atmosphere, and 150,000 or 200,000 ft in the low or high density atmosphere, respectively. There is also a region of sensitivity caused by the -50% 20,000 ft density pulses. These latter regions are located at slightly higher altitudes and are not as severe as those caused by the larger magnitude pulses. In all of these plots there is a region at extremely low altitudes, where the pulses have little or no effect. This robust region occurs because these pulses are either located below the minimum altitude of the trajectory and the satellite never flies in the perturbed atmosphere, or they are very near the minimum altitude of the trajectory and the satellite does not spend much time in the density fluctuations.

There are two primary failure modes for these trajectories. When the large magnitude density pulse affects the atmosphere in the altitude region where the satellite is in the equilibrium glide phase, the density filter is fooled into believing the entire atmosphere has higher density than that measured during the descent. The effect is to initiate the exit phase early, and predict a relatively high altitude rate for the exit phase. When the vehicle moves out of a high density region, there is a time lag before the density filter records the change. By the time the controller responds, the vehicle has moved even higher and the

a)

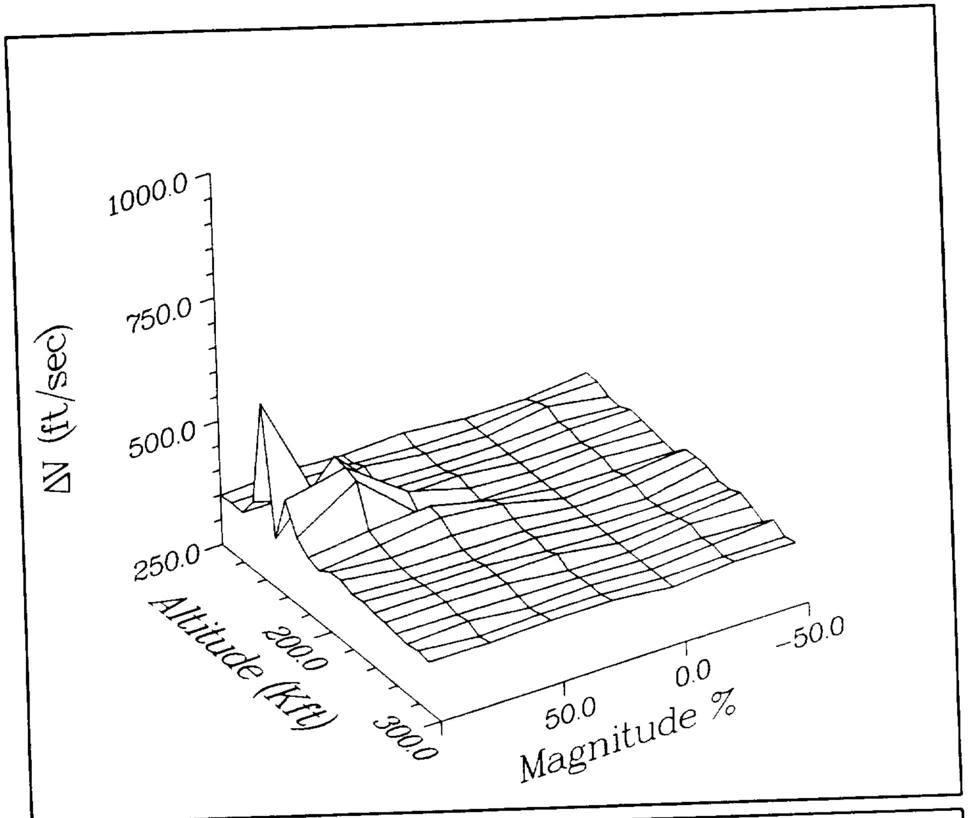

b)

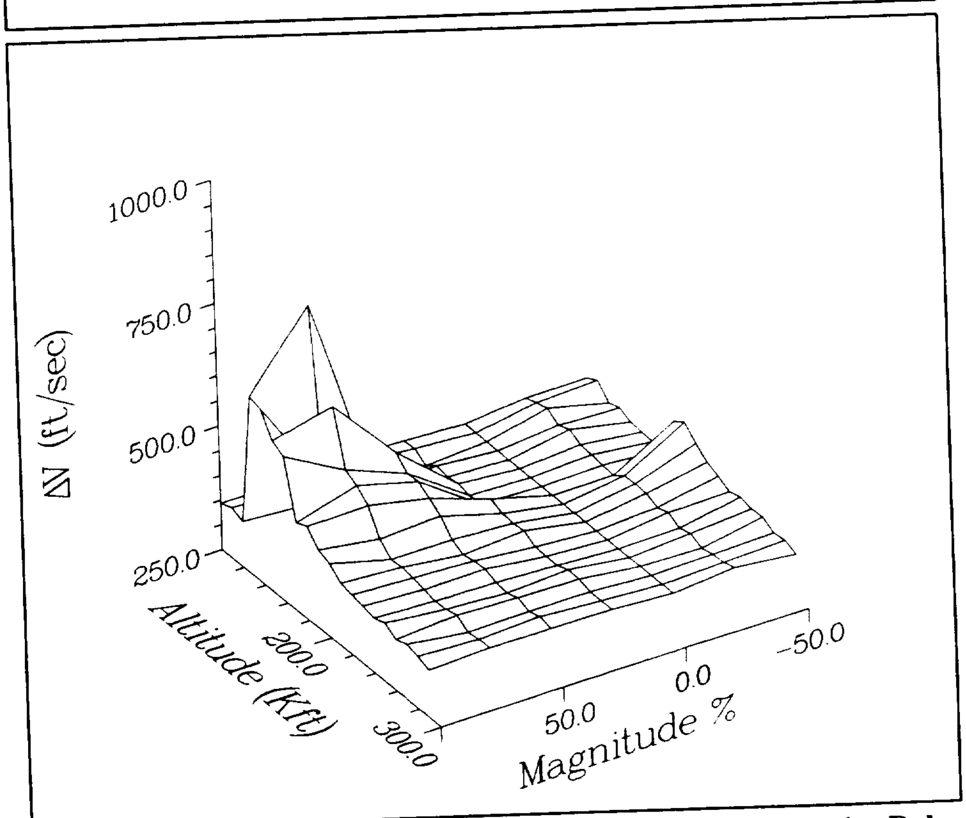

Fig. 44 MHPC Sensitivity to Outbound Leg Square Wave Density Pulses in Nominal Atmosphere. a) 10000 feet Duration; b) 20000 feet Duration

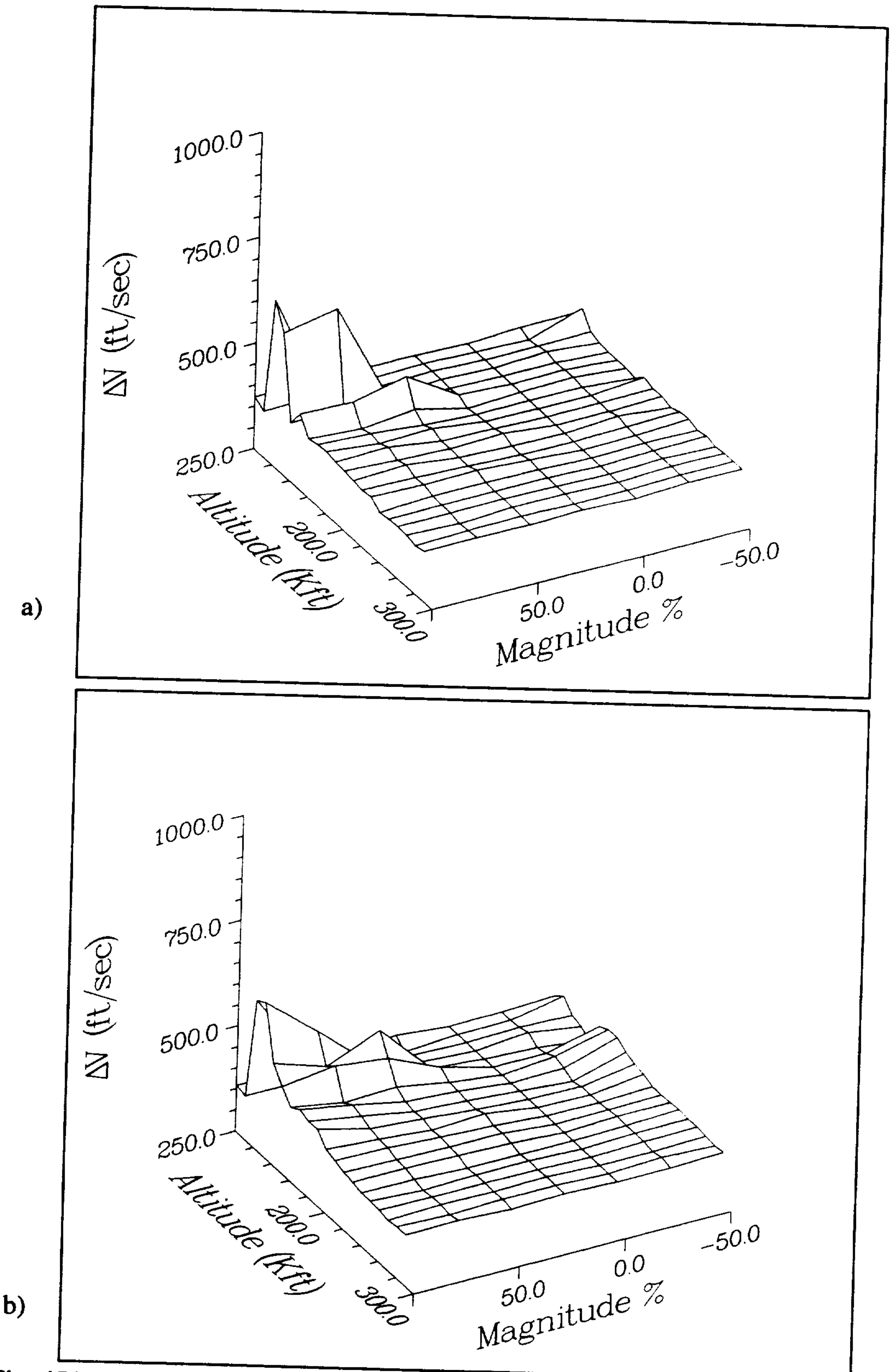

Fig. 45 MHPC Sensitivity to Outbound Leg Square Wave Density Pulses in Low Density Atmosphere. a) 10000 feet Duration; b) 20000 feet Duration

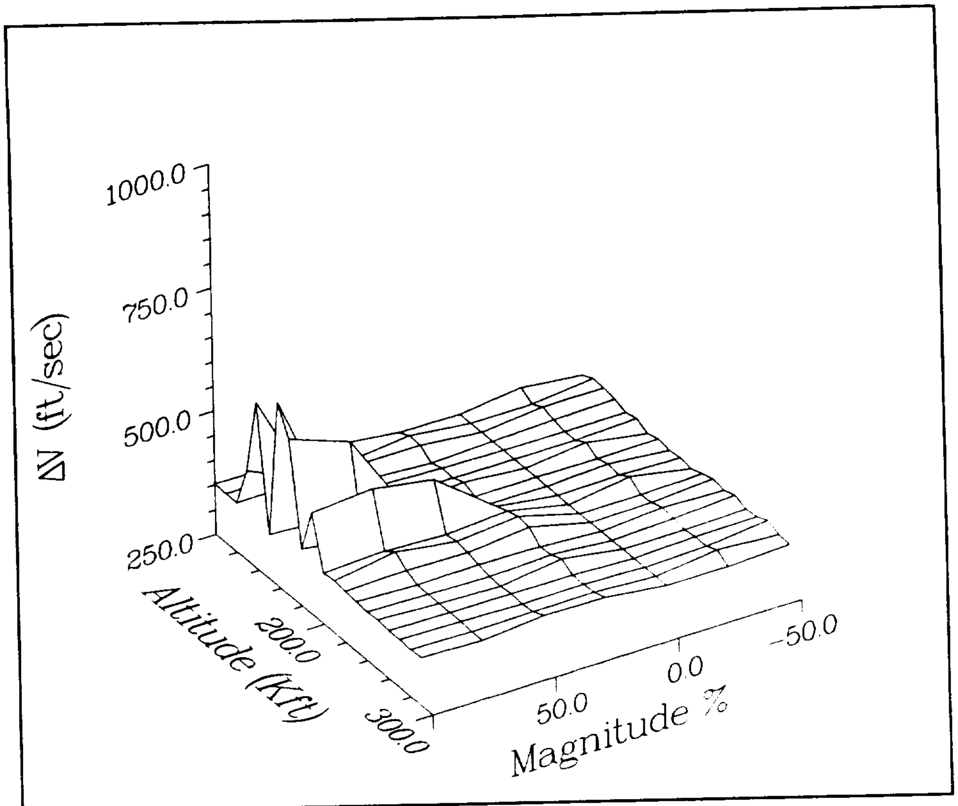

a)

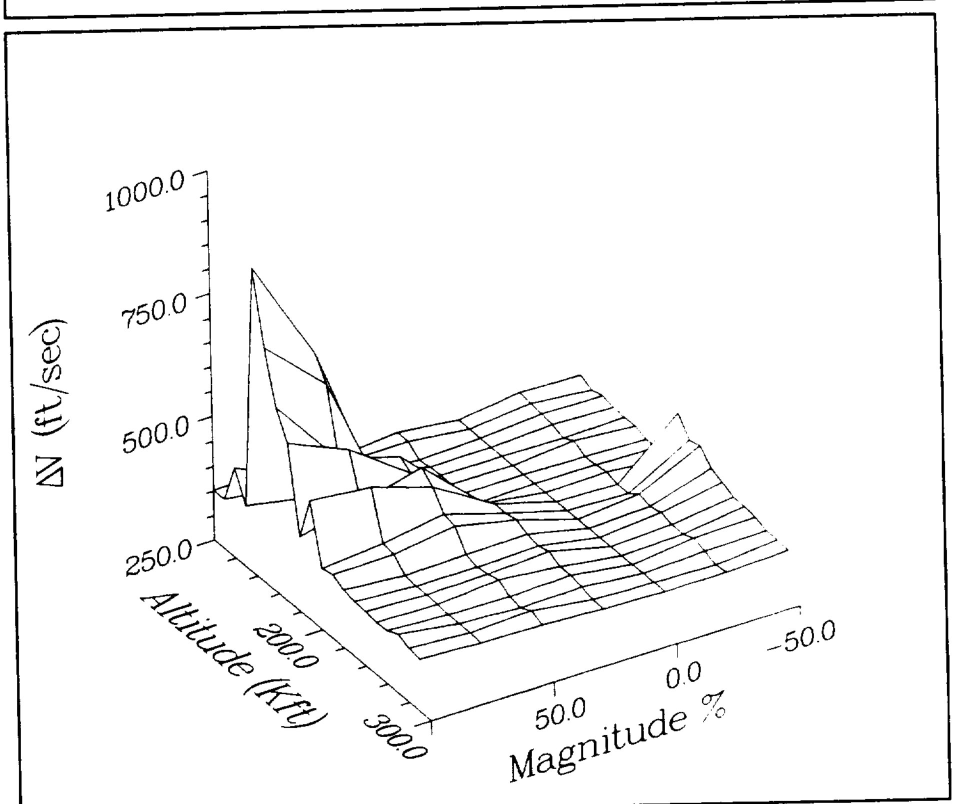

b)

Fig. 46 MHPC Sensitivity to Outbound Leg Square Wave Density Pulses in High Density Atmosphere. a) 10000 feet Duration; b) 20000 feet Duration

vehicle has less control authority. As a result the vehicle leaves the atmosphere with too much energy, and overshoots the desired apocenter altitude. The second failure mode is caused by higher altitude density pulses. All of the failures caused by the -50% pulses exhibited this failure mode. The vehicle flies the equilibrium glide phase in the unperturbed atmosphere. After the vehicle initiates the exit phase it encounters the perturbed atmosphere. The large magnitude density pulses dissipate more energy than predicted, resulting in a steeper exit phase, and in some cases, a lower apocenter than desired. Conversely, the small magnitude density pulses cause the vehicle to lose less energy than predicted and result in an apocenter altitude higher than desired.

MPC Performance

The MPC definitely performs better than the MHPC under these conditions. Again, the performance is presented in three figures, Figs. 47, 48, and 49, with the first figure showing results from the nominal atmosphere, the second from the low density atmosphere and the third from the high density atmosphere.

The 10,000 ft density pulses has almost no effect on the performance of this control algorithm. Even the 20,000 ft pulses produce reasonably good results. There is only one soft failure noted during this test sequence and two very near failures for the MPC. All three of these events are caused by 20,000 ft +100% density pulses perturbing the low density atmosphere. The pulse between 120,000 and 140,000 ft requires a ΔV of 584 ft/sec, while the pulse 10,000 ft higher (between 130,000 and 150,000 ft) requires 498ft/sec. The pulse between 140,000 and 160,000 ft requires just 458 ft/sec, but the one between 150,000 and 170,000 ft requires 492 ft/sec. These high ΔVs are caused by the same failure modes as described above with the pulses having lower edges at 120,000 and 130,000 ft causing the density estimator to overreact and force the vehicle to exit with too much ener-

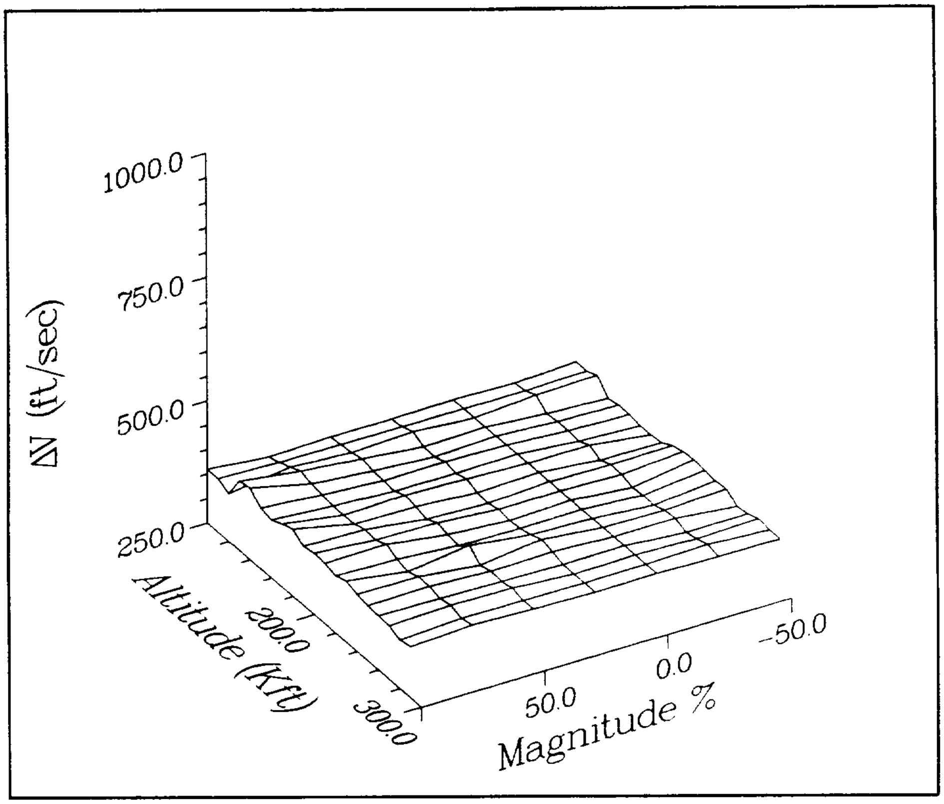

a)

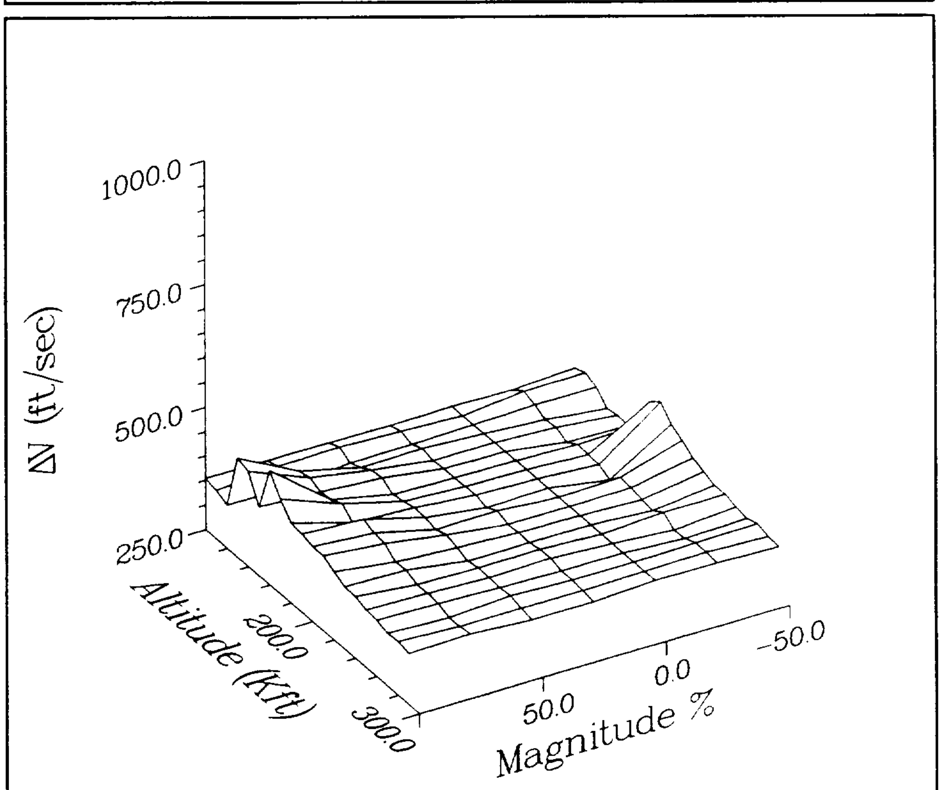

b)

Fig. 47 MPC Sensitivity to Outbound Leg Square Wave Density Pulses in Nominal Atmosphere. a) 10000 feet Duration; b) 20000 feet Duration

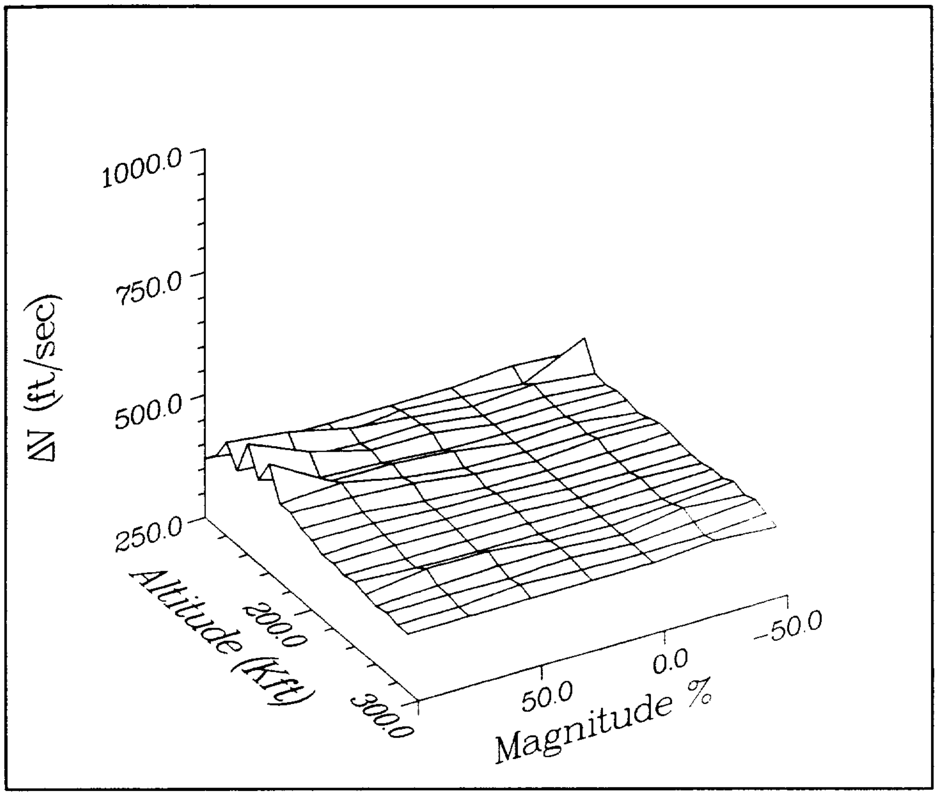

a)

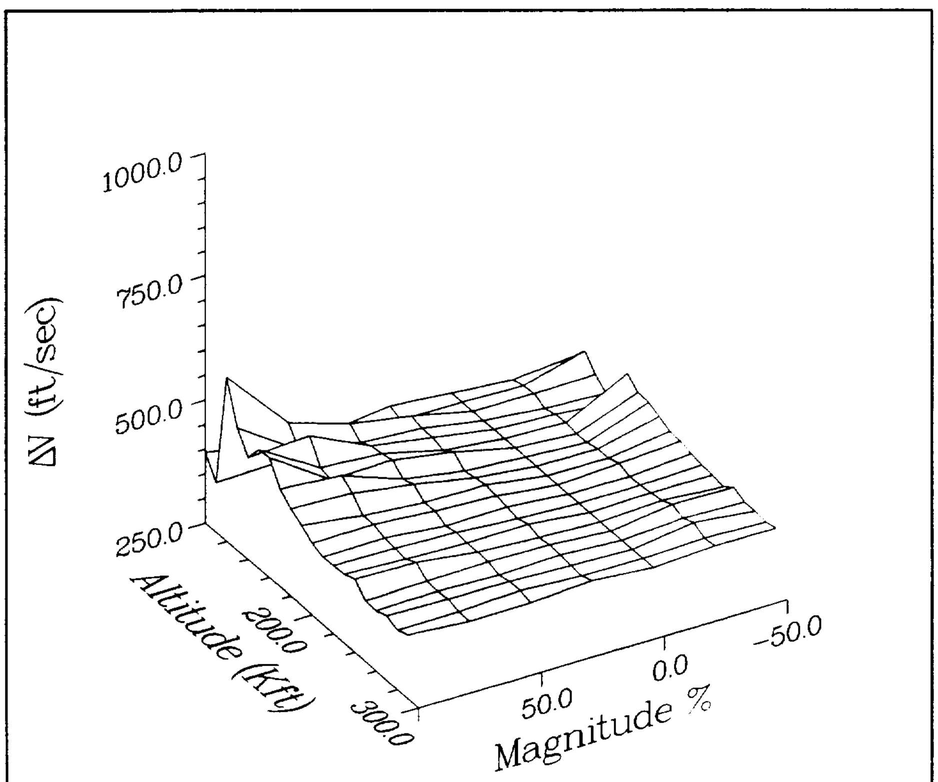

b)

Fig. 48 MPC Sensitivity to Outbound Leg Square Wave Density Pulses in Low Density Atmosphere. a) 10000 feet Duration; b) 20000 feet Duration

a)

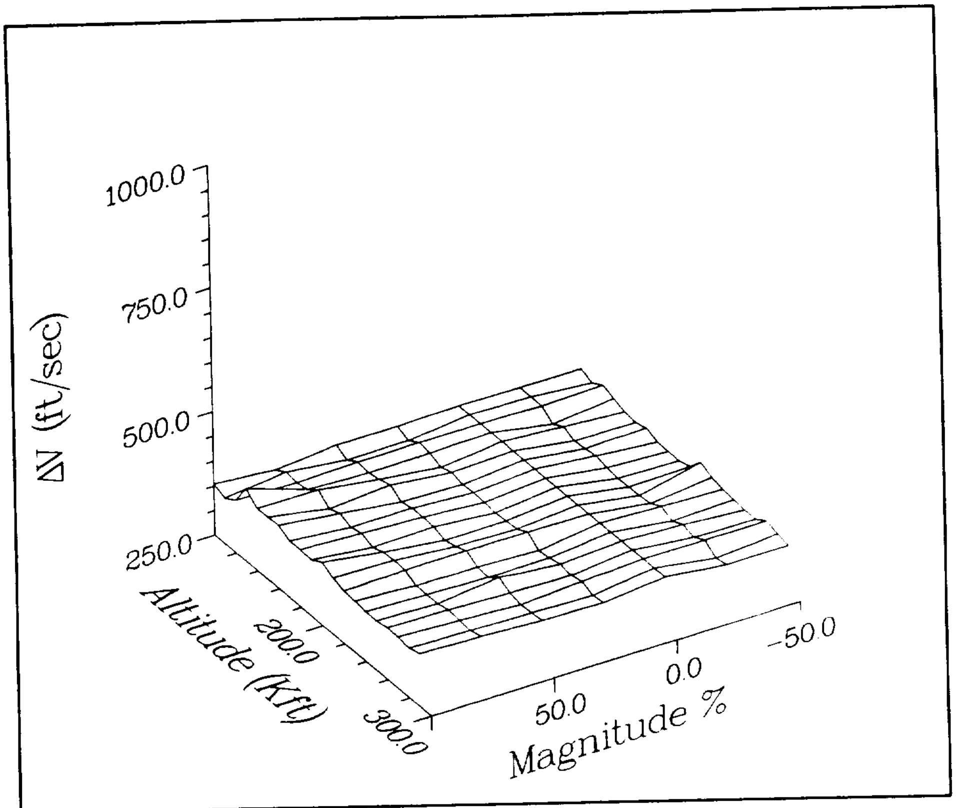

b)

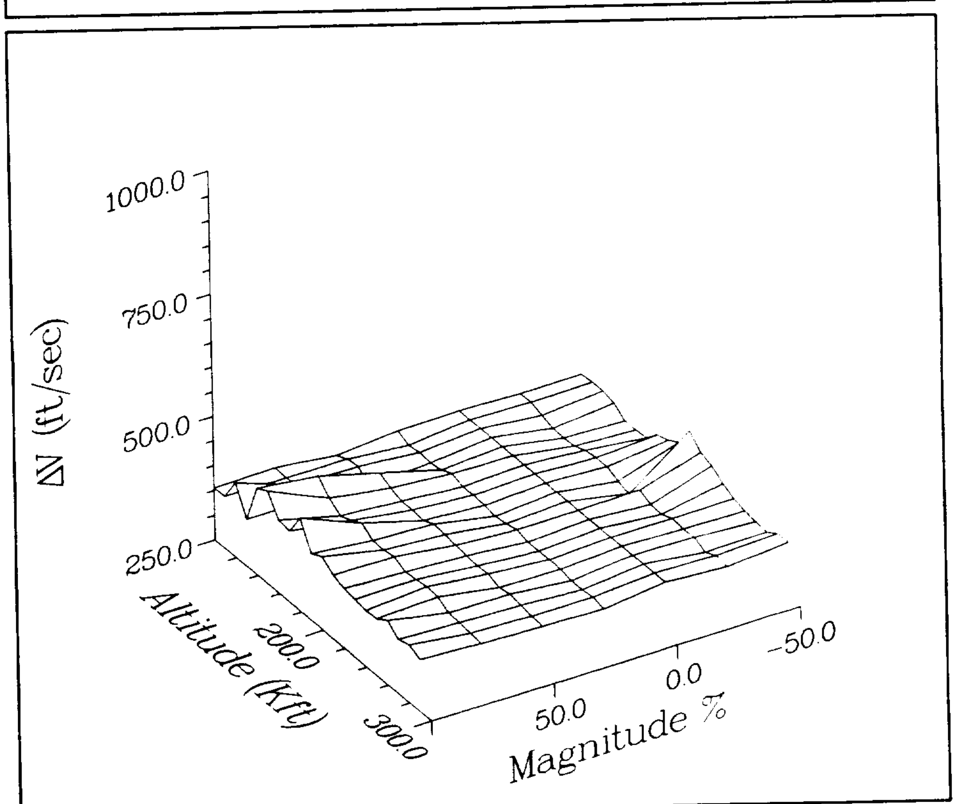

Fig. 49 MPC Sensitivity to Outbound Leg Square Wave Density Pulses in High Density Atmosphere. a) 10000 feet Duration; b) 20000 feet Duration

gy, while the pulse at 150,000 ft causes the vehicle to lose more energy than planned. Overall, the polynomial density estimator used in the MPC shows improvement over the hybrid density estimator of the MHPC. As suggested in Chapter 4, the promise of this density estimation technique is realized when the inbound and outbound density functions are different.

LHTC Performance

Performance of the LHTC is mixed. For the majority of density perturbations calculated here this controller performs better than either the MHPC or the MPC. Yet there are a few isolated instances where the controller performs extremely poorly. The controller even produces two hard failures. Presentation of this controller's performance follows the same format as before with the nominal atmosphere results in Fig. 50, the low density atmosphere results in Fig. 51 and the high density atmosphere results in Fig. 52.

One noteworthy aspect of the Lyapunov Tracking exit phase is that it almost always commands either full lift up or full lift down. When the vehicle is exactly on the desired path, the commanded bank angle chatters between ±15° and ±165° (commanded bank angles less than 15° or greater than 165° are allowed only when the orbit plane error is less than .03°). Of course, the vehicle roll rate and roll acceleration limits prevent the vehicle from oscillating too wildly. But, when the vehicle is not on the desired path the control system will command near full lift up, or full lift down to approach the trajectory. This feature allows the vehicle to respond more quickly than it does for the predictor corrector algorithms to pull the vehicle back onto the desired path. However, when the desired path is computed poorly because of a poor density estimate, the control system still responds by commanding full lift to approach the computed path as rapidly as possible. This controller also suffers from the same problems with the density estimator as the MHPC. This phenomena causes the two hard failures seen in Fig. 50b and Fig. 52b. The onboard accelerometer measurements records high drag measurements while the vehicle decelerates in the region of high density caused by the density pulse. The density filter predicts that, because of the measured high drags, the remainder of the atmosphere is also of higher density than that recorded during the descent. The effect is to predict higher energy loss due to this drag than actually occurs. This inaccurate prediction causes the control system to initiate the exit phase earlier than desired and to command a path which climbs out of the atmosphere at relatively high speed. As noted above, the Lyapunov optimal control solution pulls onto this path as rapidly as possible. By the time the satellite moves out of the high density region, and the density filter recognizes the change, the satellite is too high and is at a velocity which is too high too allow recovery. The result wis a post aerobraking apocenter altitude of 836 nm for the hard failure in Fig. 50b and 1,165 nm in Fig. 52b. Again, the target apocenter is 270 nm.

The Lyapunov Tracking exit phase, in spite of the two hard failures described in the previous paragraph, seems better able to cope with these density estimation problems than the predictor corrector algorithms. The rapid response of the vehicle is largely advantageous. The nature of the Lyapunov control system, though its agressive technique causes the two hard failures discussed above, is still desirable. As accelerometer measurements are taken and the density filter is continually updated, the desired path varies. The rapid response of the Lyapunov control law helps track this moving path as long as the vehicle has enough aerodynamic control authority to respond. In the LTC controller simulation results which follow, the effect of combining the polynomial density estimation technique with the fast response of the Lyapunov control scheme is further explored.

a)

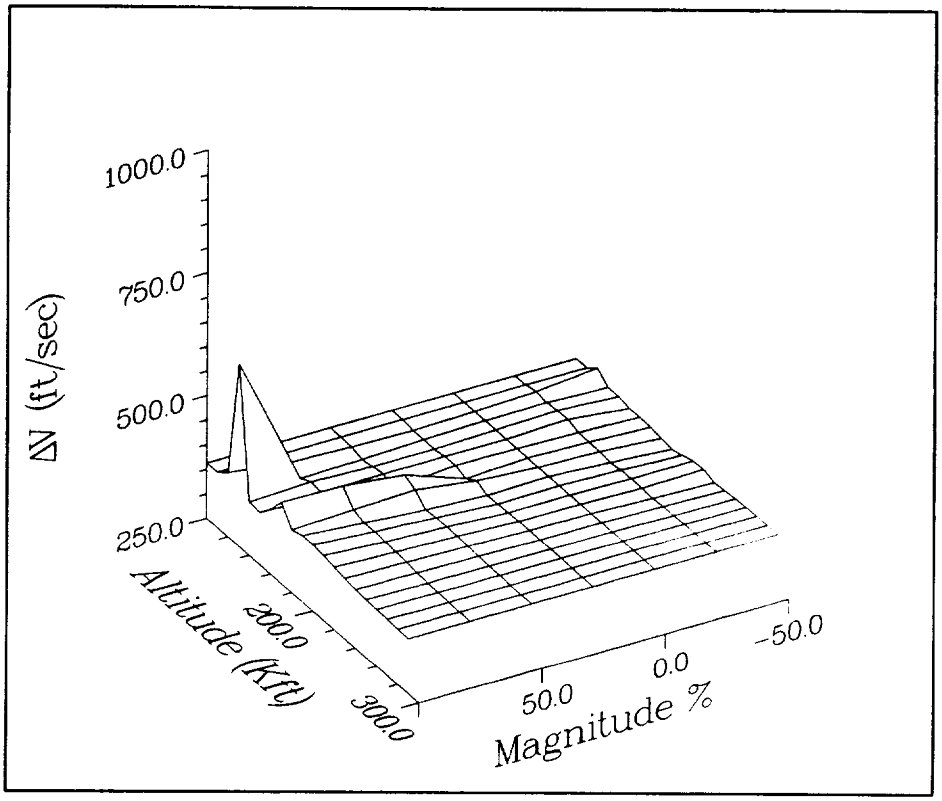

b)

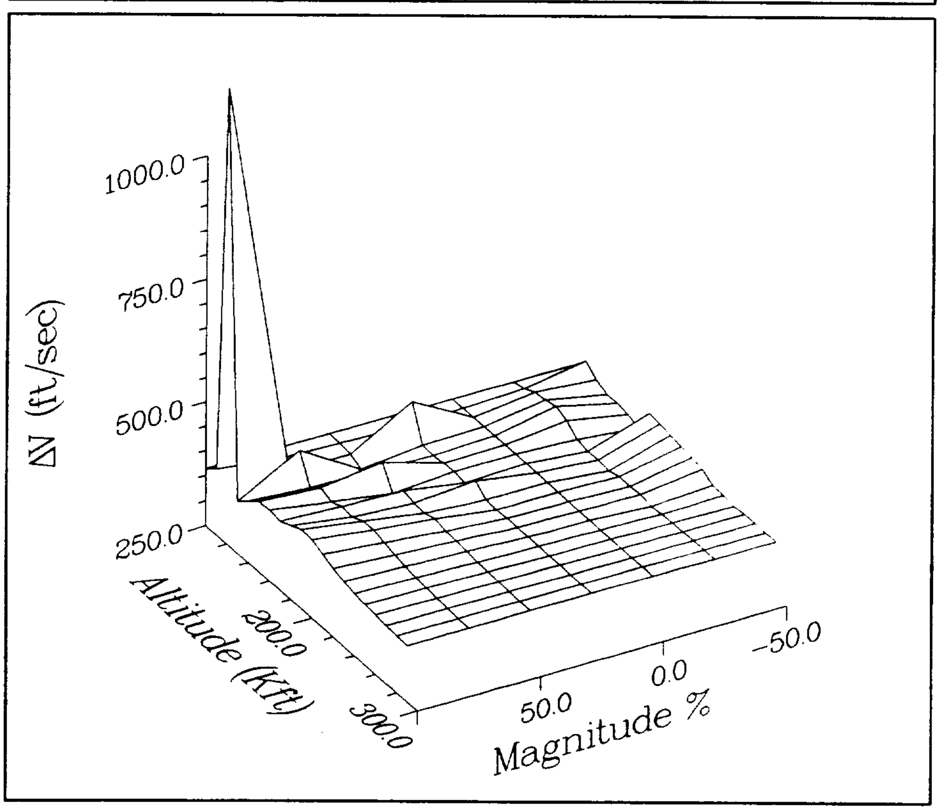

Fig. 50 LHTC Sensitivity to Outbound Leg Square Wave Density Pulses in Nominal Atmosphere. a) 10000 feet Duration; b) 20000 feet Duration

a)

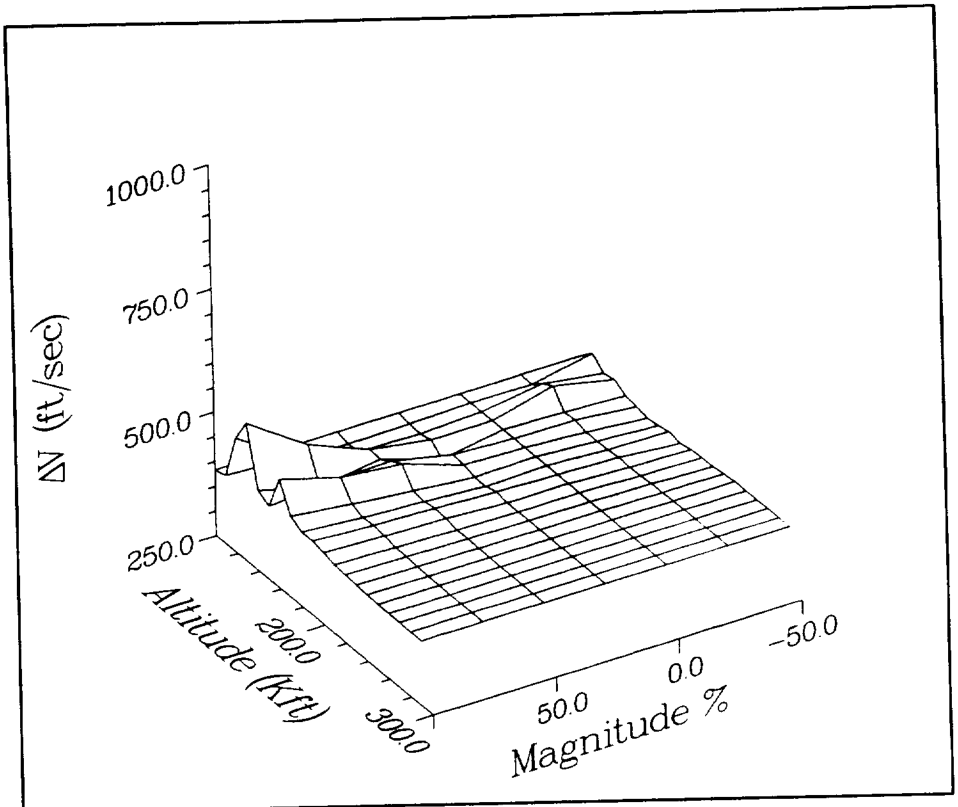

b)

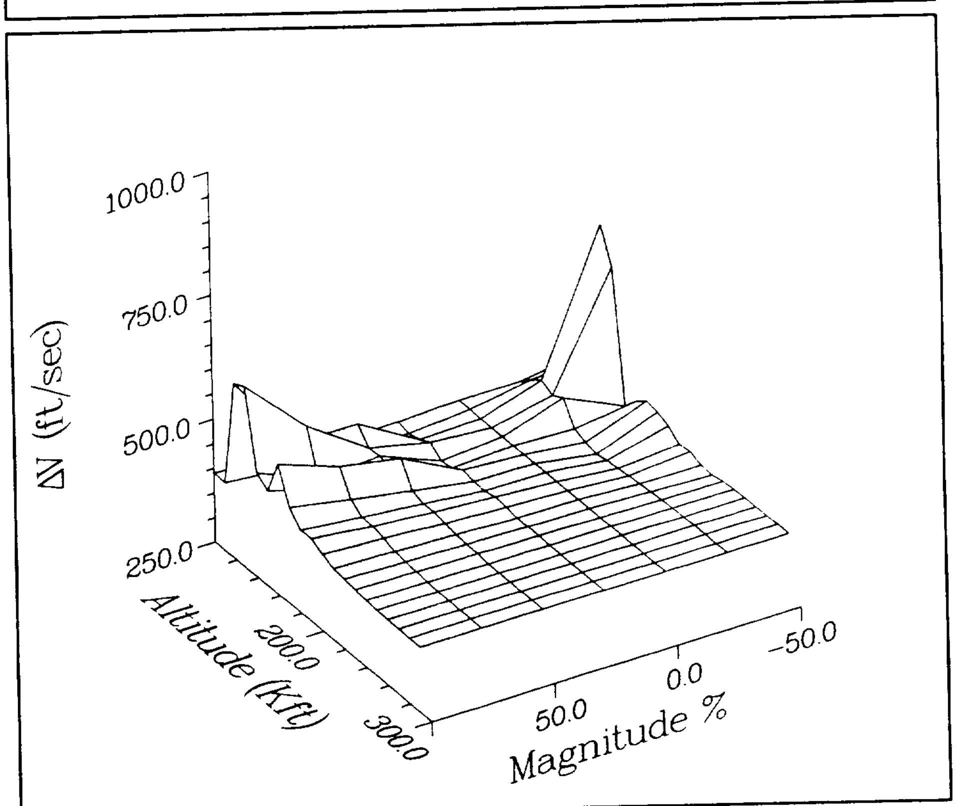

Fig. 51 LHTC Sensitivity to Outbound Leg Square Wave Density Pulses in Low Density Atmosphere. a) 10000 feet Duration; b) 20000 feet Duration

a)

b)

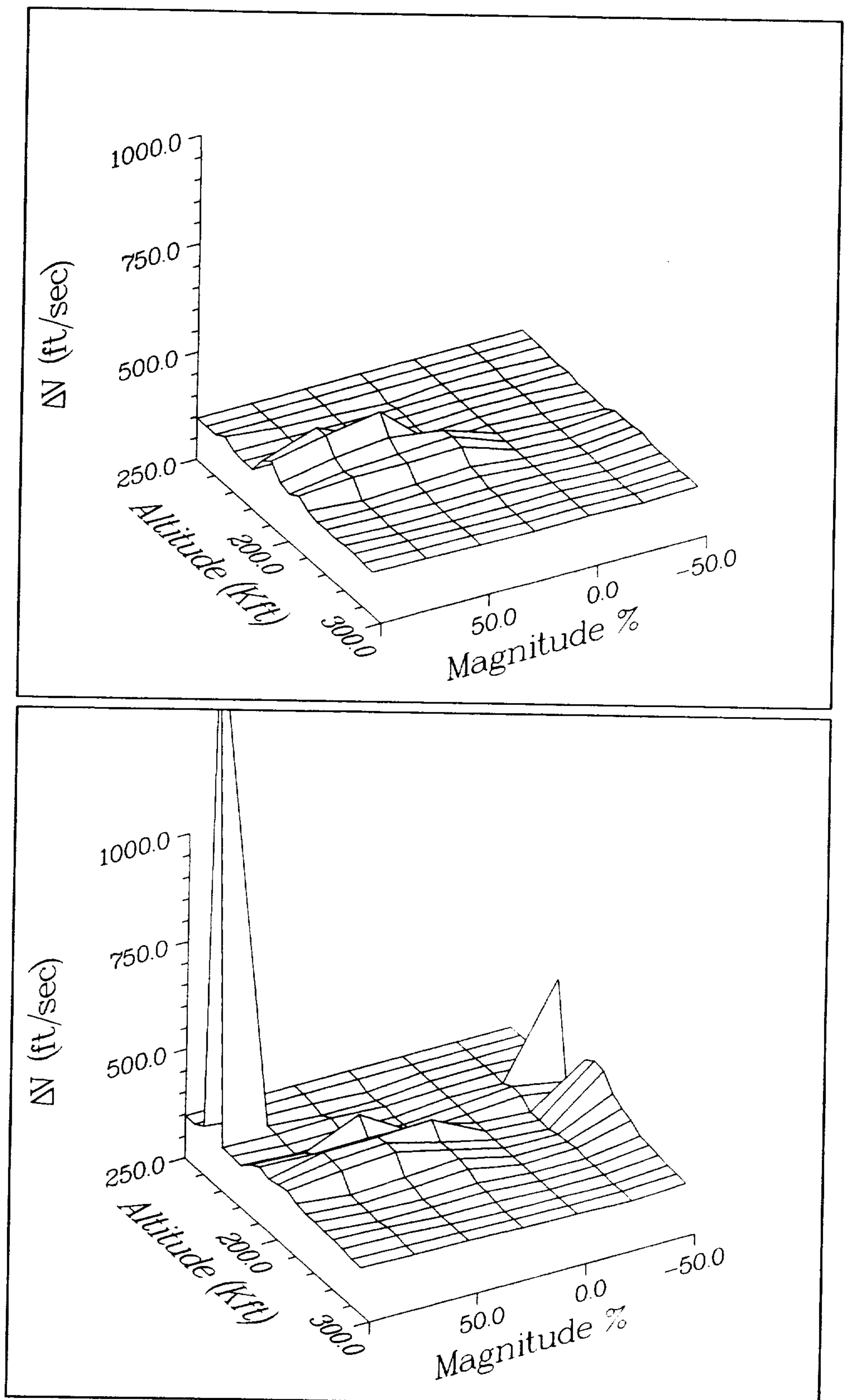

Fig. 52 LHTC Sensitivity to Outbound Leg Square Wave Density Pulses in High Density Atmosphere. a) 10000 feet Duration; b) 20000 feet Duration

LTC Performance

The LTC performance is presented in Figs. 53, 54, and 55. The 10,000 ft density pulses have almost negligible effect on the performance of this control algorithm, as is the case with the MPC. Also, the 20,000 ft pulses produce reasonably good results with the LTC. There are only three soft failures observed during this test sequence for the LTC. All three of the failures are caused by the same 20,000 ft +100% density pulses perturbing the low density atmosphere which caused the soft failure and the two other near failures in the MPC performance. The pulse between 120,000 and 140,000 ft requires a ΔV of 542 ft/sec, while the pulse 10,000 ft higher (between 130,000 and 150,000 ft) requires 505 ft/sec. The pulse between 140,000 and 160,000 ft does not result in a soft failure, requiring 493 ft/sec, but the one between 150,000 and 170,000 ft does, requiring 533 ft/sec. These failures are caused by the same failure modes as described earlier. The pulses located at 120,000 and 130,000 ft cause the density estimator to overreact, forcing the vehicle to exit with too much energy, while the pulse at 150,000 ft causes the vehicle to lose more energy than planned.

Overall, though, the polynomial density estimator used in combination with the Lyapunov control scheme shows excellent performance. The performance of this control algorithm during this evaluation sequence very nearly parallels that of the MPC.

Sinusoidal Density Variations

The next set of simulations involves perturbing the density function with sine waves. Sine waves in altitude and sine waves in range are used. These sine waves vary in amplitude (K_a), wavelength (λ) and phase angle (ϕ). The sine wave perturbations in altitude took the form

a)
b)

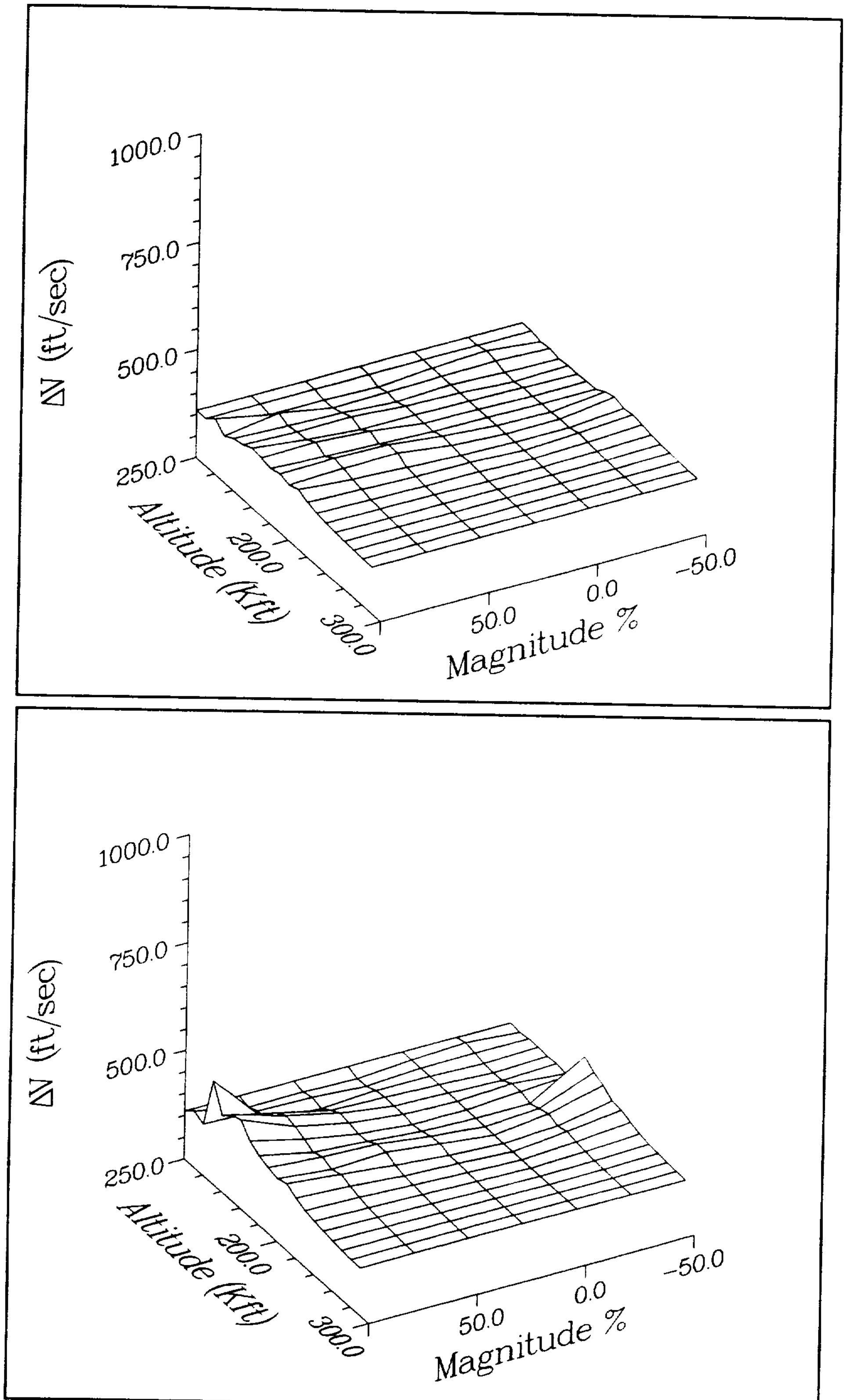

Fig. 53 LTC Sensitivity to Outbound Leg Square Wave Density Pulses in Nominal Atmosphere. a) 10000 feet Duration; b) 20000 feet Duration

a)

b)

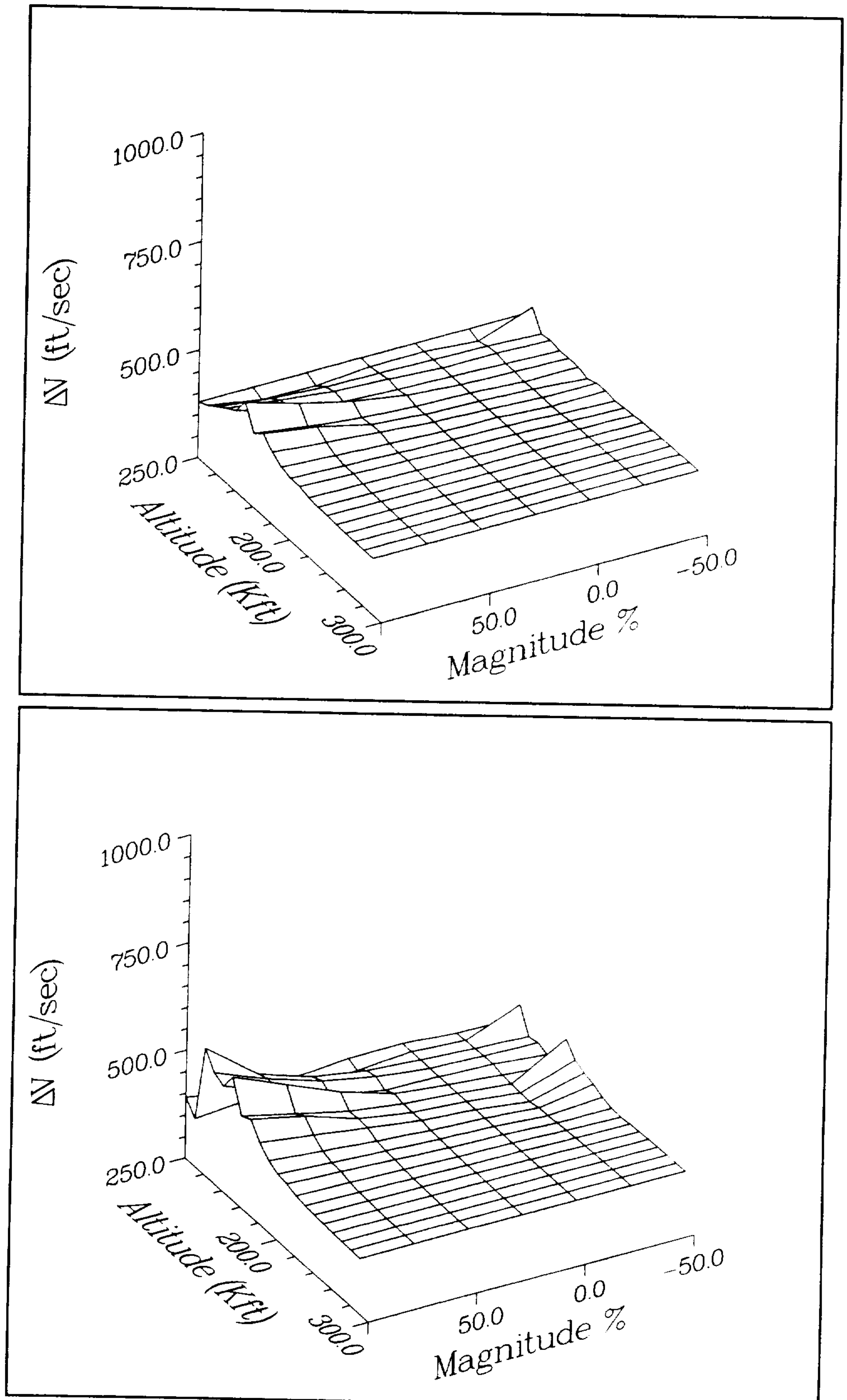

Fig. 54 LTC Sensitivity to Outbound Leg Square Wave Density Pulses in Low Density Atmosphere. a) 10000 feet Duration; b) 20000 feet Duration

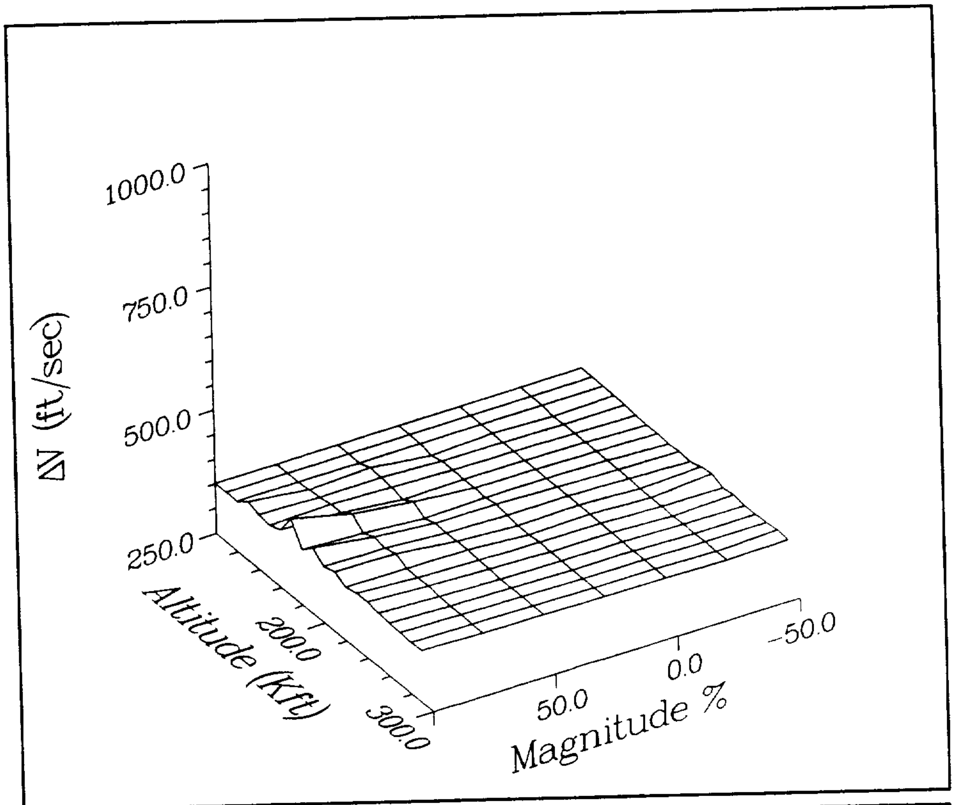

a)

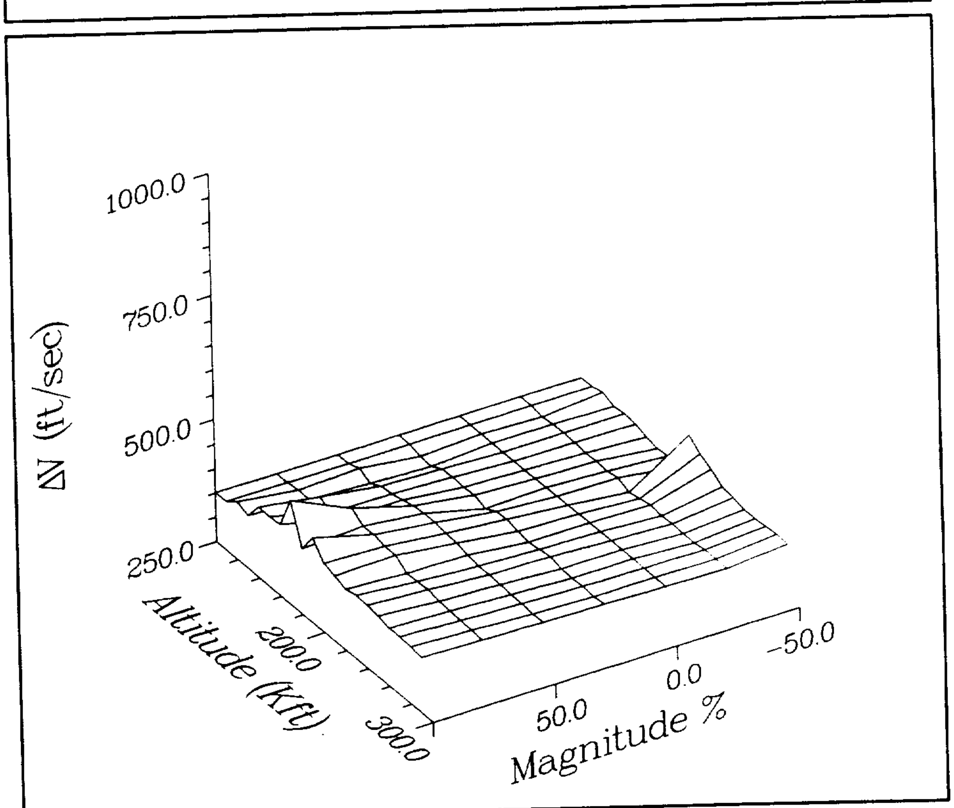

b)

Fig. 55 LTC Sensitivity to Outbound Leg Square Wave Density Pulses in High Density Atmosphere. a) 10000 feet Duration; b) 20000 feet Duration

$$\rho = \rho_{model}\left[1 + K_a \sin\left(\frac{2\pi h}{\lambda} + \phi\right)\right] \tag{84}$$

while those in range took the form

$$\rho = \rho_{model}\left[1 + K_a \sin\left(\frac{2\pi Range}{\lambda} + \phi\right)\right]. \tag{85}$$

The range of amplitudes used included 0.1, 0.25 and 0.5 for both forms of perturbations. The wavelengths selected for the altitude variations included 1000, 2000, 5000, 10,000, 20,000, 50,000, 100,000, 200,000 and 500,000 feet. For the variations in range the wavelengths selected included 1, 5, 10, 20, 50, 100, 200, 500, 1000, 2000 and 5000 nautical miles. In both cases, the phase angles included zero through $\frac{7\pi}{4}$ in $\frac{\pi}{4}$ increments.

The sinusoidal variations with amplitude of 0.1 appears to be very much in line with the actual density profiles measured by Viking 1 and Viking 2 landers during their descent through the Martian atmosphere (Figs. 7 and 8). All of the results with an amplitude of 0.1 for both forms of the sinusoidal variations and all four controllers examined in this chapter are successful. The highest ΔV requires 490 ft/sec, but the vast majority of the trajectories (over 99%) require less than 400 ft/sec. Only 13 of the 1920 trajectories tested with a 0.1 amplitude sine wave density variation need more than 400 ft/sec of ΔV. Likewise, the results generated using 25% and 50% amplitude sine waves in altitude are almost as benign as the 10% results. All of the trajectories which used 25% amplitude sine waves in altitude are successful. Of the 864 trajectories checked using 50% amplitude sine waves in altitude, none result in hard failures and only 8 produce soft failures. Of these, only 3 demand more than 600 ft/sec, with the worst calling for 732 ft/sec. A complete breakdown of these failures is presented in Table 2. Because these results generated using 10% sine waves in altitude and range and 25% sine waves in altitude are all successful, and the 8 soft failures generated using 50% sine waves in altitude are adequately described in Table 2, they are notpresented graphically. It is interesting to note that 3 of the 4 soft failures

Table 2 Soft Failures Caused by 50% Amplitude Altitude Sine Wave Density Variations

Controller	Atmosphere	λ (ft)	ϕ	Apocenter Altitude (nm)	Pericenter Altitude (nm)	Wedge Angle (deg)	Delta-V (ft/sec)
MHPC	High Density	1000	$\frac{3\pi}{2}$	402.8	41.3	.0470	538.2
MHPC	High Density	1000	$\frac{7\pi}{4}$	532.6	41.56	.0709	731.6
MPC	Low Density	20000	$\frac{3\pi}{2}$	227.9	-49.20	.0240	517.7
MPC	Nominal	50000	$\frac{7\pi}{4}$	512.9	37.0	.0968	728.6
MPC	High Density	50000	$\frac{3\pi}{2}$	398.5	37.9	.0462	541.9
LHTC	Low Density	1000	$\frac{3\pi}{4}$	255.3	-74.9	.0079	518.1
LHTC	Low Density	5000	π	229.3	-103.3	.0598	610.0
LTC	Nominal	500000	$\frac{\pi}{2}$	267.9	21.3	.812	504.0

which occurred with controllers using the hybrid density estimation technique, have wavelengths of 1000 ft, while the fourth has a wavelength of 5000 ft. The 1000 ft wavelength sine waves in altitude seem to be corrupting the stored density data used in the density estimation process. Thess data are stored at 1000 ft altitude intervals. Though the density filter should be able to compensate for this eventuality, it does not appear to do so well enough to prevent these failures. Three of the four failures which occurred with controllers employing the polynomial density estimation technique have wavelengths of 20,000 and 50,000 ft. Shorter wavelengths tend to have a cancelling effect, with the additional drag of high density regions being offset by the lower drag of low density regions. Longer wavelengths are easy for the sixth order polynomial to follow, provided there are no more than five extremes in the density function. The problem with the 20,000 and 50,000 ft wavelength sine waves is they do not oscillate fast enough to cancel high density regions against low density regions, yet they still have six to fifteen complete sine waves, with twelve to thirty density extremes in the aerobraking region. This variation is simply more than a sixth order polynomial can follow. The final failure is caused by an excessive orbit plane error (wedge angle) at exit.

25% and 50% Sine Waves in Range

The 25% amplitude sine wave density perturbations, which use vehicle range from entry as the argument to the sine function, are probably the truest measure used here to test controller robustness in the presence of a realistic worst case Martian atmosphere. These perturbations are of somewhat higher magnitude than the perturbations measured by the Viking 1 and Viking 2 landers, but, most probably, the Viking 1 and Viking 2 landers did not sample the worst case atmospheric perturbations. Though the amplitude of the perturbing sine wave is increased to 50% for the simulations, the probability is extremely low that the Martian atmosphere ever experiences high frequency oscillations in density with amplitudes this large.

The performance of the MHPC when tested against the 25% amplitude perturbations is presented in Figs. 56a, 57a, and 58a for the nominal, low density and high density atmospheres respectively. Figures 56b, 57b, and 58b present similar results when the amplitude of the perturbing sine wave increases to 50%. Similarly, Figs. 60 and 61 present the results for the MPC, while the results for the LHTC are in Figs. 62, 63, and 64 and the LTC results are depicted in Figs. 65, 66, and 67.

The 25% amplitude perturbations are significant enough to cause problems in some of the trajectories. Though they do not induce any hard failures, there are many soft failures. The 50% amplitude perturbations are severe enough to cause several hard failures for all of the controllers except the LTC. The 25% and the 50% amplitude sine waves are each used to simulate 264 perturbed atmospheres for each controller (11 wavelengths × 8 phase angles × 3 base atmospheres). Of these 264 trajectories tested using the MHPC and the 25% amplitude sinusoidal variation, six trajectories result in soft failures. Six trajectories also resulted in soft failures when the MPC controller is used, though they are not the same six perturbations. The LHTC has four soft failures while the LTC only has two. When the amplitude of the perturbing sine wave is increased to 50%, the MHPC had fourteen hard failures, the MPC had ten and the LHTC had fourteen. These three controllers also experienced many soft failures during these simulations. The LTC did not result in any hard failures, but it did produce twenty-nine soft failures.

All of these failures are the result of exit phase failures, which are in turn attributable to related directly to density estimation difficulties. Nonetheless, the equilibrium glide phase is robust enough to keep the vehicle in the atmosphere and prevent a skip out for all of these trajectories. None of the trajectories fail to exit the atmosphere, although some of

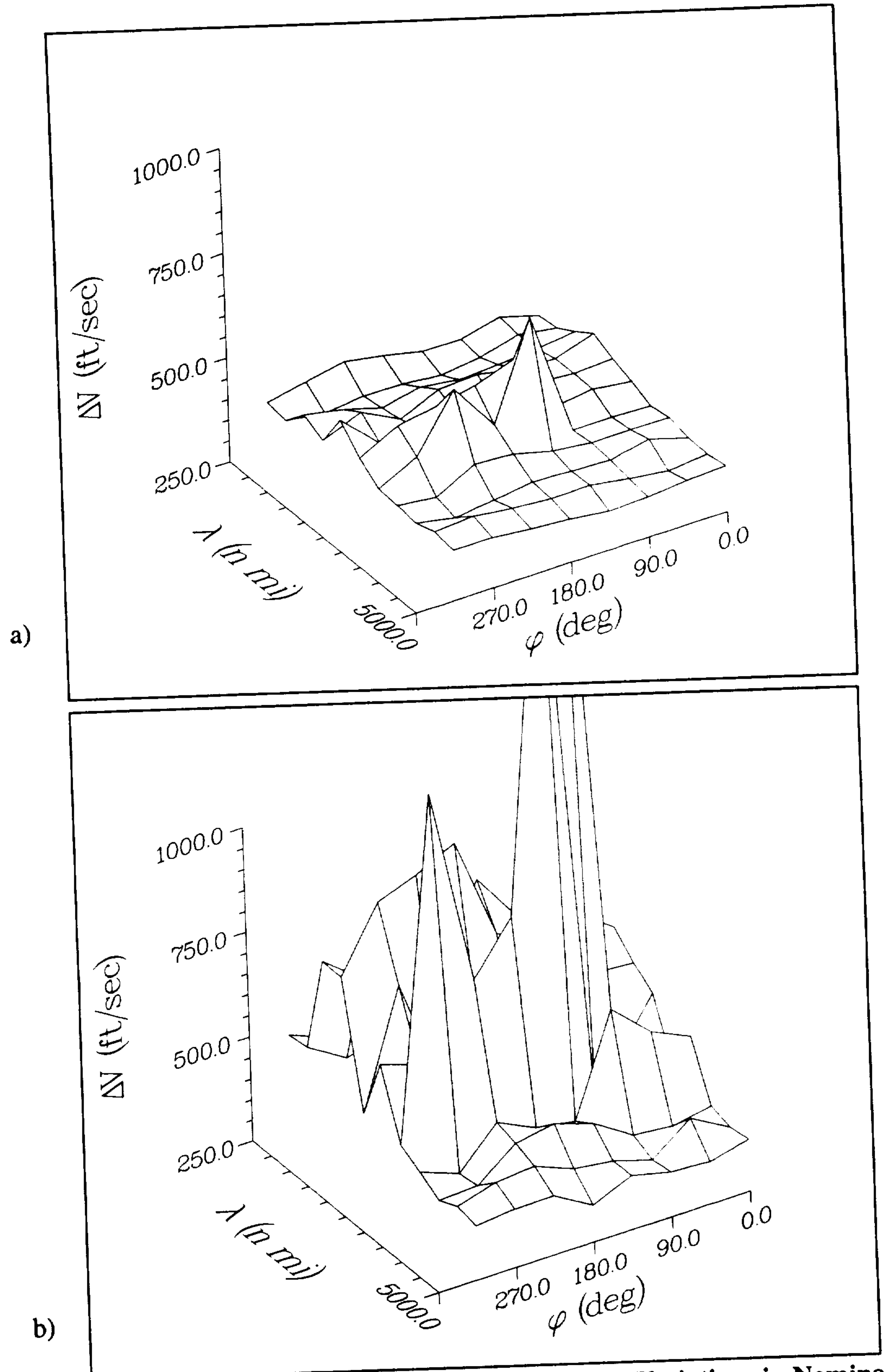

Fig. 56 MHPC Sensitivity to Sinusoidal Density Variations in Nominal Atmosphere. a) 25% Amplitude; b) 50% Amplitude

a)

b)

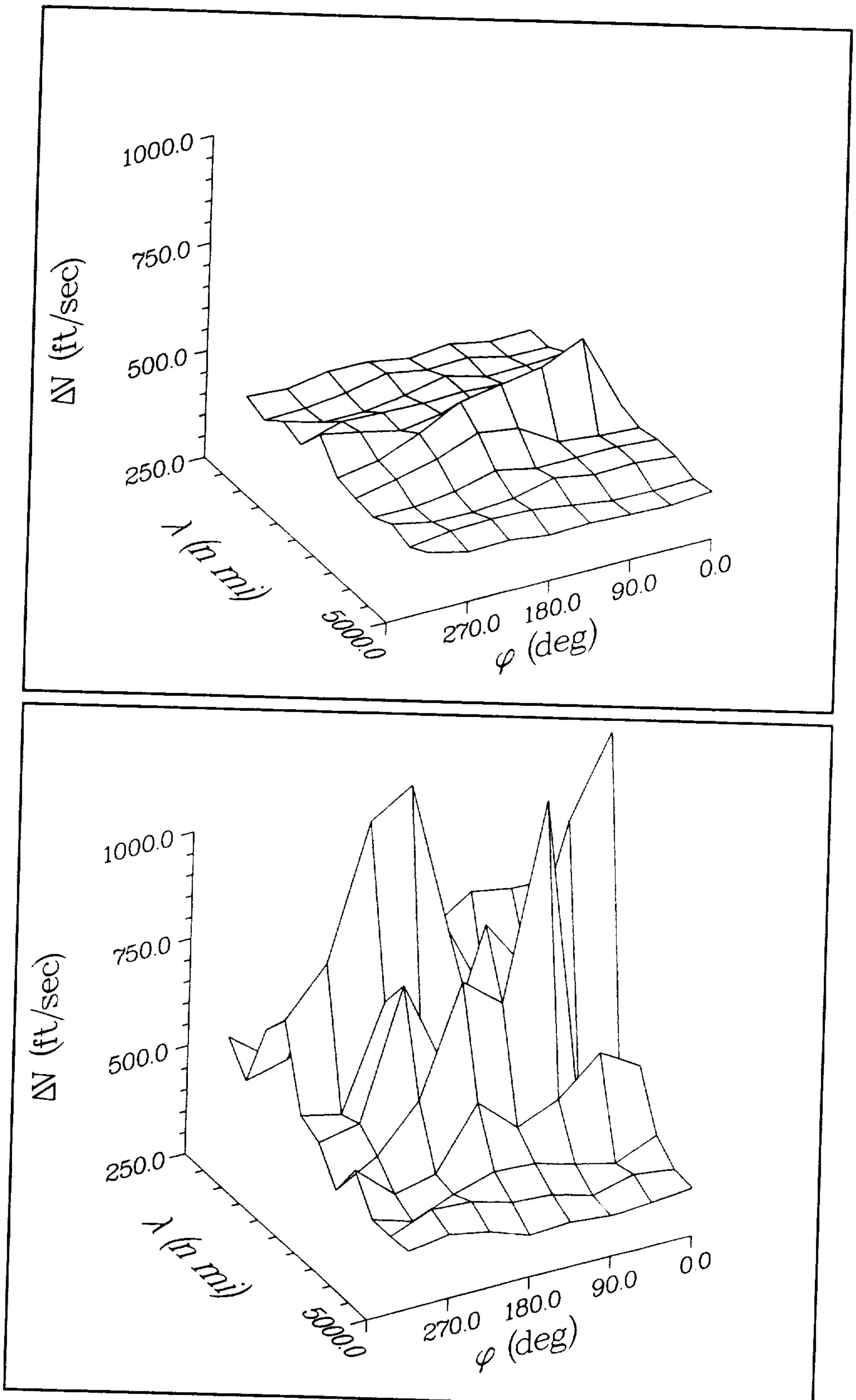

Fig. 57 MHPC Sensitivity to Sinusoidal Density Variations in Low Density Atmosphere. a) 25% Amplitude; b) 50% Amplitude

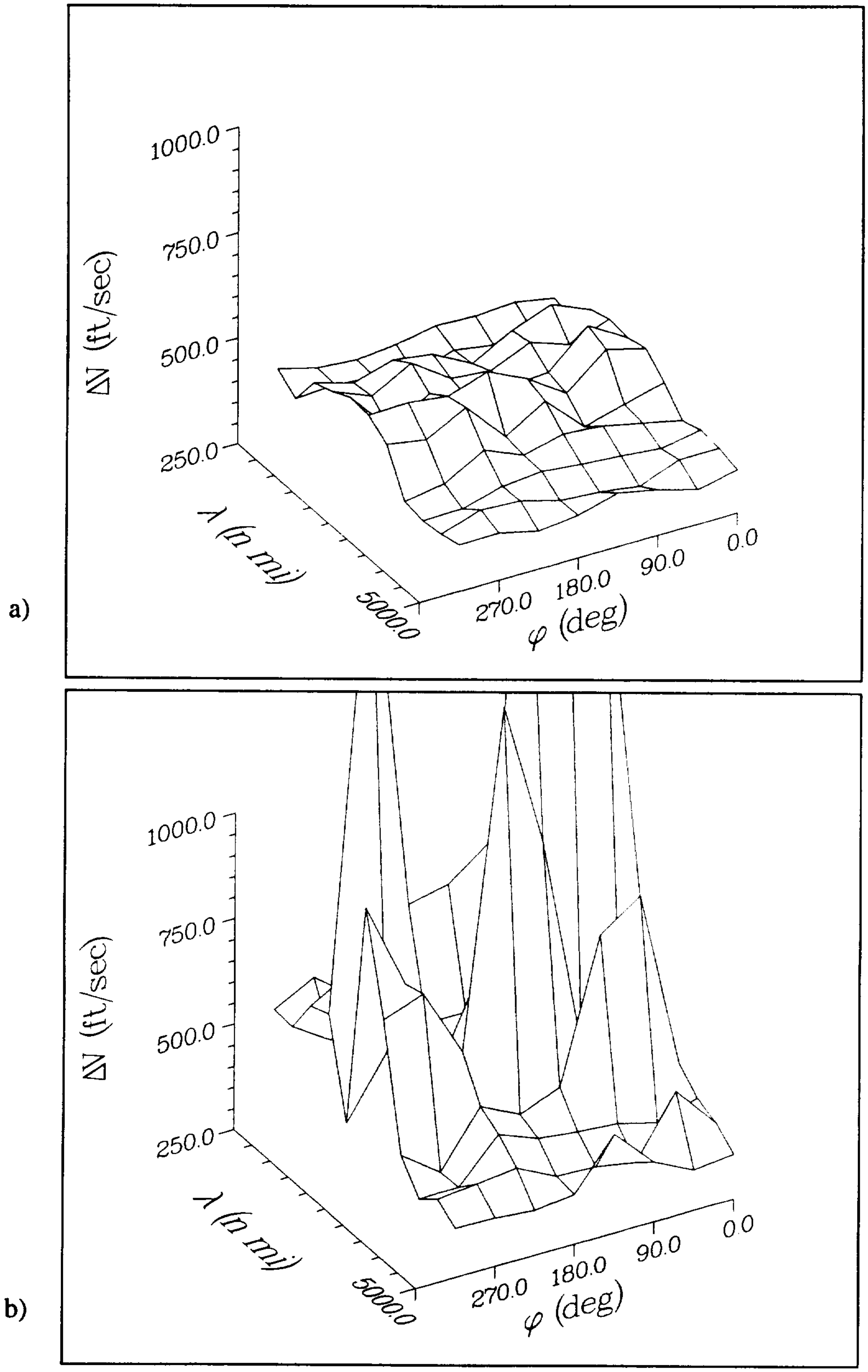

Fig. 58 MHPC Sensitivity to Sinusoidal Density Variations in High Density Atmosphere. a) 25% Amplitude; b) 50% Amplitude

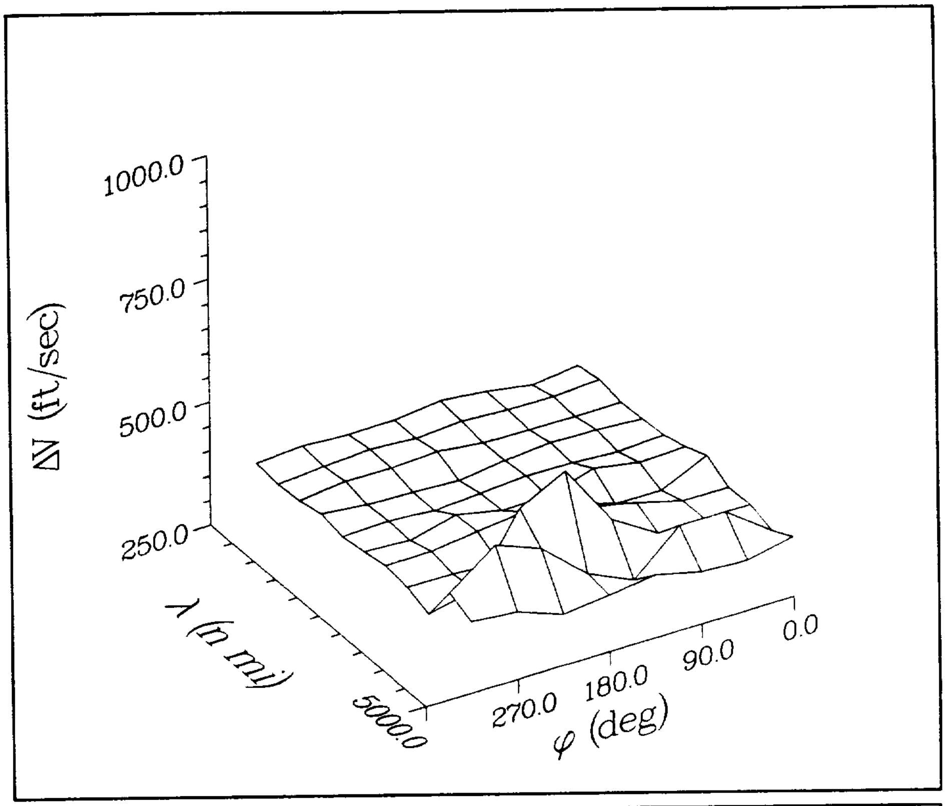

a)

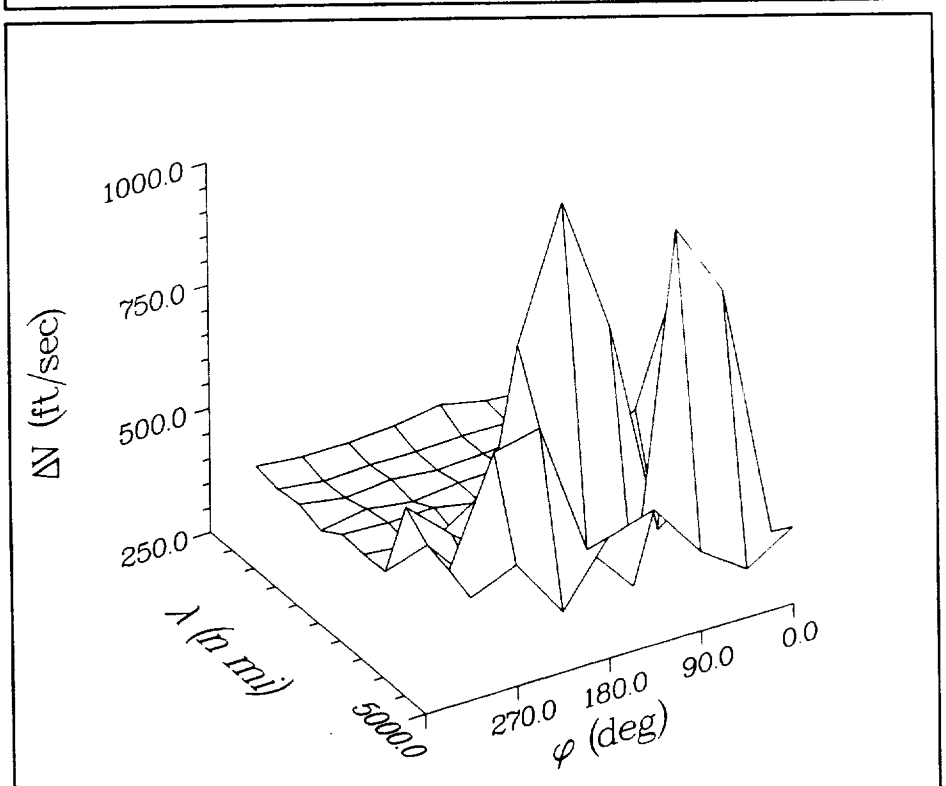

b)

Fig. 59 MPC Sensitivity to Sinusoidal Density Variations in Nominal Atmosphere. a) 25% Amplitude; b) 50% Amplitude

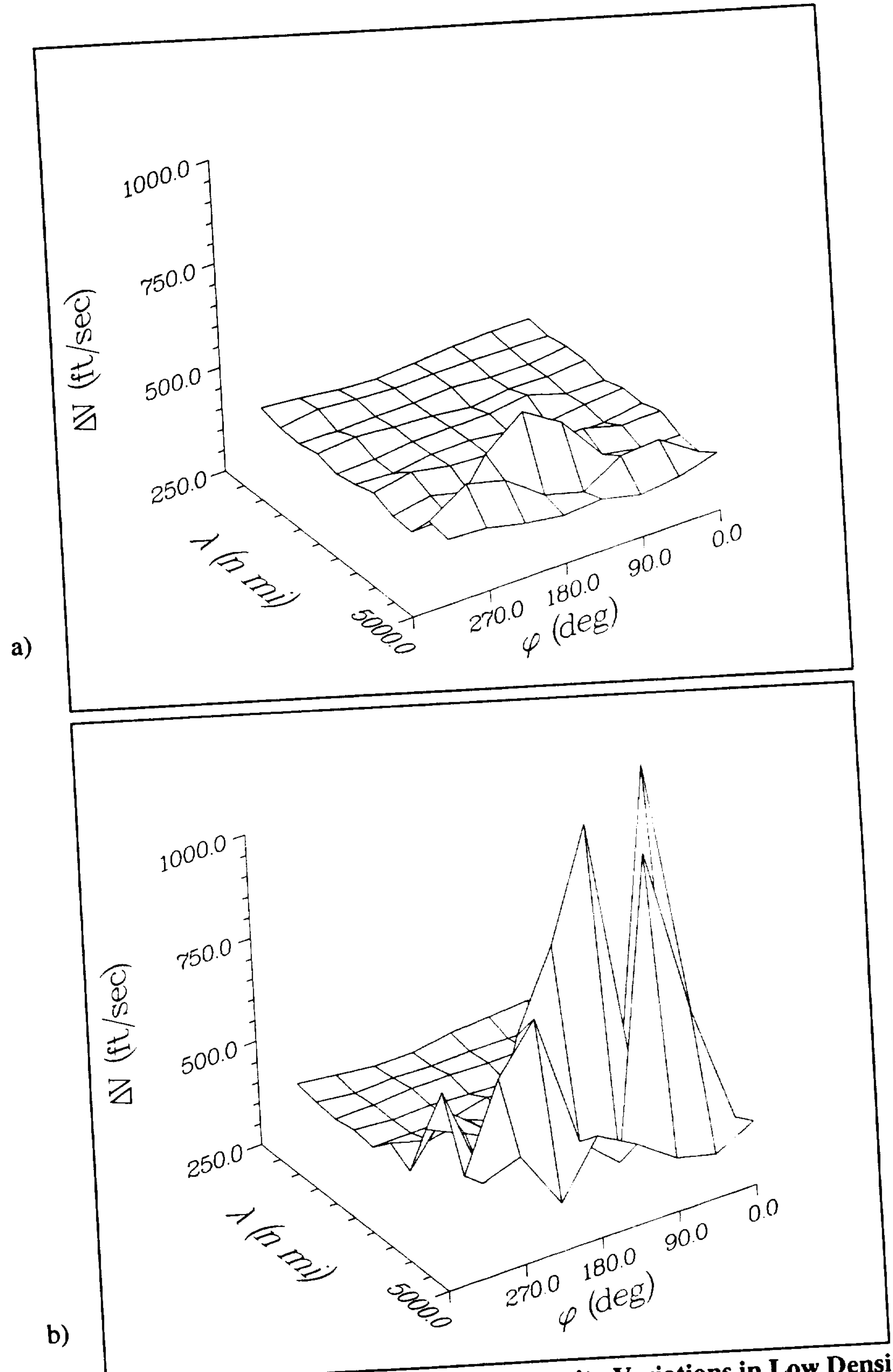

Fig. 60 MPC Sensitivity to Sinusoidal Density Variations in Low Density Atmosphere. a) 25% Amplitude; b) 50% Amplitude

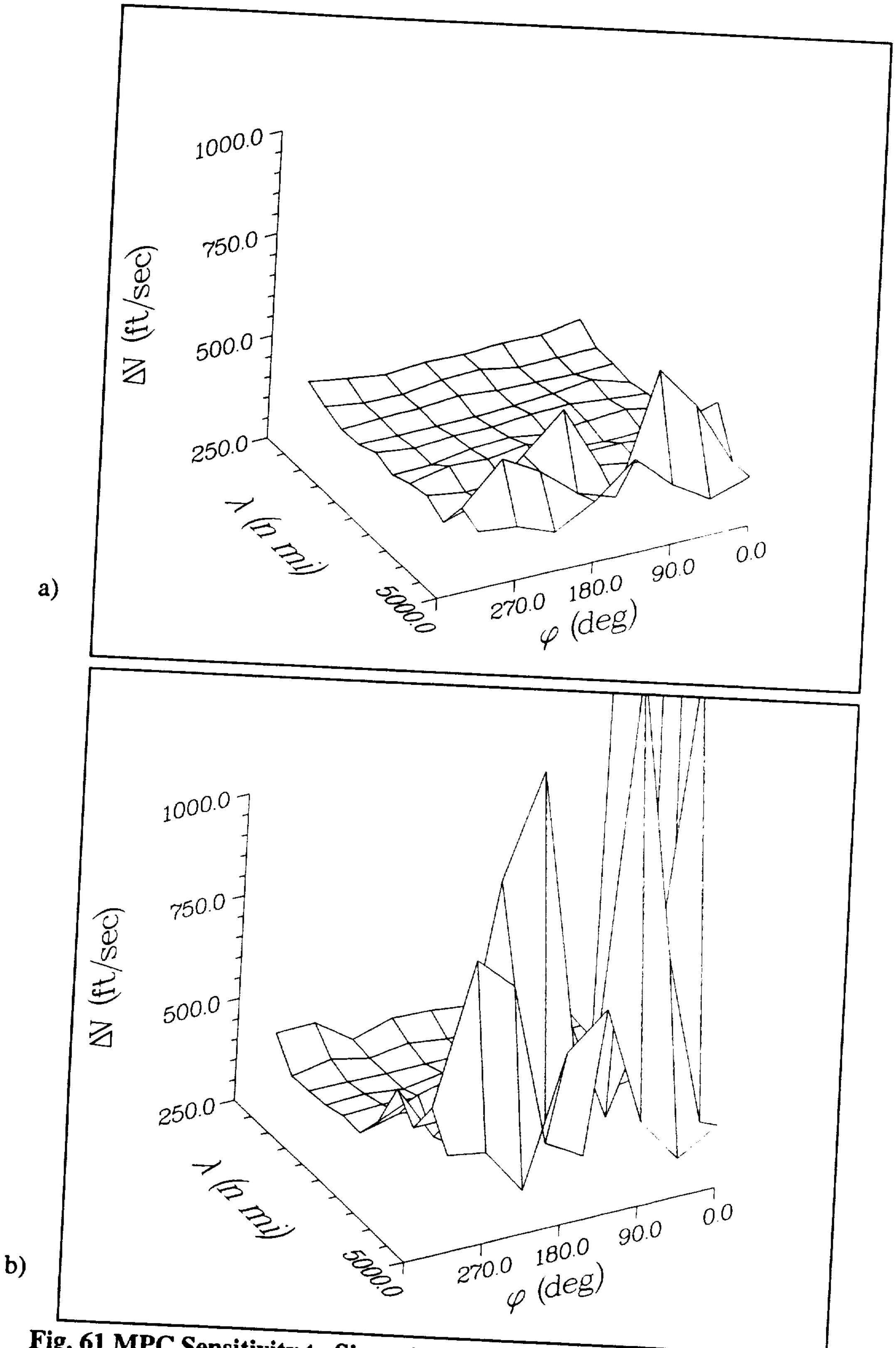

Fig. 61 MPC Sensitivity to Sinusoidal Density Variations in High Density Atmosphere. a) 25% Amplitude; b) 50% Amplitude

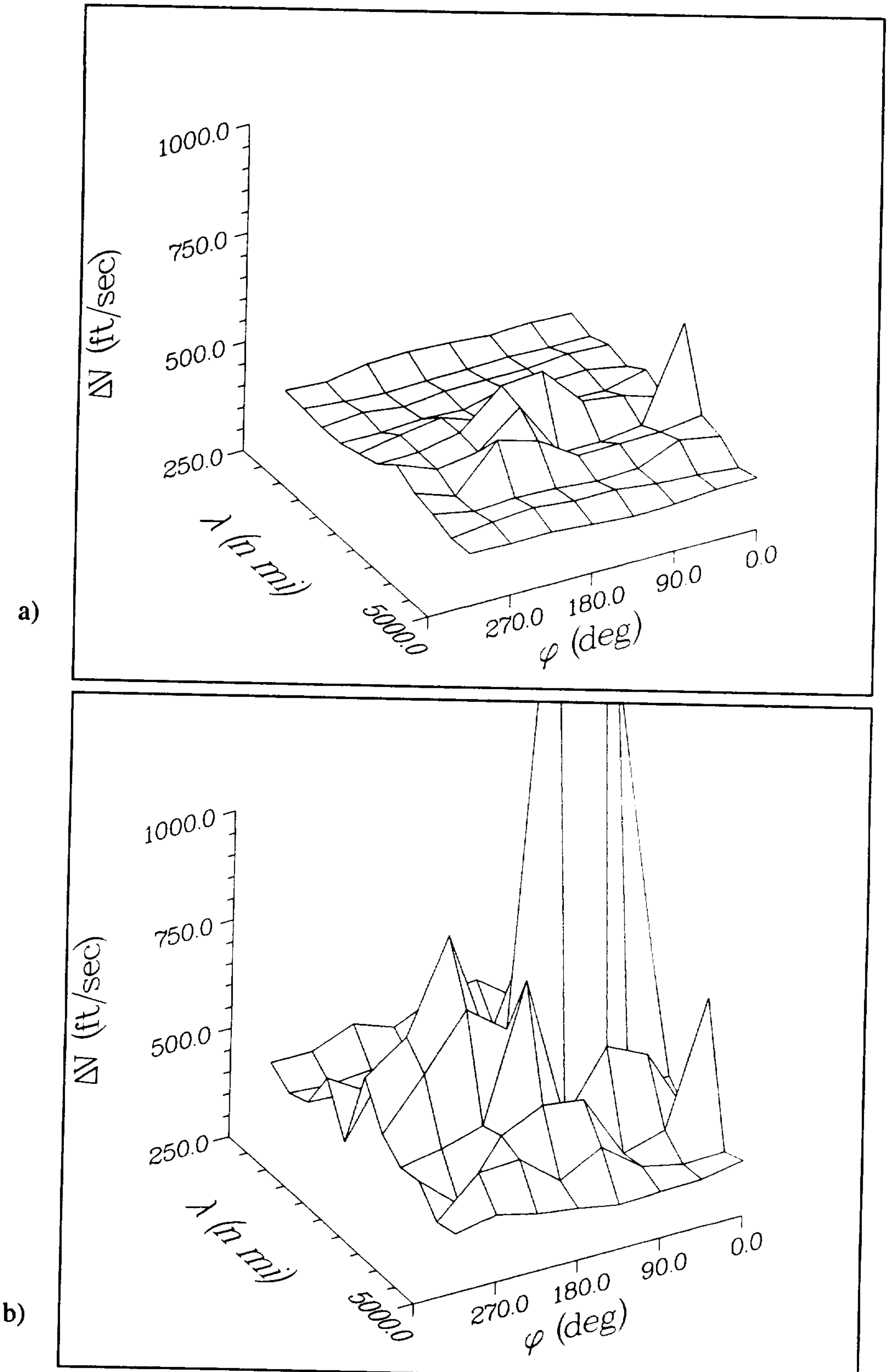

Fig. 62 LHTC Sensitivity to Sinusoidal Density Variations in Nominal Atmosphere. a) 25% Amplitude; b) 50% Amplitude

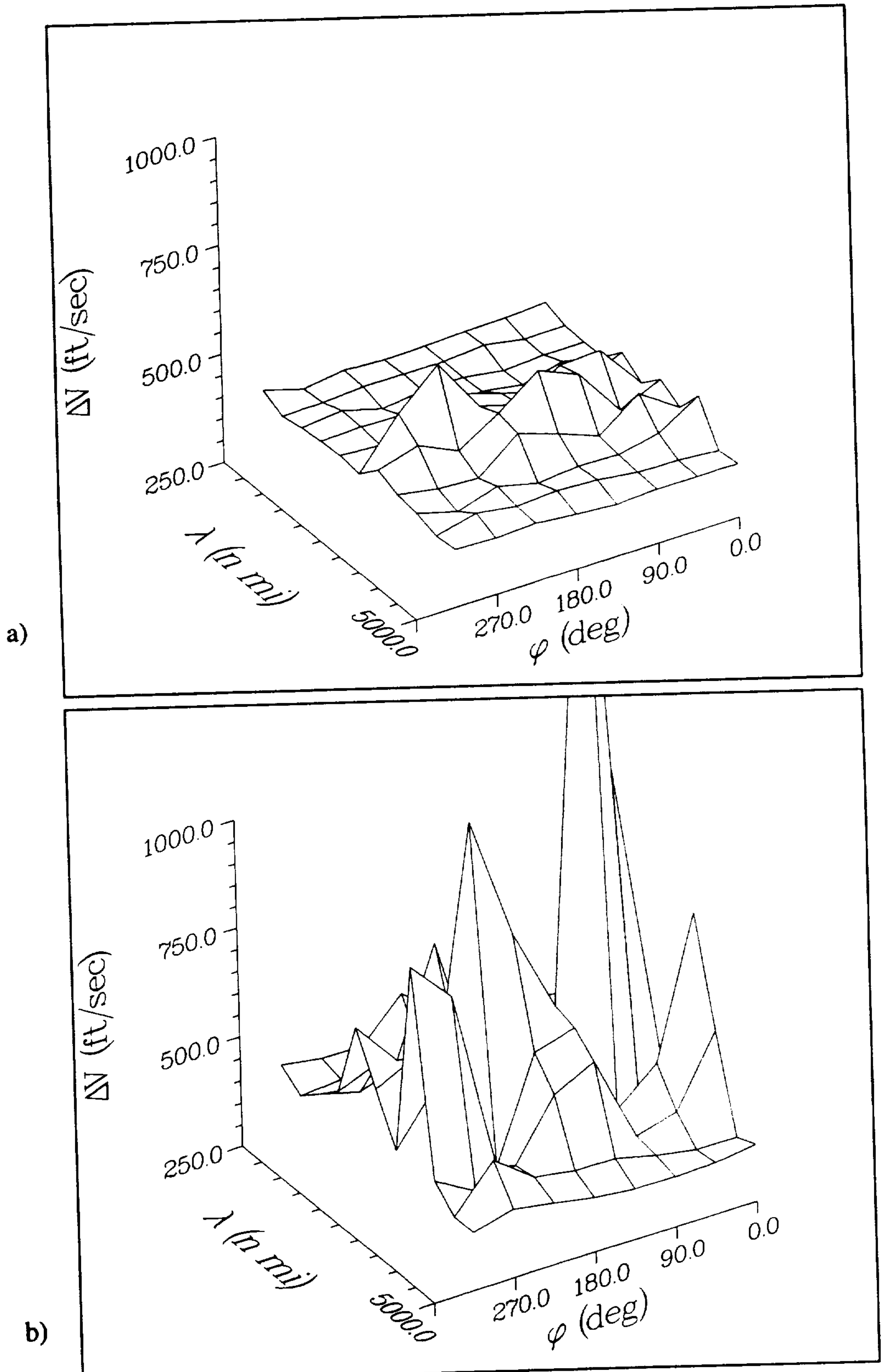

Fig. 63 LHTC Sensitivity to Sinusoidal Density Variations in Low Density Atmosphere. a) 25% Amplitude; b) 50% Amplitude

a)

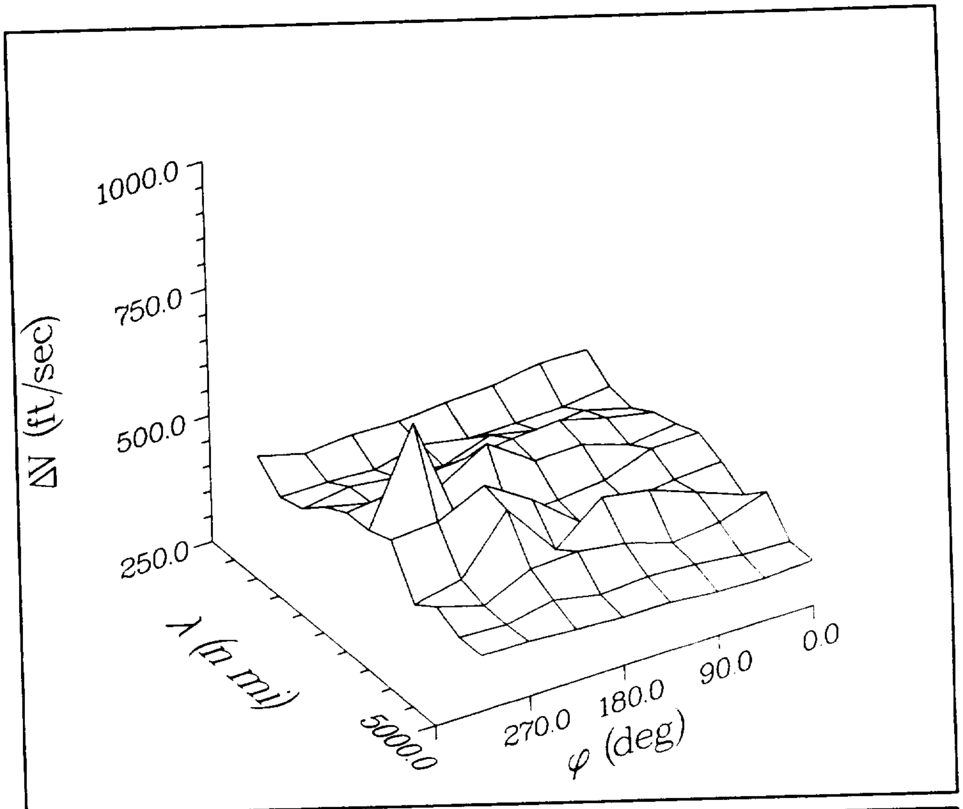

b)

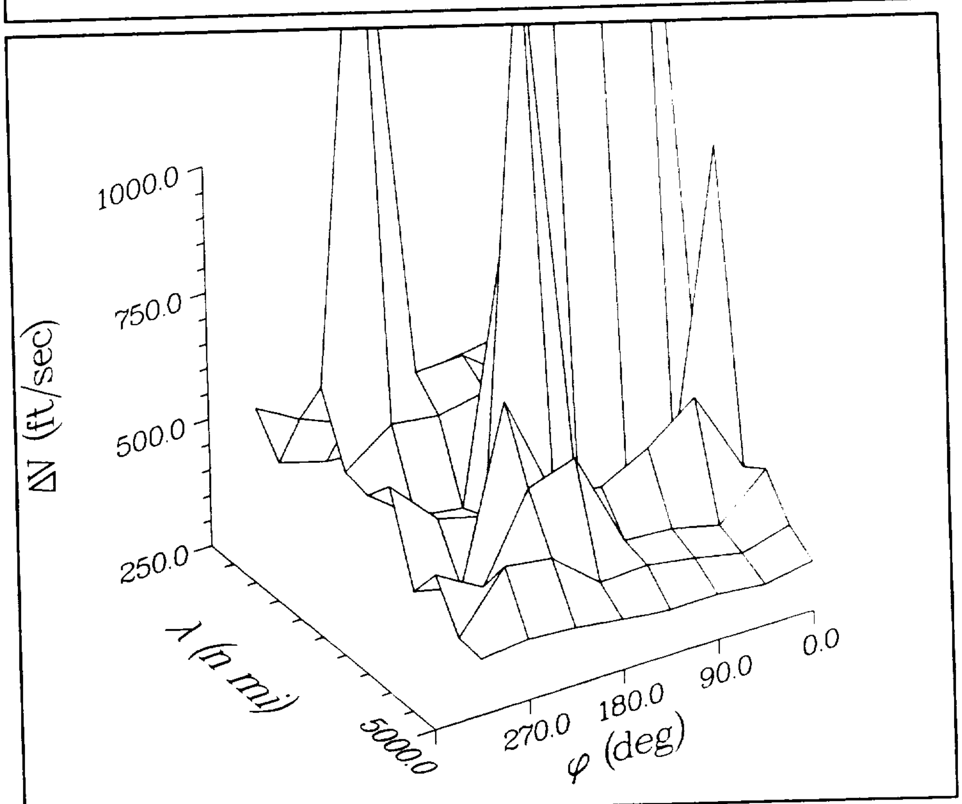

Fig. 64 LHTC Sensitivity to Sinusoidal Density Variations in High Density Atmosphere. a) 25% Amplitude; b) 50% Amplitude

a)

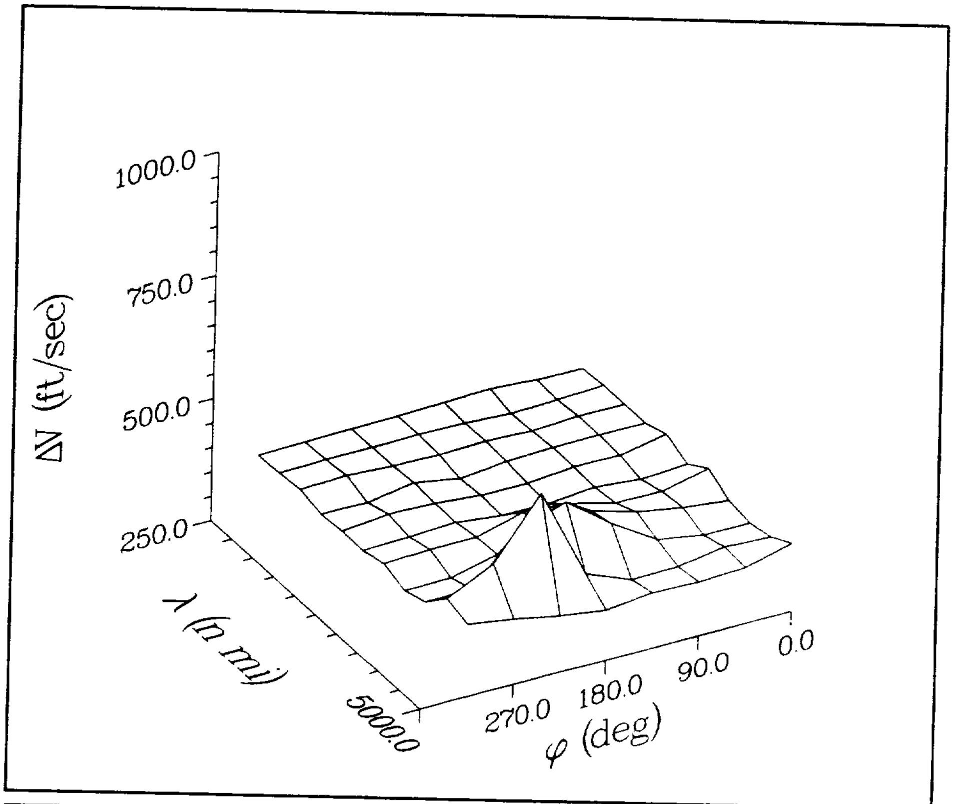

b)

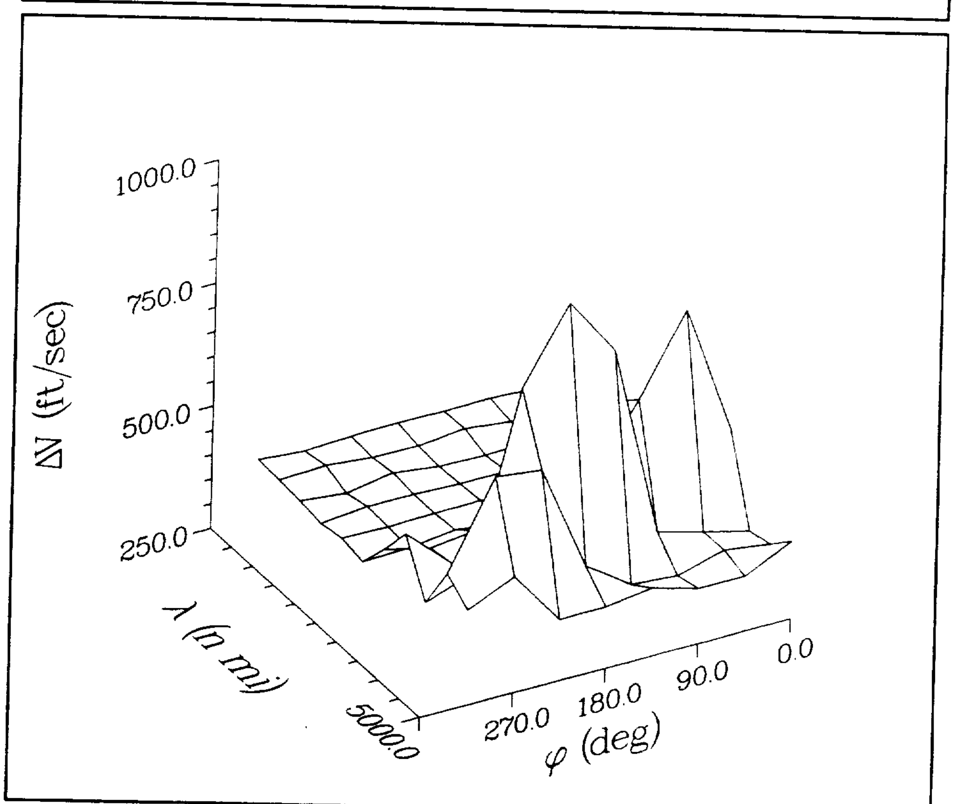

Fig. 65 LTC Sensitivity to Sinusoidal Density Variations in Nominal Atmosphere. a) 25% Amplitude; b) 50% Amplitude

a)

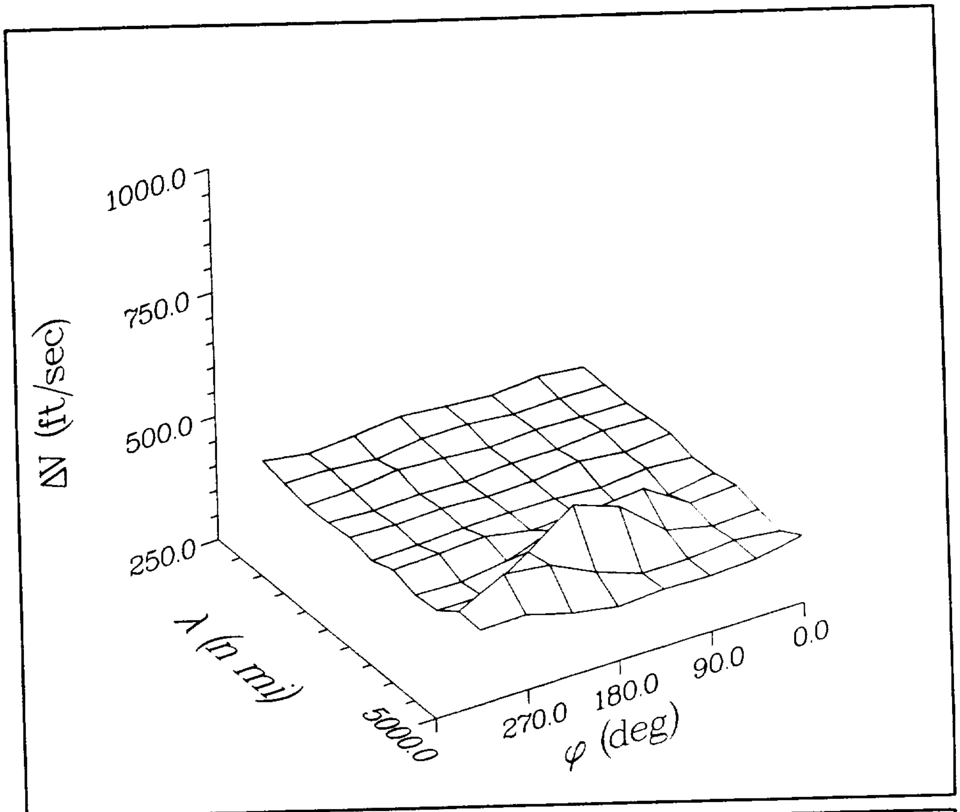

b)

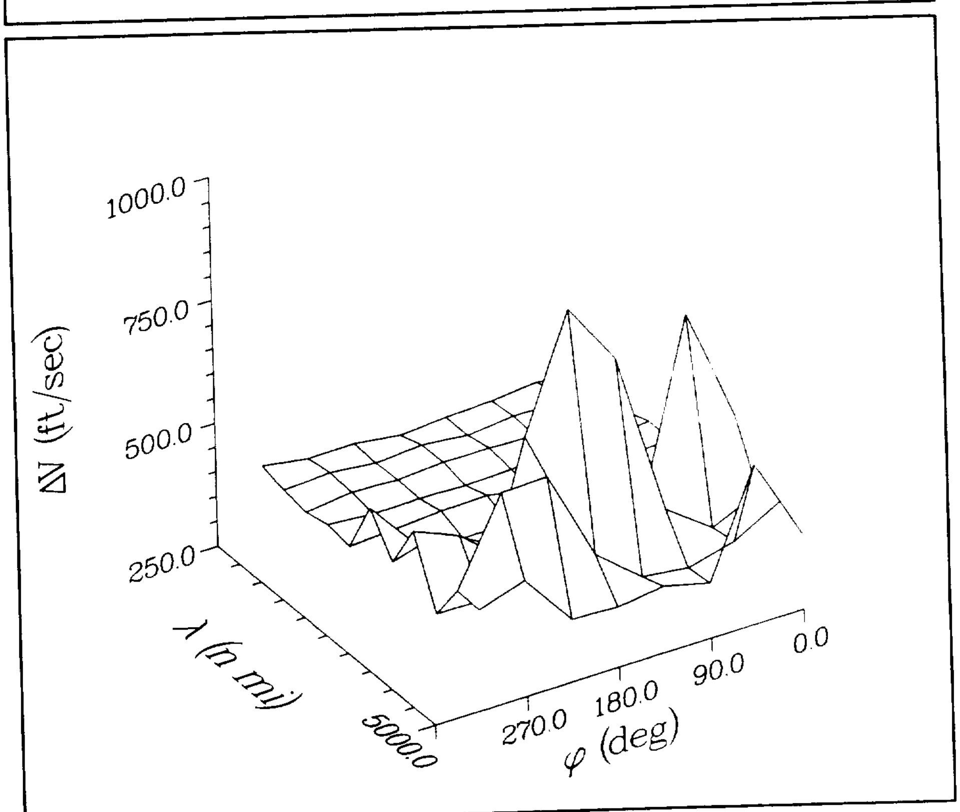

Fig. 66 LTC Sensitivity to Sinusoidal Density Variations in Low Density Atmosphere. a) 25% Amplitude; b) 50% Amplitude

a)

b)

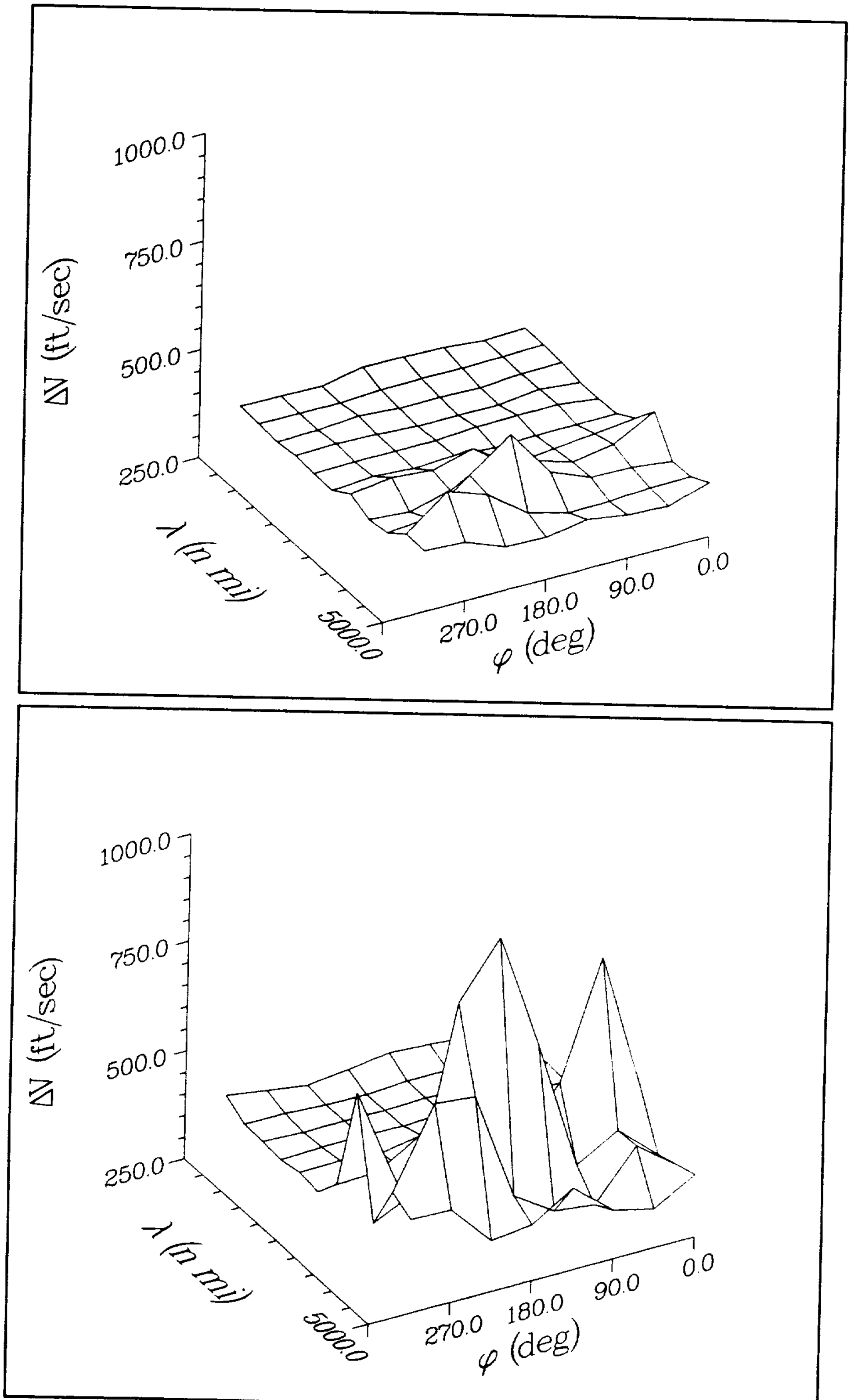

Fig. 67 LTC Sensitivity to Sinusoidal Density Variations in High Density Atmosphere. a) 25% Amplitude; b) 50% Amplitude

them barely do so. The problem with all of the failures centered around the inability of the density estimation technique to adequately predict the density function and thus the amount of drag expected by the controller for the duration of the trajectory. Both density estimation techniques appropriately ignored the high frequency density variations (those with wavelength less than 10 nm). These oscillations occur so quickly that the high and low density regions have a cancelling effect.

The hybrid density estimator shows increased sensitivity to wavelengths of 20 to 200 nm. The polynomial density estimator, on the other hand handles these wavelengths very well. It is the 500 to 2000 nm wavelengths which produce problems for this estimator. These sensitivities to different wavelengths are easy to understand. The hybrid density estimation technique uses the density filter to adjust its estimate for the entire atmosphere based on current density measurements. The long wavelength sine waves have the same effect as a slowly increasing or decreasing density bias during the trajectory. The density filter of the hybrid density estimator is able to sense this slow drift and appropriately adjust the measurements taken during descent to compensate for the drift. The wavelengths which give the hybrid density estimator trouble are those which perturb a portion of the atmosphere and then reverse that perturbation fast enough to confuse the density filter but not fast enough to have a cancelling effect. The polynomial density estimator, on the other hand, fits the sixth order polynomial in altitude to the normalized density function. This density estimation technique remembers the density which was measured at the various altitude intervals. It takes the most recent density measurement and adds this information to the knowledge base and fits a smooth polynomial curve through the data. When the local density is biased, but then that bias reverses later in the trajectory, as it does when the intermediate wavelength sine waves perturb the atmosphere, this density estimation technique excels. But, when the density function is monotonically increasing or decreasing during the trajectory, as is the case for the longer wavelength sine waves, this estimation technique does not respond fast enough. An attempt to place more weight on the most recent data should help, but attempts to do so made the oldest data obsolete; that is, the higher altitude densities, with the density estimator sometimes missing the density at exit by an order of magnitude or more. Clearly, the development of better density estimation modules deserves further study.

Overall, the Lyapunov control scheme performed better than the predictor corrector. The rapid response of the Lyapunov tracking exit phase compensates well for slowly developing density estimates. The polynomial density estimator also performs better than the hybrid density estimator, as it most clearly seen from the LTC results. The LTC kept ΔV below 500 ft/sec for all but two of the 25% amplitude sine wave perturbed atmospheres, and those two only required a ΔV of 509 or 577 ft/sec. Additionally, the 50% amplitude trajectories are all completed with ΔV below 1000 ft/sec. The LTC also copes with the square wave density pulses, both those presented in Chapter 4 which perturbed the entire atmosphere and those of this chapter which only effect the outbound leg of the trajectory. Since the LTC required less than 500 ft/sec for all of the trajectories tested in Chapter 4, and responded better than any of the other controllers to all the robustness tests of this chapter, the LTC is the most robust aerobraking controller examined.

CHAPTER VI

CONCLUSIONS AND RECOMMENDATIONS

Conclusions

The Analytic Predictor Corrector algorithm selected as the control algorithm for the AFE is generally a robust control algorithm, especially with respect to large scale density variations. The algorithm is fairly robust to short period density variations, but does demonstrate a definite sensitivity to variations in the entry flight path angle and vehicle lift and drag coefficients. These sensitivities are due, in large part, to the fixed transition velocity employed to switch the control algorithm from the entry phase to the exit phase and the rather simplistic density estimation scheme used. It is necessary to increase the $K_{\bar{q}}$ term in the equilibrium glide phase to prevent rapid large scale density variations from causing a premature exit from the Martian atmosphere.

The Energy Controller is slightly more robust than the APC to variations in the entry flight path angle and to uncertainty in vehicle lift and drag coefficients. It is also robust to large scale density variations. However, short period density variations were unacceptable to this control algorithm and the increased trajectory loads caused by the EC led to its early dismissal from the list of potential control algorithms.

The Numerical Gradient technique, and then the Conjugate Gradient technique are used to compute idealized optimal (minimum ΔV) trajectories. It was hoped that these methods could be adapted as an on-board control algorithm. But, these algorithms require about two orders of magnitude more computational time than the APC or EC to generate a solution. Additionally, the optimization technique assumes all pertinent density and vehicle lift and drag characteristics are known precisely. The trajectories produced by these optimization techniques fly the exit phase using the full lift available to remain in the atmosphere. Any decrease in density from that modeled in the optimization process allows the vehicle to exit early with too much velocity. These algorithms, with the current performance index, do not produce robust trajectories even if they are able to compute a solution fast enough to control the satellite in real time. A more general performance index which seeks to minimize ΔV while retaining robustness and also reducing control activity should be sought if these techniques are to become practical.

The modifications proposed to the APC to produce the MHPC and MPC convert that algorithm into a robust control algorithm capable of guiding the aerobraking trajectory to near minimum ΔV exit state for most of the perturbations considered

s mentioned before, it is necessary to increase $K_{\bar{q}}$ for the equilibrium glide phase to prevent a premature exit from the atmosphere. But in addition, the change to the more computationally straight forward and efficient exit phase, combined with the better density estimation techniques and the variable transition velocity, made significant improvements to overall robustness of the control algorithms. Between the MHPC and the MPC, the MPC responded better on the whole to the perturbations examined here. There were two areas where the MHPC did slightly better than the MPC. The first situations occurs when density is simply a function of altitude and the entry and exit density functions are identical. The probability of such a coincidence is rather low, but the MPC is still able to handle these situations well (though not as well as the MHPC), without producing any failures. The second area is when the large amplitude sinusoidal variations, which used range from entry as the argument to the sine function, had wavelengths between 500 and 2000 nm. This possibility is still a concern and leads to several of the recommendations that follow. Overall, however, the MPC reacted more appropriately to realistic perturbations than did the MHPC.

The Lyapunov Steepest Descent Control algorithm is implemented, but its inability to compensate for varied energy depletion rates due to density variations, variations in entry flight path angle or vehicle drag coefficient made this algorithm unusable. However, when the Lyapunov control algorithm is recast as a tracking controller designed to follow a reference trajectory, it shows much more promise. The algorithm still has trouble exiting with just the right amount of energy to achieve the desired apocenter altitude and produces peak trajectory loads higher than those of the predictor corrector algorithms. To cure the first ailment a scheme to vary the gain values in the Lyapunov function is developed, while the second is fixed by employing the equilibrium glide entry phase and using the Lyapunov Tracking Controller as an exit phase.

With the two density estimation techniques developed for the MHPC and the MPC used to define the reference trajectory, and the transition velocity from entry to exit phase computed as for the predictor correctors, the LHTC and LTC performed extremely well. The performance of the LHTC and LTC essentially mirror that of the MHPC and MPC, respectively. Generally, the strengths of the MHPC are the strong points of the LHTC, while they share common weaknesses as well. Perturbations which cause problems for the MPC are also likely to cause problems for the LTC. In most cases, the problems are initiated because the density estimation technique is unable to follow a specific perturbation. The Lyapunov tracking algorithm, with its more rapid response, compensates better and produces exit states which require less ΔV than the predictor correctors. There were a few notable exceptions where the rapid response moved the vehicle into a less dense region too rapidly resulting in loss of control authority and an exit state with too much energy. But, predominantly, the Lyapunov trackers performs better than the predictor correctors. As in the predictor corrector analysis, the polynomial density estimation technique works better than the hybrid density estimation technique. Overall, the LTC performs better than the

LHTC, MPC or MHPC and is the recommended control algorithm for performing an interplanetary aerobraking maneuver at Mars.

Recommendations

Based on these conclusions, the following recommendations are made:

1) Robustness to density variations should be a prime issue in selecting the control algorithm for the aerobraking phase of the MRSR. This characteristic must be considered along with decisions such as entry velocity, vehicle lift requirements, ballistic coefficient, or navigational accuracy requirements.

2) The expected wavelengths and maximum amplitude of the short period density oscillations in the Martian atmosphere should be characterized. The nature of these short period oscillations should be determined. It would be beneficial in designing a density estimation technique to know if the short period density wave structure is primarily horizontal or vertical in nature, or a predominantly time-varying function.

3) Once the frequency of the expected density variations is determined, the density estimation technique employed in the aerobraking control system should be tuned to respond to the most likely frequencies which may perturb the trajectory, while ignoring those which have minimal effect on the trajectory.

4) A higher order density estimator, perhaps using Tschebechev polynomials or Legendre polynomials to bypass the numerical difficulties of a higher order polynomial in altitude, should be examined. It may also be desirable to fit a second function, in terms of arc length, or time, or range to the density function, especially if a monotonically increasing or decreasing density function is predicted.

5) The density estimation technique should be adjusted to use all available knowledge of the Martian atmosphere, including any knowledge of dust storms, solar flares, or solar heating of the atmosphere along the intended trajectory.

6) The LTC should be tested using higher entry velocities and different vehicle lift and drag characteristics or ballistic coefficient, as well as different target orbits to determine its suitability for controlling some of the other mission scenarios proposed for MRSR. The fast trip manned precursor mission is clearly a candidate. Also, trading off nominal performance for robustness by varying the exit phase altitude rate should be studied.

7) A statistical method of evaluating controller performance should be developed based on the probability of various atmospheric perturbations occurring. This method may extend further to include the probability of variations in entry conditions or vehicle aerodynamic characteristics.

8) A new performance index should be developed which will minimize ΔV while retaining a level of robustness. With this new performance index, the calculus of variations optimization techniques should be revisited in an attempt to construct a controller which computes a truly optimal solution.

REFERENCES

[1]Mease, K. D., and Vinh, N. X., "Minimum-Fuel Aeroassisted Coplanar Orbit Transfer Using Lift-Modulation," *Journal of Guidance, Control, and Dynamics*, Vol 8, No. 1, Feb. 1985, pp. 134-141.

[2]Park, C., "A Survey of Aerobraking Orbital Transfer Vehicle Design Concepts," AIAA Paper 87-0514, presented at the AIAA 25th Aerospace Sciences Meeting, Reno, Nevada, Jan. 1987.

[3]Talay, T. A., White, N. H., and Naftel, J. C., "Impact of Atmospheric Uncertainties and Viscous Interaction Effects on the Performance of Aero-Assisted Orbital Transfer Vehicles," AIAA Paper 84-0408, presented at the AIAA 22nd Aerospace Sciences Meeting, Reno, Nevada, Jan. 1984.

[4]Vinh, N. X., "Optimal Control of Orbital Transfer Vehicles," AIAA Paper 83-2092, presented at the AIAA Atmospheric Flight Mechanics Conference, Gatlinburg, Tennessee, Aug. 1983.

[5]Johannesen, J. R., Vinh, N., and Mease, K., "Effect of Maximum Lift to Drag Ratio on Optimal Aeroassisted Plane Change," *AIAA 12th Atmospheric Flight Mechanics Conference*, Snowmass, Colorado, Vol I, Aug. 1985, pp. 399-407.

[6]Mease, K. D., and McCreary, F. A., "Atmospheric Guidance Law for Planar Skip Trajectories," *AIAA 12th Atmospheric Flight Mechanics Conference*, Snowmass, Colorado, Vol I, Aug. 1985, pp. 408-415.

[7]Lee, B., and Grantham, W. J., "Aeroassisted Orbital Maneuvering Using Lyapunov Optimal Feedback Control," *AIAA Guidance, Navigation, and Control Conference*, Monterey, California, Vol II, Aug. 1987, pp. 994-1000.

[8]Letts, W. R., and Pelekanos, A., "Aeroassisted Orbital Transfer Mission Evaluation," AIAA Paper 82-1380, presented at the AIAA 9th Atmospheric Flight Mechanics Conference, San Diego, California, Aug. 1982.

[9]Cerimele, C. J., and Gamble, J. D., "A Simplified Guidance Algorithm for Lifting Aeroassist Orbital Transfer Vehicle," AIAA Paper 85-0348, presented at the AIAA 23rd Aerospace Sciences Meeting, Reno, Nevada, Jan. 1985.

[10]Fitzgerald, S. M., and Ward, D. T., "Aeroassisted Orbital Transfer Vehicle Guidance Performance in the Presence of Density Dispersions," AIAA Paper 88-0302, presented at the AIAA 26th Aerospace Sciences Meeting, Reno, Nevada, Jan. 1988.

[11]Fitzgerald, S. M., "Aeroassisted Orbital Transfer Vehicle Guidance Performance in the Presence of Density Dispersions," M.S. Thesis, Dept. of Aerospace Engineering, Texas A&M University, College Station, Texas, Aug. 1988.

[12]"Aeroassist Flight Experiment Preliminary Design Document," National Aeronautics and Space Administration, Marshall Space Flight Center, Huntsville, Alabama, May 1986.

[13]Meyerson, R. E., and Cerimele, C. J., "Aeroassist Vehicle Requirements for a Mars Rover/Sample Return Mission," AIAA Paper 88-0303, presented at the AIAA 26th Aerospace Sciences Meeting, Reno, Nevada, Jan. 1988.

[14]Joels, K. M., *The Mars One Crew Manual,* Ballantine Books, New York, New York, 1985, pp. 4.1.1-4.1.4.

[15]Findley, J. T., Kelly, G. M., and Troutman, P. A., "Final Report-Shuttle Derived Density Model," Analytical Mechanics Associates, Inc., NASA Contractor Report 171824, Dec. 1984.

[16]Champion, K. S. W., "Atmospheric Structure for Low Altitude Satellites and Aerobraking Orbital Transfer Vehicles," AIAA Paper 86-0186, presented at the AIAA 24th Aerospace Sciences Meeting, Reno, Nevada, Jan. 1986.

[17]Blanchard, R. C., Hinson, E. W., and Nicholson, J. Y., "Shuttle High Resolution Accelerometer Package Experiment Results: Atmospheric Density Measurements Between 60-160 km," AIAA Paper 88-0492, presented at the AIAA 26th Aerospace Sciences Meeting, Reno, Nevada, Jan. 1988.

[18]Pitts, D. E., Tillman, J. E., Pollack, J., and Zurek, R., "Model Profiles of the Mars Atmosphere for the Mars Rover and Sample Return Mission," National Aeronautics and Space Administration, Johnson Space Center, Houston, Texas, n.d.

[19]Kaplan, D., "Environment of Mars, 1988," National Aeronautics and Space Administration, NASA Technical Memorandum 100470 , Oct. 1988.

[20]"Mars Aeronomy Observer: Report of the Science Working Team," National Aeronautics and Space Administration, NASA Technical Memorandum 89202 , Oct. 1986.

[21]"Report of the MAO Precursor Workshop, Vol. 1," National Aeronautics and Space Administration, Goddard Space Flight Center, Greenbelt, Maryland, June 1989.

[22]Brace, L. H., "Mars Atmosphere and Dust Storms," Presented at the Aerobraking Technology Workshop, National Aeronautics and Space Administration, Johnson Space Center, Houston, Texas, May 1990.

[23]Gamble, J. D., Cerimele, C. J., and Spratlin, K., "Aerobraking of a Low L/D Manned Vehicle from GEO Return to Rendezvous with the Space Shuttle," AIAA Paper 83-2110, presented at the AIAA Atmospheric Flight Mechanics Conference, Gatlinburg, Tennessee, Aug. 1983.

[24]Cerimele, C. J.., Skalecki, L. M., and Gamble, J. D., "Meteorological Accuracy Requirements for Aerobraking Orbital Transfer Vehicles," AIAA Paper 84-0030, presented at the AIAA 22nd Aerospace Sciences Meeting, Reno, Nevada, Jan. 1984.

[25]Powell, R. W., Stone, H. W., and Naftel, J. C., "Performance Evaluation of the Atmospheric Phase of Aeromaneuvering Orbital Transfer Vehicles," AIAA Paper 84-0405, presented at the AIAA 22nd Aerospace Sciences Meeting, Reno, Nevada, Jan. 1984.

[26]Roberts, B. B., "Systems Analysis and Technology Development for the NASA Orbit Transfer Vehicle," AIAA Paper 85-0965, presented at the 20th AIAA Thermophysics Conference, Williamsburg, Virginia, June 1985.

[27]Vinh, N. X.,Johannesen, J. R., Mease, K. D., and Hanson, J. M., "Explicit Guidance of Drag Modulated Aeroassisted Orbital Transfer Between Elliptical Orbits," *AIAA Guidance and Control Conference*, Seattle, Washington, Vol I, Aug. 1984, pp. 133-142.

[28]Kechichian, J. A., Cruz, M. I., and Rinderle, E. A., "Optimization and Closed-Loop Guidance of Drag Modulated Aeroassisted Orbital Transfer," AIAA Paper 83-2093, presented at the AIAA Atmospheric Flight Mechanics Conference, Gatlinburg, Tennessee, Aug. 1983.

[29]Hull, D. G., Giltner, J. M., Speyer, J. L., and Mapar, J., "Minimum Energy-Loss Guidance for Aero-Assisted Orbital Plane Change," *AIAA Guidance and Control Conference*, Seattle, Washington, Vol I, Aug. 1984, pp. 19-26.

[30]Vinh, N. X., Busemann, A., and Culp, R. D., *Hypersonic and Entry Flight Mechanics*, 1st Edition, The University of Michigan Press, Ann Arbor, Michigan, 1980, pp. 129.

[31]Hull, D. G., "New Analytical Results for AOTV Guidance," *AIAA 12th Atmospheric Flight Mechanics Conference*, Snowmass, Colorado, Vol I, Aug. 1985, pp. 416-420.

[32]Hull, D. G., McClendon, J. R., Speyer, J. L., "Aero-Assisted Orbital Plane Change Using an Elliptic Drag polar," AIAA Paper 86-0268, presented at the AIAA 24th Aerospace Sciences Meeting, Reno, Nevada, Jan. 1986.

[33]Hull, D. G., McClendon, J. R., Speyer, J. L., "Improved Aero-Assisted Plane Change Using Successive Approximations," *AIAA Atmospheric Flight Mechanics Conference*, Williamsburg, Virginia, Vol I, Aug. 1986, pp. 253-258.

[34]Gamble, J. D., Cerimele, C. J., Moore, T. E., and Higgins, J., "Atmospheric Guidance Algorithm Concepts for an Aeroassist Flight Experiment," *Journal of the Astronautical Sciences*, Vol 36, Nos. 1/2, Jan.-June 1988, pp. 45-71.

[35]Justus, C. G., Chimonas, G., Johnson, D. L., and James, B. F., "The Mars Global Reference Atmosphere Model (MARS - GRAM)," National Aeronautics and Space Administration, NAG8-078, Oct. 1989.

[36]Brauer, G. L., Cornick, D. E., Olson, D. W., Peterson, F. M., and Stevenson, R., "Six-Degree-Of-Freedom Program to Optimize Simulated Trajectories (6D POST)," National Aeronautics and Space Administration, NAS1-18147 , Sept. 1987.

[37]Menees, G. P., and Park, C., "Determination of Atmospheric Density Using a Space-Launched Projectile," AIAA Paper 85-0327, presented at the AIAA 23rd Aerospace Sciences Meeting, Reno, Nevada, Jan. 1985.

[38]Cruz, M. I., and Ilgen, M. R., "21st Century Early Mission Concepts for Mars Delivery and Earth Return," AIAA Paper 90-2889, presented at the AIAA 28th Aerospace Sciences Meeting, Reno, Nevada, Jan. 1990.

[39]Ess, R. H., "Atmospheric Effects on Martian Aerocapture," AIAA Paper 90-2818, presented at the AIAA 28th Aerospace Sciences Meeting, Reno, Nevada, Jan. 1990.

[40]Bryson, A. E., and Ho, Y. C., *Applied Optimal Control*, Blaisdell, Waltham, Masachusetts., 1969.

[41]Pierson, B. L., "Panel Flutter Optimization by Gradient Projection," *International Journal for Numerical Methods in Engineering*, Vol 9, No. 2, 1975, pp. 271-296.

[42]Junkins, J. L., *An Introduction to Optimal Estimation of Dynamical Systems*, Sijthoff & Noordhoff, Alphen aan den Rijn, The Netherlands, 1978, pp. 1-29.

[43]McHenry, L., "Analytic Aerobrake Exit Altitude Rate Predictor-Corrector", Letter EGB-90-133/AFE-90-017, The Charles Stark Draper Laboratory, Inc., Pasadena, California, May 1990.

[44]McHenry, L., "Analytic Aerobrake Exit Radial Velocity Predictor-Corrector: Derivation Clarification", Letter EGB-90-315/AFE-90-046, The Charles Stark Draper Laboratory, Inc., Pasadena, California, Nov. 1990.

[45]Lee, B., "Aeroassisted Orbital Maneuvering Using Lyapunov Optimal Feedback Control," M.S. Thesis, Dept. of Mechanical and Materials Engineering, Washington State University, Pullman, Washington, Aug. 1988.

[46]Shepperd, S. W., Fuhry, D. P., and Brand, T. J., "Onboard Preaerocapture Mavigation Performance at Mars," AAS Paper 91-119, presented at the AAS/AIAA Spaceflight MechanicsMeeting, Houston, Texas, Feb. 1991.

[47]Kirk, D. E., *Optimal Control Theory*, Prentice-Hall, Englewood Cliffs, New Jersey, 1970.

[48]Shipley, B. W., Jr., "Control Algorithms for Aerobraking in the Martian Atmosphere," PhD Dissertation, Dept. of Aerospace Engineering, Texas A&M University, College Station, Texas, Sep. 1991.

APPENDIX A

IDEALIZED MINIMUM ΔV OPTIMAL SOLUTION

A numerical gradient technique was employed to determine the minimum ΔV solution for a nominal Martian aerobraking maneuver[40]. The MRSR mission scenario calls for the aerobraking maneuver to reduce the vehicle velocity relative to the planet using aerodynamic drag and then to exit the atmosphere on an elliptical intermediate orbit. A series of propulsive maneuvers are then performed to transfer the vehicle from the intermediate orbit to the desired final orbit. The total ΔV required to transition from the intermediate orbit to the desired orbit is determined by the vehicle's atmospheric exit velocity vector and is a good measure of control system performance. The open loop solution presented here assumes that initial conditions as well as all pertinent vehicle and atmospheric properties are known precisely. Limits are not placed on trajectory loads. Robustness to atmospheric dispersions is not considered in computing this optimal solution. This solution produces the minimum ΔV attainable to transition from the post aerobraking intermediate orbit to the desired final orbit for a given atmosphere, vehicle and entry condition and is used as a benchmark to evaluate the performance of the feedback controllers.

Equations of Motion

The formulation begins with the equations of motion. The equations of motion were presented in Chapter III but are repeated again here for completeness.

$$\frac{dr}{dt} = \frac{dh}{dt} = V\sin\gamma \tag{86}$$

$$\frac{dV}{dt} = \frac{-C_D \rho S V_r^2}{2m} - \frac{\mu}{r^2}\sin\gamma \tag{87}$$

$$\frac{d\gamma}{dt} = \frac{-C_L \rho S V_r^2}{2mV}\cos\Phi - \left[\frac{\mu}{Vr^2} - \frac{V}{r}\right]\cos\gamma \tag{88}$$

Equation (86) is simply the radial velocity in terms of the inertial velocity and flight path angle. Equation (87) gives the time rate of change of velocity in two parts: 1) the velocity loss rate due to aerodynamic drag and 2) the change in velocity due to gravitational acceleration (the inertial component). Similarly, Eq. (88) is the time rate of change in the flight path angle also composed of two parts: 1) the change in flight path angle due to the component of aerodynamic lift in the vertical plane and 2) the change in flight path angle due to gravitational acceleration (the inertial component). The control variable Φ, the bank angle, determines the amount of lift exerted in the vertical plane to bend the trajectory and change the flight path angle.

Nondimensional State Variables

Dimensionless state variables are introduced:

$$\bar{x} = \begin{bmatrix} x_1 \\ x_2 \\ x_3 \end{bmatrix} = \begin{bmatrix} h/h_e \\ V/(\sqrt{\mu/R}) \\ \gamma \end{bmatrix} \tag{89}$$

along with a dimensionless time variable τ

$$\tau = (t/h_e)\sqrt{\mu/R}. \tag{90}$$

The equations of motion may now be written:

$$\dot{x}_1 = x_2 \sin x_3 \tag{91}$$

$$\dot{x}_2 = -B\sigma x_{2_r}^2 - \frac{c}{(c-1+x_1)^2}\sin x_3 \tag{92}$$

$$\dot{x}_3 = \frac{A\sigma x_{2_r}^2}{x_2}\cos\Phi + \frac{\cos x_3}{c-1+x_1}\left[x_2 - \frac{c}{(c-1+x_1)x_2}\right] \tag{93}$$

where $\sigma = \rho/\rho_0 = exp\,[(-(h-h_0))/hS]$, $A = (\rho_0 S h_e C_L)/(2m)$, $B = (\rho_0 S h_e C_D)/(2m)$ and $c = R/h_e$.

The Performance Index

To minimize total ΔV required to transition to the desired orbit it is sufficient to minimize the exit flight path angle provided the apocenter of the intermediate orbit equals the desired apocenter. This procedure maximizes the pericenter of the post-aero orbit. Two terminal constraints are employed. The first requires the final altitude to be the atmospheric interface altitude and the second fixes the intermediate orbit apocenter. The cost function is therefore the exit flight path angle $(J = \gamma_x)$ and the goal is to minimize the cost function subject to

$$\psi_1 = x_{1_f} - 1 = 0 \tag{94}$$

and

$$\psi_2 = -\left(\frac{r_a}{R}\right)^2\left[x_2^2 - \frac{2c}{c-1+x_1}\right] - 2\frac{r_a}{R} + \left[\frac{c-1+x_1}{c}\right]^2 x_2^2(\cos x_3)^2 = 0. \tag{95}$$

To derive Eq. (95), set the orbital angular momentum at exit equal to the angular momentum at apocenter.

$$h = r_x V_x \cos\gamma_x = r_a V_a . \tag{96}$$

From this equation solve for the velocity at apocenter in terms of the terminal radius, velocity, flight path angle and the radius of apocenter.

$$V_a = \frac{r_x V_x \cos\gamma_x}{r_a} \tag{97}$$

Equate the orbital energy at exit to that at apocenter, using the expression for velocity at apocenter from above

$$\frac{(r_x V_x \cos\gamma_x)^2}{2 r_a^2} - \frac{\mu}{r_a} = \frac{V_x^2}{2} - \frac{\mu}{r_x} \tag{98}$$

Obtain Eq. (95) after some algebra and after replacing the physical state variables with the nondimensional variables given in Eqs. (89) and (90).

The Numerical Gradient Technique

This problem is solved using a first order numerical gradient procedure. To formulate the optimal control problem begin with the performance index. In general terms this index may be written

$$J = \phi(x_f) + \int_{t_0}^{t_f} \{L(x^*, u^*)\}\, dt \tag{99}$$

The performance index is then augmented with penalty functions to impose the terminal constraints and the equations of motion.

$$J_a = \phi(x_f) + [\nu]^T \{\psi(x_f)\} + \int_{t_0}^{t_f} \{L(x^*, u^*) + [\lambda]^T [f(x^*, u^*) - \dot{x}^*]\} dt \quad (100)$$

For this problem $[\nu]$ is a 2×1 column matrix of constants, $\{\psi(x_f)\}$ is a 2×1 column matrix of terminal constraints given by Eqs. (94) and (95) and $[\lambda]$ is a 3×1 time varying matrix of Lagrange multipliers or influence functions. $\{\dot{x}\} = \{f(x, u)\}$ are the 3 first order differential equations of motion Eqs. (91), (92) and (93). $\{u\}$ is the control variable Φ. To customize this general augmented cost function for the problem at hand delete $L(x^*, u^*)$ since there is not an integral term in our performance measure, and substitute γ_f for $\phi(x_f)$ to obtain

$$J_a = \gamma_f + [\nu]^T \{\psi(x_f)\} + \int_{t_0}^{t_f} \{[\lambda]^T [f(x^*, u^*) - \dot{x}^*]\} dt \quad (101)$$

The numerical solution process begins with a guess of the control time history. The values for the state variables are computed from initial conditions and then integrated forward in time using this postulated control time history. Differential equations for the Lagrange multipliers, which are developed later, are used to integrate $[\lambda]$ backward in time beginning with the value of $[\lambda]$ computed at t_f. A new control time history is derived by setting the first variation in the augmented cost function to zero. The process is repeated until the terminal constraints are satisfied to within an acceptable tolerance.

The first variation in J_a is formed

$$\delta J_a = \frac{\partial \gamma_f}{\partial x_f} \delta x_f + [\nu]^T \frac{\partial \psi}{\partial x_f} \delta x_f + \int_{t_0}^{t_f} \{([\lambda]^T \frac{\partial f}{\partial x}) \delta x + ([\lambda]^T \frac{\partial f}{\partial u}) \delta u - [\lambda]^T \delta \dot{x}\} dt. \quad (102)$$

Integrate $[\lambda]^T \delta\dot{x}$ by parts to obtain

$$-\int_{t_0}^{t_f} ([\lambda]^T \delta\dot{x})\, dt = -[\lambda_f]^T \delta x_f + \int_{t_0}^{t_f} ([\dot{\lambda}]^T \delta x)\, dt \tag{103}$$

Substitute Eq. (103) into Eq. (102) to obtain

$$\delta J_a = \left(\frac{\partial\gamma_f}{\partial x_f} + [\nu]^T \frac{\partial\psi}{\partial x_f} - [\lambda_f]^T\right)\delta x_f$$

$$+\int_{t_0}^{t_f}\left[\left([\lambda]^T\frac{\partial f}{\partial x} + [\dot{\lambda}]^T\right)\delta x + \left([\lambda]^T\frac{\partial f}{\partial u}\right)\delta u\right]dt \tag{104}$$

Define a new Lagrange multiplier

$$[\lambda]^T \equiv [\lambda^J]^T + [\nu]^T [\lambda^i]^T \tag{105}$$

$[\lambda^J]$ is the 3×1 column of Lagrange multipliers normally used to impose the equations of motion while $[\lambda^i]$ is dimensioned 3×2 and contains additions to the Lagrange multipliers which arise from the terminal constraints. The first variation in J_a may now be written

$$\delta J_a = \left(\frac{\partial\gamma_f}{\partial x_f} + [\nu]^T \frac{\partial\psi}{\partial x_f} - [\lambda_f^J]^T - [\nu]^T [\lambda_f^i]^T\right)\delta x_f$$

$$+\int_{t_0}^{t_f}\Bigg[\left(\left([\lambda^J]^T + [\nu]^T [\lambda^i]^T\right)\frac{\partial f}{\partial x} + [\dot{\lambda}^J]^T + [\nu]^T [\dot{\lambda}^i]^T\right)\delta x$$

$$+\left(\left([\lambda^J]^T + [\nu]^T [\lambda^i]^T\right)\frac{\partial f}{\partial u}\right)\delta u\Bigg]dt \tag{106}$$

The performance index is minimized by setting the first variation in J_a equal to zero. Choose differential equations for the Lagrange multipliers so that the coefficient of δx goes to zero to obtain the two equations

$$[\dot{\lambda}^J]^T = -[\lambda^J]^T \frac{\partial f}{\partial x} \quad (107)$$

and

$$[\dot{\lambda}^i]^T = -[\lambda^i]^T \frac{\partial f}{\partial x} \quad (108)$$

The gradient of f is

$$\frac{\partial f}{\partial x} = \begin{bmatrix} 0 & \sin x_3 & x_2 \sin x_3 \\ \frac{\partial f_2}{\partial x_1} & \frac{\partial f_2}{\partial x_2} & \frac{\partial f_2}{\partial x_3} \\ \frac{\partial f_3}{\partial x_1} & \frac{\partial f_3}{\partial x_2} & \frac{\partial f_3}{\partial x_3} \end{bmatrix} \quad (109)$$

where

$$\frac{\partial f_2}{\partial x_1} = \frac{h_e}{hS} B\sigma \frac{x_{2r}^2}{x_2} + \frac{2c \sin x_3}{(c - 1 + x_1)^3} \quad (110)$$

$$\frac{\partial f_2}{\partial x_2} = -2B\sigma x_{2r} \quad (111)$$

$$\frac{\partial f_2}{\partial x_3} = -\frac{c \cos x_3}{(c - 1 + x_1)^2} \quad (112)$$

$$\frac{\partial f_3}{\partial x_1} = -\frac{h_e}{hS}A\sigma\frac{x_{2r}^2}{x_2}\cos\Phi + \frac{2c\cos x_3}{(c-1+x_1)^3 x_2} - \frac{x_2\cos x_3}{(c-1+x_1)^2} \tag{113}$$

$$\frac{\partial f_3}{\partial x_2} = A\sigma\cos\Phi + \frac{\cos x_3}{(c-1+x_1)} + \frac{c\cos x_3}{(c-1+x_1)^2 x_2^2} \tag{114}$$

and

$$\frac{\partial f_3}{\partial x_3} = -\frac{\sin x_3}{(c-1+x_1)}\left[x_2 - \frac{c}{(c-1+x_1)x_2}\right]. \tag{115}$$

Integrate the costates backwards in time using Eqs. (107) and (108) with the boundary conditions obtained by requiring the coefficient of δx_f in Eq. (106) to be zero

$$[\lambda_f^J]^T = \frac{\partial \gamma_f}{\partial x_f} = \begin{bmatrix} 0 & 0 & 1 \end{bmatrix} \tag{116}$$

$$[\lambda_f^i]^T = \frac{\partial \psi}{\partial x_f} = \begin{bmatrix} 1 & 0 & 0 \\ \frac{\partial \psi_2}{\partial x_{1f}} & \frac{\partial \psi_2}{\partial x_{2f}} & \frac{\partial \psi_2}{\partial x_{3f}} \end{bmatrix} \tag{117}$$

where

$$\frac{\partial \psi_2}{\partial x_{1f}} = -\left(\frac{r_a}{R}\right)^2\left[\frac{2c}{(c-1+x_{1f})^2}\right] + 2(c-1+x_{1f})\left(\frac{x_{2f}\cos x_{3f}}{c}\right)^2 \tag{118}$$

$$\frac{\partial \psi_2}{\partial x_{2f}} = (2x_{2f})\left[-\left(\frac{r_a}{R}\right)^2 + \left(\frac{(c-1+x_{1f})\cos x_{3f}}{c}\right)^2\right] \tag{119}$$

and

$$\frac{\partial\psi_2}{\partial x_{3f}} = -2\left[\frac{(c-1+x_{1f})x_{2f}}{c}\right]^2 \cos x_{3f} \sin x_{3f}. \tag{120}$$

Since the coefficients of δx and δx_f have been set to zero, the first variation of J_a reduces to

$$\delta J_a = \int_{t_0}^{t_f}\left[\left(\left([\lambda^J]^T + [\nu]^T[\lambda^i]^T\right)\frac{\partial f}{\partial u}\right)\delta u\right]dt = \delta J + [\nu]^T\{\delta\psi\} \tag{121}$$

where

$$\delta J = \int_{t_0}^{t_f}\left[\left([\lambda^J]^T\frac{\partial f}{\partial u}\right)\delta u\right]dt \tag{122}$$

and

$$\{\delta\psi\} = \int_{t_0}^{t_f}\left[\left([\lambda^i]^T\frac{\partial f}{\partial u}\right)\delta u\right]dt \tag{123}$$

Defining two new variables

$$\Lambda_\phi \equiv [\lambda^J]^T\frac{\partial f}{\partial u} \tag{124}$$

$$\Lambda_\psi \equiv [\lambda^i]^T\frac{\partial f}{\partial u}. \tag{125}$$

Λ_ϕ is a scalar, while Λ_ψ is a 2×1 column matrix and

$$\frac{\partial f}{\partial u} = \left[0\ 0\ -A\sigma x_2 \sin\Phi\right]. \tag{126}$$

To make J_a as small as possible, choose the variation in the control δu to be

$$\delta u = -K[\Lambda_\phi + [\nu]^T \Lambda_\psi]^T \tag{127}$$

K is a scalar weight which fixes the relative importance placed on minimizing the cost function versus satisfying the terminal constraints. A value of 200 for K places sufficient weight on the cost function and still allows the terminal constraints to be satisfied within an acceptable tolerance. By substituting Eqs. (127) and (125) into Eq. (123) obtain

$$\{\delta\psi\} = -\mathrm{K}\int_{t_0}^{t_f} [\Lambda_\psi]\,[\Lambda_\phi + [\nu]^T \Lambda_\psi]^T dt. \tag{128}$$

Again, introduce two additional variables

$$\{g\} \equiv \int_{t_0}^{t_f} [\Lambda_\psi]\,[\Lambda_\phi]^T dt \tag{129}$$

$$[Q] \equiv \int_{t_0}^{t_f} [\Lambda_\psi]\,[\Lambda_\psi]^T dt \tag{130}$$

Substitute these variables into Eq. (128) to obtain

$$\{\delta\psi\} = -K\,[g + Q\,[\nu]]\,. \tag{131}$$

To drive $\{\delta\psi\}$ to zero, choose $\{\delta\psi\} = -\{\psi_f\}$, where $\{\psi_f\}$ is the value of the terminal constraints, computed after integrating the state equations forward. solving Eq. (131) for $\{\nu\}$

$$\{\nu\} = -[Q]^{-1}\left[g - \frac{1}{K}\psi_f\right]. \tag{132}$$

Use this value for $\{\nu\}$ in Eq. (127) to obtain $\{\delta u\}$. The control update is then computed

$$\{u_{new}\} = \{u_{old}\} + \{\delta u\}. \tag{133}$$

Since the final time is free, we must also minimize

$$\frac{\partial J_a}{\partial t_f}\delta t_f = \left[\frac{\partial \phi}{\partial t_f} + \nu^T \frac{\partial \psi}{\partial t_f}\right]\delta t_f. \tag{134}$$

Now let

$$\delta t_f = -\frac{1}{b}\left[\frac{\partial \phi}{\partial t_f} + \nu^T \frac{\partial \psi}{\partial t_f}\right]_{t = t_f}. \tag{135}$$

Replace ϕ with γ_f and ψ with the expressions given in Eqs. (94) and (95) to obtain

$$\delta t_f = -\frac{1}{b}\left(f_{3f} + \nu_1 f_{1f} + \nu_2\left(\frac{\partial \psi_2}{\partial x_{1f}} f_{1f} + \frac{\partial \psi_2}{\partial x_{2f}} f_{2f} + \frac{\partial \psi_2}{\partial x_{3f}} f_{3f}\right)\right). \tag{136}$$

Use the new control time history {Eq. (133)}, along with the change in t_f {Eq. (136)}, to again integrate the state equations forward. Compute the terminal value of the Lagrange multipliers and integrate these backwards in time, then recompute the control time history. This process is repeated until the terminal constraints are satisfied within an acceptable error bound. The final apocenter altitude is required to be within 5 nm of the target value while the terminal altitude is required to be within 25,000 ft of the defined atmospheric interface altitude. Apocenter errors of 5 nm require very little ΔV to correct and are attainable using this optimization method although thirty or more iterations may be required to converge this closely. The 25,000 ft terminal altitude error band was chosen because the aerodynamic effects decrease exponentially with altitude and are almost negligible at altitudes above 300,000 ft. To converge closer than 25,000 ft to the selected atmospheric interface altitude of 410,105 ft (125 km) requires many more iterations. Furthermore, the terminal altitude generally converges toward the target altitude from above.

Conjugate Gradient Projection Method

The conjugate gradient projection method was employed to speed convergence of this problem[40, 41]. The gradient obtained in Eq. (127) was again used in this method to compute the search direction for correcting the control variable. However, after the first control update the previous search direction is used in conjunction with the computed gradient to give the problem near second-order convergence characteristics. The procedure follows. First, compute the gradient direction using Eq. (127)

$$g_i = -\delta u \tag{137}$$

where the i subscript denotes the ith iteration of control updates. Next, compute the search direction

$$s_i = -g_i \tag{138}$$

for the first iteration, while for subsequent iterations

$$s_i = -g_i + \frac{\langle g_i, g_i \rangle}{\langle g_{i-1}, g_{i-1} \rangle} s_{i-1}. \tag{139}$$

where $\langle a, b \rangle$ is the inner product of a and b.

Once the search direction is determined, it is necessary to properly scale the magnitude of the correction.